In presenting the dissertation as a partial fulfillment of the requirements for an advanced degree from the Georgia Institute of Technology, I agree that the Library of the Institute shall make it available for inspection and circulation in accordance with its regulations governing materials of this type. I agree that permission to copy from, or to publish from, this dissertation may be granted by the professor under whose direction it was written, or, in his absence, by the Dean of the Graduate Division when such copying or publication is solely for scholarly purposes and does not involve potential financial gain. It is understood that any copying from, or publication of, this dissertation which involves potential financial gain will not be allowed without written permission.

7/25/68

FAST NEUTRON THERAPY TREATMENT PLANNING

A THESIS

Presented to

The Faculty of the Division of Graduate

Studies and Research

by

Patton H. McGinley

In Partial Fulfillment

of the Requirements for the Degree

Doctor of Philosophy

in the School of Nuclear Engineering

Georgia Institute of Technology

August, 1971

GEORGIA INSTITUTE OF TECHNOLOGY LIBRARY

Regulations for the Use of Theses

Unpublished theses submitted for the Master's and Doctor's degrees and deposited in the Georgia Institute of Technology Library are open for inspection and consultation, but must be used with due regard for the rights of the authors. Passages may be copied only with permission of the authors, and proper credit must be given in subsequent written or published work. Extensive copying or publication of the thesis in whole or in part requires the consent of the Dean of the Graduate Division of the Georgia Institute of Technology.

This thesis by PATTON HOPKINS MCGINLEY has been used by the following persons, whose signatures attest their acceptance of the above restrictions.

A library which borrows this thesis for use by its patrons is expected to secure the signature of each user.

NAME AND ADDRESS OF USER	BORROWING LIBRARY	DATE

FAST NEUTRON THERAPY TREATMENT PLANNING

Approved: _____

_____

_____

_____

_____

Date approved by Chairman: 8/16/71

ACKNOWLEDGMENTS

This report is based upon a thesis submitted to the Georgia Institute of Technology in partial fulfillment of the requirements for the Doctor of Philosophy Degree. The report describes research carried out in the School of Nuclear Engineering at the Georgia Institute of Technology.

The author acknowledges support by the Atomic Energy Commission by the award of a Special Fellowship in Radiation Science and Protection administered by Oak Ridge Associated Universities. He wishes to express gratitude to Professor F. W. Chambers, Jr., thesis advisor, for suggesting the area of study and for help in all aspects of this work. The author is also very grateful to the members of his reading committee, Dr. G. G. Eichholz, Dr. L. J. Gallaher, and Dr. D. S. Harmer, for their encouragement and guidance.

The author also wishes to express his gratitude for the assistance of many of the members of the Health Physics Staff at the Oak Ridge National Laboratory and for the use of the DLEA neutron generator. In particular, the suggestions and technical assistance of Dr. J. W. Poston and Mr. E. M. Robinson have been appreciated.

Thanks also go to Dr. J. B. Smathers of the Texas A & M University Department of Nuclear Engineering and to Dr. D. K. Bewley of the Hammersmith Hospital Cyclotron Unit for arranging the irradiation of a number of LiF dosimeters.

The author wishes to thank his wife and children for the moral support given him while he was in graduate school. A special thanks should be expressed to the Bennie Board Business, of which his wife is chairman of the "boards," for the generous financial aid to his education.

TABLE OF CONTENTS

TABLE OF CONTENTS (Continued)

LIST OF TABLES

LIST OF TABLES (Continued)

LIST OF ILLUSTRATIONS

LIST OF ILLUSTRATIONS (Continued)

SUMMARY

During the last two decades there has been a renewed interest in the use of fast neutrons for radiotherapy. At present, a clinical trial is being conducted at Hammersmith Hospital, London, using fast neutrons with an average energy of 7.65 MeV and future trials, in which 14 MeV neutrons will be employed, are being considered. Little information exists concerning the dose distribution produced by collimated beams of 14 MeV neutrons in tissue. Nor have the effects of bone and lung tissues on the soft tissue dose distribution been investigated for neutron beams of sizes suitable for use in radiotherapy. Information of this type is needed for treatment planning of 14 MeV neutron therapy.

In this research, dose distributions for use in neutron radiotherapy were experimentally determined. Tissue-equivalent ionization chambers were utilized in conjunction with thermoluminescent dosimeters to establish the neutron and gamma ray doses deposited in tissue irradiated by beams of 14 MeV neutrons. Dose distributions in homogeneous and heterogeneous phantoms containing lung and bone components were determined at a source-to-skin distance of 125 cm.

From these measurements it was concluded that the dose distributions due to 14 MeV neutrons have properties which make them suitable for use in radiotherapy. However, improved collimation and shielding systems will be required in order to reduce the whole-body dose received by a patient undergoing neutron therapy.

An examination of the dose distributions revealed that the percent depth dose at points within the volume of tissue irradiated could be predicted by means of an empirical equation. Based on these measurements, only a slight change in the soft tissue dose distribution was produced by bone. On the other hand, an increased dose was found for points in and behind the lungs as compared to the dose that would be obtained in a homogeneous phantom.

A discussion of the sources of error in the experimental measurements is included as well as suggestions for future work related to 14 MeV neutron therapy.

CHAPTER I

INTRODUCTION

The aim of the radiotherapist is to destroy tumors while at the same time to produce minimum damage to normal tissue surrounding the tumor. In general the radiosensitivity of normal tissue is only slightly less than that of malignant tissue. As a result of this fact it may be impossible to destroy the tumor without severe damage to normal tissue. It is felt by some researchers that the effectiveness of radiotherapy could be increased by the use of new types of radiation, such as high energy charged particles or neutrons that have an enhanced effect on the anoxic portion of tumors as compared to their effect on normal tissue.

It has been found that the response to conventional radiotherapy by X and gamma radiation is significantly influenced by the oxygen concentration in the vicinity of cells being irradiated [1,2]. Both cancerous and normal cells show greater sensitivity to radiation at higher oxygen concentration. In general the sensitivity to radiation is increased by a factor of three when the survival of well-oxygenated cells is compared to that of anoxic cells.

This oxygen effect may be one of the reasons for failure of X and gamma radiation to cure certain cancers. Healthy tissue, due to its higher oxygen concentration, tends to be more sensitive to radiation than cancerous tissue that contains anoxic regions. Under these conditions the dose that can safely be delivered to the treatment volume may be lim-

ited by the radiation tolerance of healthy tissue adjacent to the tumor and it may be impossible to deliver a dose of sufficient size to eliminate the tumor.

This problem of anoxic cells in tumors may be overcome in the following ways:

1. The sensitivity of all cells in the tumor region may be increased to the same level by increasing the oxygen concentration of the anoxic cells.

2. The sensitivity of cells in and near the tumor may all be reduced to the same level by a reduction of the oxygen concentration.

3. By use of radiation whose effect is independent of oxygen concentration both anoxic and oxygenated tissue would be affected to the same degree.

The first possibility has been tested by having the patient breathe oxygen at high pressure while receiving radiotherapy. After a decade and a half of clinical experiments, there is no substantial evidence that this method of radiotherapy is effective.

The second solution is practical only where the arterial blood can be cut off for a short time. Methods have not been found for reducing the oxygen concentration in tissue without cerebral damage. The third possibility of overcoming the oxygen effect by use of new types of radiation sources is considered in this thesis.

It has been found that the magnitude of the oxygen effect depends on the linear energy transfer (LET) of the radiation employed, with high LET radiation being relatively independent of oxygen concentration in its

effect on normal and tumor tissue [2,3,4].

The term "linear energy transfer" was introduced by Zirkle et al. [5] to describe the spatial distribution of energy dissipated in matter by ionizing radiation. The LET is usually expressed in terms of keV per micron path length of absorber.

Gamma and X ray photons with energy of more than 100 keV produce low LET (0.2 to 3 keV/μ) secondary electrons in tissue. On the other hand, alpha particles produced by the decay of naturally occurring radioactive materials have high LET values of the order of about 100 keV/μ in tissue. The LET of ionizing particles is a function of their mass and velocity with high LET being produced by low speed and high mass particles.

Charged particles of LET greater than a few keV/μ have a short range in tissue. Therefore, the effect of high-LET particles on animals or animal tissue has been studied mainly by the use of fast neutrons which have no charge and can penetrate deeply into tissue. High-LET particles, such as recoil protons and alpha particles, are produced by the interaction of neutrons with tissue. Biological changes are produced by the energy deposited in tissue by these particles. Chapter II of this thesis covers the details of neutron interactions with matter and the types of particles produced.

If high-LET radiation is employed for tumor treatment, the anoxic parts of the tumor mass will be affected almost to the same extent as normal oxygenated tissue. Therefore, radiotherapy utilizing fast neutrons or high energy charged particles may be more effective than conventional tumor therapy with low LET X ray and gamma rays.

A neutron source suitable for external beam therapy, in which the radiation source is located outside of the patient's body and a collimated beam of radiation is used to irradiate the tumor, should exhibit the following characteristics:

1. small oxygen effect for the neutrons emitted;
2. high penetration in tissue for the neutrons emitted;
3. reasonable size and cost;
4. low weight, so that positional and angular control of the beam are possible;
5. high source strength, so that a high dose rate is produced at the location of the patient to minimize treatment time.

The first factor, the oxygen effect, has been determined for neutrons produced by the following reactions: fission, $^{2}H(d,n)^{3}He$, $^{9}Be(d,n)^{10}B$, and $^{3}H(d,n)^{4}He$ [6,7,8,9]. The neutrons produced by these reactions exhibit only minor oxygen effect and may therefore be suitable for radiotherapy.

It has been found that neutrons from the first and second reactions [9,10] do not have sufficient penetration for external beam therapy. Neutrons produced by bombarding a beryllium target with deuterons have penetration that is barely acceptable for therapy [11]. Neutrons produced by the $^{3}H(d,n)^{4}He$ reaction meet the first four requirements [7,9,12], but the available source strength is too low for radiotherapy. It is felt that it is technically feasible to remedy this defect by improved target design using some of the methods reviewed in Chapter II. It is for these reasons that clinical trials are being considered at the University of

Pennsylvania Hospital utilizing neutrons produced by the $^{3}H(d,n)^{4}He$ reaction [13].

Before clinical trials are initiated, dose distributions in tissue must be obtained for use in treatment planning. Dose distributions for use in treatment planning are commonly expressed in terms of the percent depth dose ($P_{x,y}$) which is defined as

$$P_{x,y} = \frac{D_{x,y}}{D_o} \times 100 \ , \qquad (1)$$

where

D_o = dose at a reference point along the central axis (usually 0.5 cm depth below the skin surface for ^{60}Co)

$D_{x,y}$ = dose at point (x,y).

A typical geometrical arrangement of the radiation source and the patient is shown in Figure 1. The source is located at point S and the edge of the beam is shown as solid lines from S to L and L'. The surface of the patient is located along line LL'. Length ℓ is used in some of the treatment planning equations that follow. This length is the distance between point O and the point where the line from source S to point (x,y) intersects the skin of the patient. The distance from the source to the skin of the patient is given by length SO and is called the source-to-skin distance (SSD). The line through the center of the beam along SO is called the central axis. Percent depth dose values for points along this axis will be indicated by the symbol $P_{o,y}$.

The main purpose of treatment planning is to assure adequate tumor

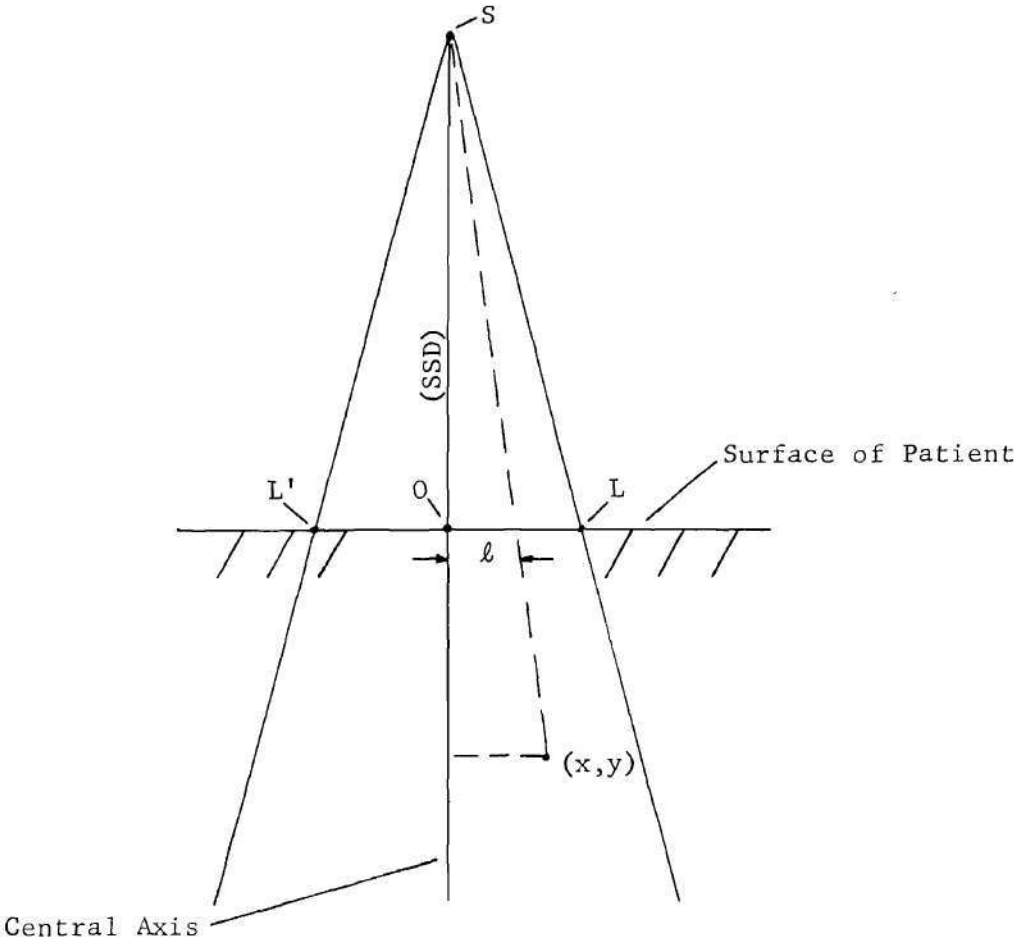

Figure 1. Geometry for Depth Dose Determination

dose and minimum dose to healthy tissue. This goal is attained by use of multifield techniques, rotational methods and control of field size and treatment distance. An outline of these methods is given in Chapter II and a brief summary of a typical treatment plan is given below.

In tumor treatment it is inevitable to expose some healthy tissue to almost the same dose as that delivered to the tumor. Figure 2 shows several regions associated with a tumor mass. In computing the exposed tissue volume the actual tumor and a surrounding region referred to as the "safety margin" are assumed to constitute the mass to be exposed. The safety margin is added to the outermost boundaries of the tumor to allow for uncertainties in tumor size and to possibly include sub-clinical extensions from the main tumor.

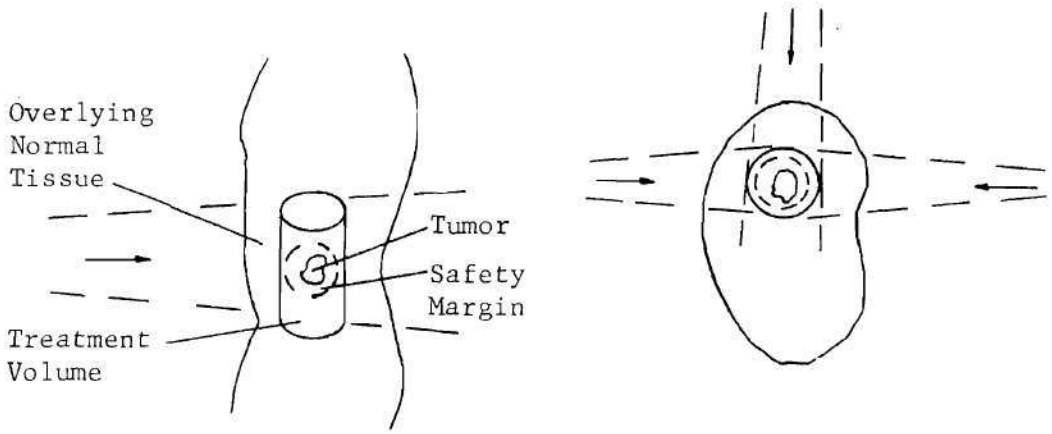

Figure 2. Tumor Volume, Safety Margin, and Treatment Volume (From Reference 13)

Irradiation of the tumor mass is achieved by exposure to several converging radiation fields in the same horizontal plane. This procedure considerably reduces the skin dose and the dose to overlying normal tissue. By employing this multifield method a roughly cylindrical volume, somewhat larger than the safety margin volume, receives a high absorbed dose.

The "treatment volume" usually contains part or all of some essential organ whose sensitivity to radiation limits the dose deliverable to the nearby tumor mass. Irreparable damage may be done to surrounding normal tissue at dose levels less than that required to "kill" the tumor. Therefore, an evaluation of each treatment procedure must be made based on the dose distribution in the volume of irradiated tissue.

The objective of this investigation is to obtain tissue-dose distributions for collimated beams of 14 MeV neutrons and to develop treatment planning equations for fast neutron therapy. The investigation can be divided into four related parts. They are

1. design and construction of a fast neutron collimator and shield,

2. measurement of physical properties of the fast neutron beam produced by the collimator in air and tissue-equivalent material,

3. determination of percent dose distributions due to 14 MeV neutrons in tissue equivalent material, and

4. analysis of the depth dose data to obtain relationships between the percent depth dose and parameters such as depth in tissue, distance off central axis, field size, and source-to-skin distance.

CHAPTER II

GENERAL CONCEPTS

The purpose of this chapter is to summarize the problems and requirements associated with the prediction of dose distributions for use in 14 MeV neutron treatment planning. Also considered are the concepts necessary for an understanding of these problems.

Dose Concept

Specifying biological effects produced by a given radiation exposure in terms of a single parameter is difficult. It has been the general approach to assume that the effect of radiation can be correlated with the energy absorbed. The basic concept of "absorbed dose" was defined by the International Commission on Radiological Units [14] as

$$D = \frac{\Delta E_d}{\Delta m} , \tag{2}$$

where

D = absorbed dose

ΔE_d = energy imparted by ionizing radiation to matter in a volume of mass Δm.

The unit of absorbed dose is the rad which is equivalent to 100 ergs of energy absorbed per gram of matter. It should be noted that this definition of radiation dose is more general than some of the older units

such as the roentgen in that neither the absorbing material or the type of radiation is specified.

The degree of ionization produced in air by X or gamma radiation is used to determine the exposure (X) as shown by equation 3.

$$X = \frac{\Delta Q}{\Delta m} . \tag{3}$$

The term ΔQ represents the sum of the electrical charges on all ions of one sign produced in air when all secondary electrons liberated by photons in a volume of air of mass Δm are completely stopped in air. The roentgen (R) which represents the liberation of 2.58×10^{-4} Coulombs of charge of one sign per kg of air is used as the unit of exposure.

The magnitude of damage produced by the exposure of a biological system to equal absorbed doses of different radiations may be quite different. In the medical field the "RBE dose" is used to indicate the degree of biological damage produced by an absorbed dose (D) of a given type of radiation. The RBE dose for a particular type of radiation (type A) is defined as

$$\text{RBE dose} = (D)(RBE) , \tag{4}$$

where

D = absorbed dose(rad)

RBE = relative biological effectiveness of radiation (type A) compared with the effect of X or γ radiation.

For a given type of radiation the RBE factor can be defined as

$$\text{RBE} = \begin{pmatrix}\text{Dose of 250 keV X rays}\\ \text{or gamma rays producing}\\ \text{a given biological effect}\end{pmatrix} \Big/ \begin{pmatrix}\text{Dose of radiation-}\\ \text{A producing the same}\\ \text{biological effect}\end{pmatrix} \qquad (5)$$

The RBE dose is a relatively awkward concept in the sense that many different factors influence RBE values. For example, the RBE of a radiation may depend on the type of biological effect considered, temperature, the dose, the dose rate, LET, oxygen concentration, etc. It has been estimated that the conditions encountered in fast neutron therapy may result in a RBE of 2.5 to 3.0 [4,13,15].

Deposition of Energy in Matter by Fast Neutrons

In order to develop instruments and techniques for use in the determination of the absorbed dose in patients undergoing neutron therapy, knowledge of the mechanism of energy deposition in matter by fast neutrons is desirable. The following section is a survey of the basic interaction of neutrons with matter with special emphasis on neutron interactions in tissue.

When matter is irradiated with neutrons the primary interaction is at the nuclear level since neutrons are uncharged and there will be only slight interaction with orbital electrons. In general the interactions are of two types, scatter and absorption of neutrons by the target nuclei. Neutron scattering reactions may be of the elastic or inelastic type. Elastic scattering events are those in which the neutron collides with the nucleus of an atom and some of the kinetic energy of the neutron is transferred to kinetic energy of the struck nucleus. The struck nucleus is not left in an excited state and kinetic energy is con-

served in the collision. The energy of the neutron (E') after collision is given by

$$E' = E \frac{A^2 + 2A\,\omega + 1}{(A + 1)^2} , \qquad (6)$$

where

E = initial energy of the neutron

A = atomic weight of scattering material

ω = cosine of the scattering angle in the center-of-mass coordinate system.

Maximum loss of kinetic energy of the neutron occurs for scattering materials with low atomic weight and for large angles of scatter. The probability for elastic scattering tends to increase as the neutron's energy becomes small. The neutron may also undergo scatter and leave the nucleus in an excited state. Scattering of this type is called inelastic scattering and it occurs with increasing probability as the energy of the neutron becomes large. Above 3.0 MeV neutron energy, about half of the total cross section for materials with medium and high atomic weight is due to inelastic scattering [16]. On the average the energy of the neutron is reduced to below 2.0 MeV as the result of any single inelastic scattering event in matter [16].

Neutron absorption by the target nucleus may result in such reactions as the following types (n,α), (n,2n), and (n,p). These reactions are prevalent for neutrons with energy of several MeV and their cross sections increase with energy. Exceptions to this general rule are the

$^{10}B(n,\alpha)^{7}Li$ and the $^{6}Li(n,\alpha)^{3}H$ reactions which have large cross sections at low neutron energy. The (n,2n) reaction becomes energetically possible when the energy of the incident neutron is larger than the binding energy of the last neutron in the target nucleus. Depending on the nucleus in question, the binding energy of the last neutron varies from 1.67 to 20.4 MeV.

An absorption reaction in which the neutron enters the nucleus and no particle is emitted is usually called neutron capture. This reaction occurs with high probability at low neutron energy and a compound nucleus is formed in an excited state due to the binding energy released as a result of neutron absorption. The compound nucleus usually releases this excess energy by the emission of one or more capture gamma rays and the product nucleus undergoes radioactive decay.

In tissue neutron interactions are primarily with nuclei of hydrogen, carbon, oxygen, and nitrogen. Less important reactions occur with calcium and phosphorus. Heavy charged particles (protons, deuterons, alpha particles, and recoil C, N, and O nuclei) with high LET are released in tissue by fast neutrons through recoil effects and absorption reaction.

In summary, the five main reactions by which fast neutrons deposit energy in tissue are listed below.

1. Elastic scattering of neutrons by hydrogen is the most important interaction in terms of energy deposited per gram of tissue. Recoil protons contribute 94 percent of the absorbed dose at 0.3 MeV and this percentage drops to 70 percent at 14 MeV neutron energy due to the decreasing cross section for this interaction.

2. Neutron absorption by oxygen is the second most important fast neutron interaction in tissue. In particular, the reaction $^{16}O(n,\alpha)^{13}C$ will result in high LET α particles being produced in tissue. About 11 percent of the absorbed dose due to 14 MeV neutrons is produced by this reaction in tissue [17].

3. Recoil nuclei other than hydrogen recoils are produced in tissue due to fast neutron interactions. These recoil nuclei have short track length and very high LET. About 10 percent of the absorbed dose due to 14 MeV neutrons is due to this process.

4. Radiative capture of slow neutrons by hydrogen in tissue leads to the production of 2.21 MeV gamma rays. This reaction has low probability at high neutron energies, but becomes important after the neutron has been slowed by a series of collisions with nuclei in tissue.

5. Neutron absorption by nitrogen also has high probability at low neutron energy and results in the production of 0.6 MeV protons by the $^{14}N(n,p)^{14}C$ reaction. Less than 0.2 percent of the absorbed dose due to 14 MeV neutrons is produced by this reaction.

In addition to the interactions mentioned above, energy may be lost by neutrons in tissue by inelastic scattering. About four percent of the energy deposited in tissue by 14 MeV neutrons is due to recoil nuclei produced by inelastic scattering. Randolph [17] has indicated that there are at least 17 nuclear reactions and 25 products contributing to the absorbed dose in tissue due to 14 MeV neutrons. The principal reactions and the fraction of the absorbed dose due to the reaction prod-

ucts are outlined in Table 1.

Table 1. 14 MeV Neutron Reactions in Tissue [17]

Reaction	Ionizing Product	Fraction of Total Dose (F)	Average LET $\bar{L}_e$ (keV/μ)	$F\bar{L}_e$
H(n,n)H	p	0.704	25	17.6
$^{16}O(n,\alpha)^{13}C$	α	0.106	90	9.5
	^{13}C	0.046	750	34.2
$^{16}O(n,n)^{16}O$	^{16}O	0.030	500	15.2
$^{16}O(n,n)^{16}O^*$	^{16}O	0.035	670	23.6
$^{12}C(n,n)^{12}C$	^{12}C	0.009	700	6.3
$^{12}C(n,n)3\alpha$	α	0.017	130	2.2
11 others	19 others	0.056	291	16.3

Overall energy average LET -- 124.9 keV/μ
Energy average LET from H -- 25
Energy average LET from all other elements -- 362

About 70 percent of the dose is delivered at an energy average LET of 25 keV/μ due to elastic scatter by hydrogen. The remaining 30 percent of the absorbed dose, due to elastic scatter and nuclear reactions with O, C, and N, is at a higher LET value.

Requirements for a Dosimetry System

Neutron beams almost always have associated with them a gamma ray

component. These gamma rays are produced by capture reactions and inelastic scattering of neutrons in the shield and collimator material and in tissue. X rays are inavoidably produced in neutron generators and γ-ray dose levels near the target have been reported at 25 to 450 mR/hr [18]. In the case of well-collimated 14 MeV neutron beams the gamma dose component can be relatively small and little build-up of this component has been noted in tissue-equivalent materials [19]. For therapy purposes it is desirable to determine the absorbed dose due to neutrons and gamma rays separately. Each component can then be weighted by a clinical RBE factor to obtain the biological damage produced by the radiation.

In order to obtain depth dose values for use in neutron therapy planning a dosimetry system should be employed that has the following characteristics.

1. Capability of resolving the absorbed dose in tissue into gamma and neutron components.

2. Small size in order to produce minimum perturbation of the radiation field.

3. Capability of dose rate determination at 125 cm from the target of a conventional neutron generator (20 to 200 mR/min).

4. A high degree of stability is required since depth dose studies typically require several months time.

5. For the reasons given in the next section of this chapter, depth dose distributions are usually determined by measurements made in tissue-equivalent liquids. Therefore, the dosimeters should be rugged and waterproof since they will be used in a liquid phantom.

Tissue-Equivalent Materials

For reasons of convenience and cost, dose distribution studies are almost invariably carried out by measuring the dose at selected points within a suitably shaped solid or liquid-filled model known as a phantom. For valid comparisons such a phantom must be made of material that closely reproduces the composition and spatial distribution of body tissues.

In order for a material to be tissue-equivalent (TE) for neutrons, it must have the same elemental composition as tissue. True tissue-equivalent solid materials have not been developed due to difficulties in reproducing the required oxygen content. However, TE solutions can easily be prepared for use as a phantom to simulate the patient's body. Tables 2 and Table 3 list the composition of muscle and bone and some of the tissue-equivalent materials available at present. Since most of the energy deposited in tissue by fast neutrons is due to interactions with hydrogen, the hydrogen content of any tissue substitute material should be closely matched to that of tissue. It should be noted that the oxygen and carbon content of TE plastic (A-150) are almost reversed as compared to soft tissue or muscle. Corrections for this reversal of oxygen and carbon content in this material are discussed in Chapter III.

In order to obtain realistic dose distributions, one should use a heterogeneous phantom that contains muscle, lung, and bone components. The shape and dimensions of the phantom should be similar to those of an average patient. Lung-equivalent material should have a composition similar to that of muscle [20] but with a density in the range of 0.2 to 0.5 gm/cm^3 [21]. A lung phantom could be constructed of muscle equivalent plastic interspersed with small air spaces.

Table 2. Composition of Muscle and Muscle-Equivalent Materials in Percent by Weight

Element	Typical Muscle [22]	TE Gas* I [23]	TE Gel [23]	TE Plastic A-150 [24]	TE Gas II [23]	TE Liquid [25]
H	10.2	9.7	10.0	9.9	10.1	10.2
C	12.3	15.7	14.9	77.1	45.7	12.0
N	3.5	3.5	3.5	4.4	3.5	3.6
O	72.9	71.1	71.6	5.0	40.7	74.2
other elements	1.1	--	--	3.6	--	--

*Explosive mixture

Table 3. Composition of Bone and Bone-Equivalent Material in Percent by Weight

Element	Bone [22]	Bone-Equivalent Plastic B-100 [26]
H	6.4	6.39
C	27.8	53.41
N	2.7	2.67
O	41.0	3.06
Ca	14.7	17.69
P	7.0	---
F	---	16.77
Other Elements	0.4	---

Radiotherapy Unit

If 14 MeV neutrons are to be used for therapy, adequate shielding and collimation must be provided to minimize the exposure of healthy tissue to radiation. In general terms, a typical radiotherapy unit for fast neutron treatment may take the form shown in Figure 3. The walls, ceiling, and floor of the treatment room serve as a primary radiation barrier and are constructed of concrete. The primary barrier is used to reduce the radiation levels outside the treatment room in order to protect the hospital's patients and staff. It has been reported [27,28] that the thickness of the primary barrier must be of the order of seven feet of concrete. The neutron source itself is surrounded by a shield and collimator system in order to provide a beam of neutrons and to reduce the whole body dose to the patient. Minimum dose to tissue outside the target volume is essential due to the deleterious effects produced by neutrons on the blood forming organs, lenses of the eyes, and skin of the patient. The patient is shown in Figure 3 in the supine position on the treatment couch. Alignment of the patient and the beam is usually obtained by use of a light source that projects a beam of light through the collimator. The light beam is aligned with markings on the skin of the patient corresponding to the desired entrance port for the beam. The neutron source could also be used to make a diagnostic radiograph from which the alignment of the tumor and the beam could be determined.

The basic components of the therapy unit are the neutron source, collimator, and shield. Each of these components is discussed in the following sections.

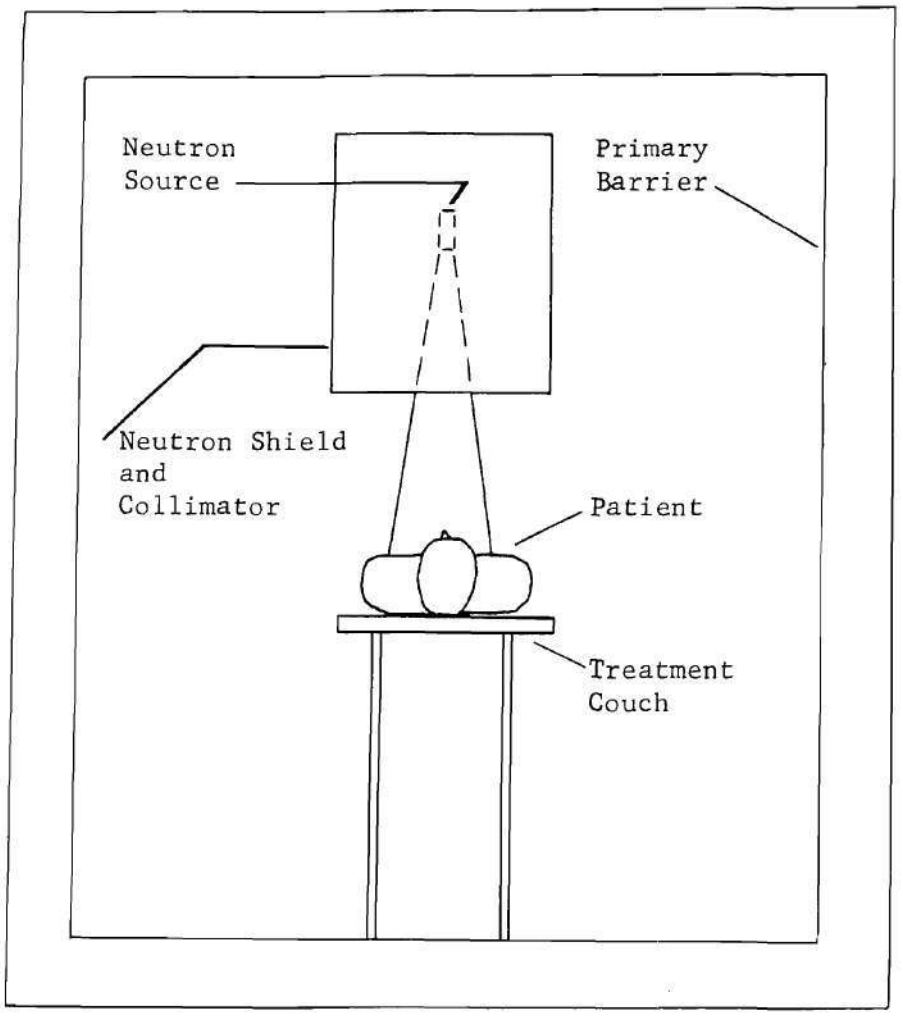

Figure 3. Plan of a Typical Fast Neutron Therapy Unit

Neutron Source

Fast neutrons of energy of approximately 14.6 MeV are produced by the $^{3}H(d,n)^{4}He$ reaction. Neutrons generated by this method are usually referred to as DT or 14 MeV neutrons. In employing this reaction, a beam of deuterons is directed against a tritium-containing metal disc. The fast neutron flux emerges almost isotropically from the tritium target and only slight variation of the neutron energy with the angle of emission from the target has been observed. For example, at an incident deuteron energy of 150 keV, neutrons with energy of 14.7 MeV are emitted in the forward direction and with 13.4 MeV energy at an angle of 180° with respect to the incident deuteron beam [29].

A typical commercial neutron generator utilizes a Cockcroft-Walton voltage generator to produce accelerating potentials of the order of 150 to 200 keV. Higher potentials result in increased cost and complexity due to insulation problems. The tritium target consists of a copper disk onto which a thin layer (2 to 2.5 mg/cm^2) of titanium has been evaporated. Several curies of tritium are incorporated into the titanium layer by absorption. A deuterium ion current of about 2.0 mA is used to achieve neutron yields of the order of 1×10^{11} neutrons/sec.

Due to the loss of tritium from the target as a result of deuteron bombardment, which heats the target and causes "boiling off" of the tritium into the beam tube vacuum system, the target half life (i.e., the time required for the neutron yield to decrease to half of the initial value) is relatively short, being of the order of an hour or less when a high beam current is used.

A neutron spectrum obtained at a distance of 125 cm from a tritium target is shown in Figure 4 [19]. The target was bombarded with 400 keV deuterons and threshold detectors were used to obtain the neutron energy spectrum. To minimize the presence of scattered neutrons the source was located on a light-weight metal floor in the middle of a cubical room measuring 40 feet on each edge.

For neutron radiotherapy it is necessary that the neutron source produce a high dose rate at the location of the patient and have relatively long life. Brennan [9] has suggested that the minimum dose rate acceptable for neutron therapy is 10 rads per minute at the surface of the patient. This dose rate corresponds to a neutron flux of approximately 2×10^7 neutrons per cm^2 per second. This value for the minimum dose rate was based on the following considerations. Accurate alignment of the beam and tumor volume can be maintained only for a relatively short time due to movement of the patient. At best, the patient can be expected to remain immobile for a period of about 15 minutes.

Also, if a statistically significant number of cases is to be treated (> 24 patients per day) for a clinical trial, a dose rate of this magnitude is required. To obtain a dose rate of 10 rads per minute, a neutron source yield of 4.0×10^{12} neutrons per second is required if the patient is to be treated at a distance of 125 cm from the target. Smaller treatment distances will probably not be used since unfavorable dose distributions result [9].

A target life time of at least 30 hours [13] is desirable for radiotherapy to minimize time loss due to target replacement. Several

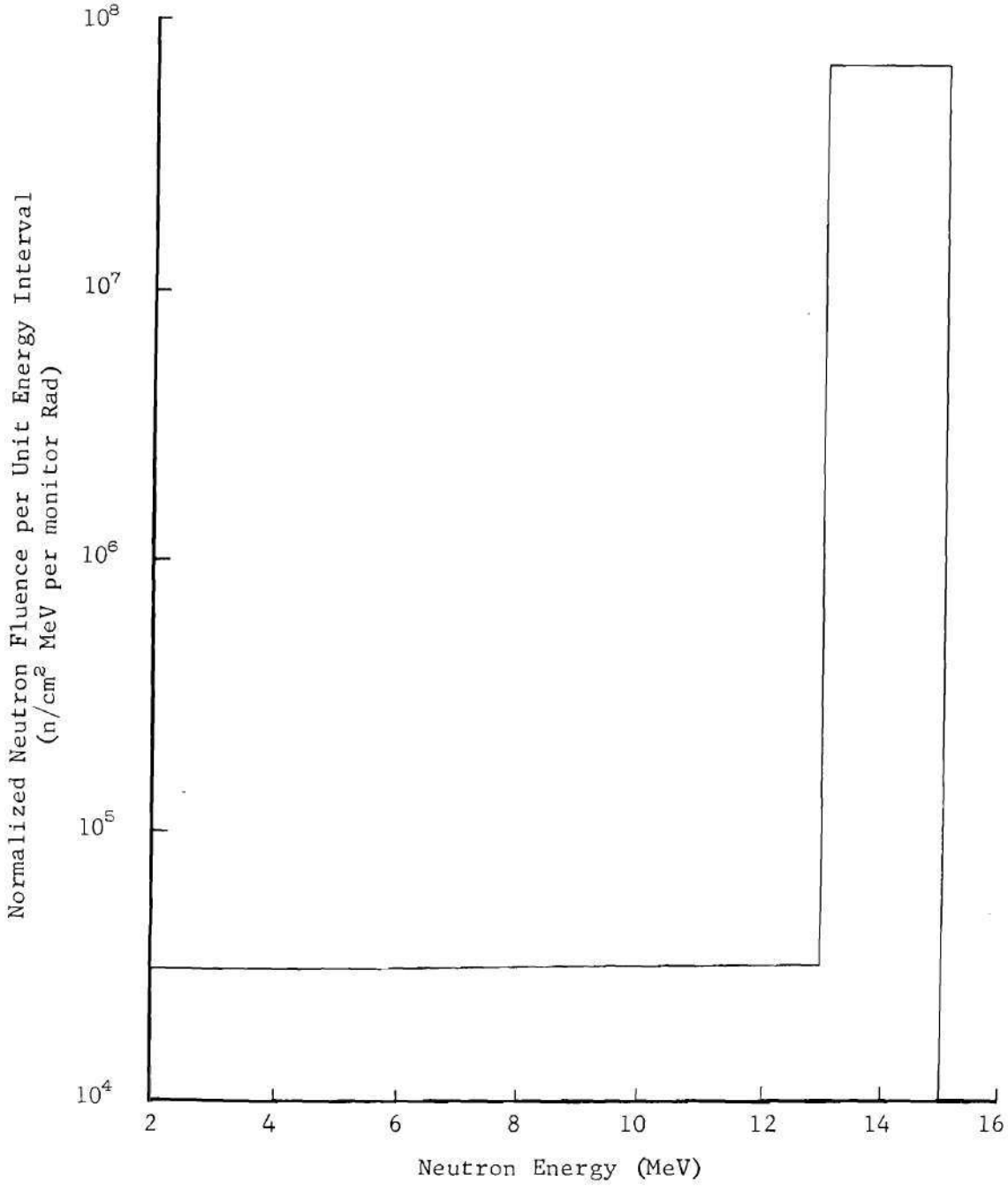

Figure 4. Neutron Spectrum in Air (15 x 15 cm field) LRL-ICT(d,t) Source (from reference 19)

approaches are being investigated at present to increase the neutron yield and target life time. The neutron output could be increased by use of large area targets and increased beam current. A neutron generator has been constructed by the Health Physics Group of the Oak Ridge National Laboratory in which a 35 cm diameter target containing 1500 to 2000 Ci of tritium was bombarded by a beam current of 500 mA [30,31]. A target life of four hours was obtained for continuous operation at a source yield greater than 1×10^{13} neutrons per second. However, it is felt that collimation problems would result if targets larger than 2.54 cm diameter are used for neutron therapy [32]; also, the use of 1500-2000 Ci of ^{3}H in a single target poses serious safety and contamination problems. Therefore, other approaches for increasing the neutron yield and target life are being explored.

A mixed beam approach is being considered by the British Services Electronic Research Laboratory [33]. The target contains both deuterium and tritium and both tritium and deuterium ions are accelerated into the target. The following reactions occur: $^{3}H(d,n)^{4}He$, $^{2}H(t,n)^{4}He$, and $^{2}H(d,n)^{3}He$, but the yield of the last reaction is relatively low. By use of tritium and deuterium in both the target and the beam, target life times of 80 to 100 hours have been obtained at a yield of 1×10^{11} neutrons per second [34]. The mixed beam method has been used with sealed tubes to eliminate the need for a vacuum pumping system and gas transfer equipment. By use of a sealed source, the tritium health hazard is reduced since large amounts of tritium gas do not have to be pumped through a vacuum system.

The Aero-Jet Corporation [35] has developed high yield ion sources for the production of 650 mA beams of deuterium or tritium ions. These ions can be focused into a beam having a diameter of two centimeters or less. At present this group is investigating the development of a radiotherapy target in which both deuterium and tritium ions are used to bombard a bare copper plate. Loss of tritium by the "sputtering off" of the Ti layer is avoided by this system.

The possibility of employing a gas target containing gaseous tritium is being investigated [36]. Preliminary studies indicate it may be possible to obtain a source yield greater than 1×10^{13} neutrons per second by use of gas targets.

One of the larger 14 MeV neutron generators in this country is located at the Lawrence Radiation Laboratory, California [19]. This neutron generator utilizes a target which consists of a disc of copper with a layer of tritium on the surface. The target is rotated at 1100 rpm and a two centimeter beam of deuterium ions strikes the edge of the disc. An emission rate of 1×10^{12} neutrons per second and a target life of 30 to 40 hours has been reported for this generator [12].

If 14 MeV neutrons are to be used for therapy, the source output must be increased and longer target life must be obtained. From the studies reviewed above, it appears to be technically feasible to achieve a neutron yield of 4×10^{12} neutrons per second and a target half life greater than 30 hours. At the moment the neutron yield obtainable from commercial generators is adequate for depth dose studies.

Neutron Shield and Collimator

To avoid exposing a major portion of the patient's body to large neutron doses, a shielding system is required for fast neutron therapy. A neutron shield suitable for external beam therapy should meet the following basic requirements.

1. The shield should produce an attenuation of the dose by a factor of at least 98 percent for points near the edge of the beam.

2. The whole body dose should be one percent or less of the tumor dose.

3. The shield weight should be minimal for easy positional and angular control of the neutron beam.

4. The maximum shield length should be less than 125 cm.

The first requirement is based on the fact that the dose due to radiation backscattered from the patient at points a few centimeters outside of the beam is about 2.0 percent of the dose at the center of the neutron beam [27]. Therefore, there is no need for the shield to produce an attenuation of the dose by a factor much greater than 98 percent for points near the beam edge. The second requirement is based on the fact that a tumor dose of several hundred rads will be required for neutron radiotherapy. If the patient's whole body is exposed to dose levels much greater than 1.0 percent of the tumor dose, unacceptable somatic injury may result.

In order to position the beam accurately with respect to the patient, a shield of relatively low weight is required. A source plus shield weight of as much as seven tons could be used with standard ^{60}Co

therapy mountings [34]. The requirement for maximum shield length of 125 cm is based on the following considerations. To obtain favorable dose distributions in tissue, the patient must be treated at a distance of at least 125 cm from the source [9]. On the other hand, to obtain an acceptable dose rate (10 rad/min) the patient may have to be treated as close to the source as possible. Thus, a treatment distance of 125 cm will probably be used for neutron therapy.

The terms field size, field flatness, and beam sharpness will be used in this thesis to describe radiation beam characteristics. A typical beam profile is shown in Figure 5. A distribution of this type will be called a traverse dose function. The value of this function at a given point (x,y) is obtained from the ratio shown below.

$$F = \frac{D_{x,y}}{D_{o,y}} , \tag{7}$$

where

F = traverse dose function

$D_{x,y}$ = dose at a point x distance from the central axis and a depth y

$D_{o,y}$ = dose at a point on the central axis and a depth y.

The field size is obtained from the traverse dose function at the surface of the patient. This quantity is determined at the point where the function F has a value of 0.5. In some of the equations that follow, the field size is represented by the symbol 2L. Beam size is used as a general term to describe the width of the beam at any depth in the patient.

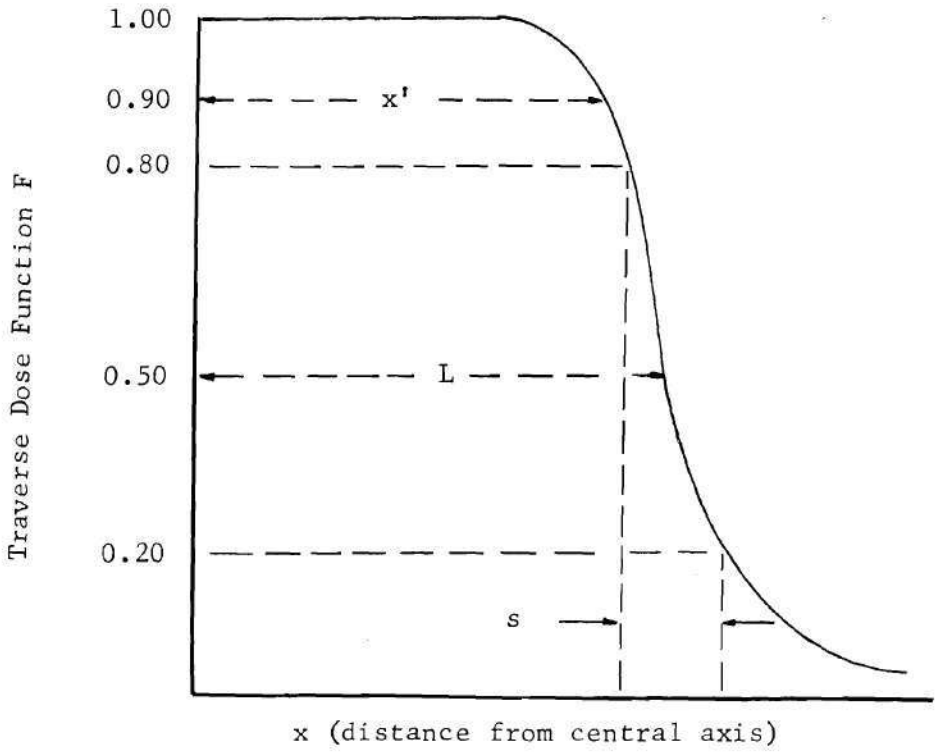

Figure 5. Traverse Dose Function at a Constant Depth

The beam size is determined at the point where the traverse dose function has a value of 0.5 for the depth in question.

The beam flatness (f) at depth y is defined as

$$f = \frac{x'}{L_y} \times 100 \ , \tag{8}$$

where

x' = traverse distance from central axis to the point where F has a value of 0.90

L_y = half-width of the beam at depth y.

The beam sharpness as used in this thesis is defined as the distance required for F to decrease from 0.80 to 0.20. This distance is measured traverse to the central axis and is shown in Figure 5 by the symbol s. These values of F were selected to describe the dose distribution at the edge of the beam due to the fact that, in this range, F decreases in nearly a linear fashion with distance x. A second term similar to the beam sharpness may be used to describe the dose distribution at the edge of the beam. The origin of the geometrical penumbra [37] is illustrated in Figure 6 and it can be calculated by use of equation 9.

$$p = \left(\frac{d\text{-SDD}}{(SDD)}\right) \times \left(\begin{matrix}\text{source} \\ \text{diameter}\end{matrix}\right) \ , \tag{9}$$

where

SDD = distance from source to distal end of collimator

d = distance from source to point where p is obtained.

Typical values of p for ^{60}Co radiotherapy units range from approximately zero to five centimeters at the surface of the patient. For

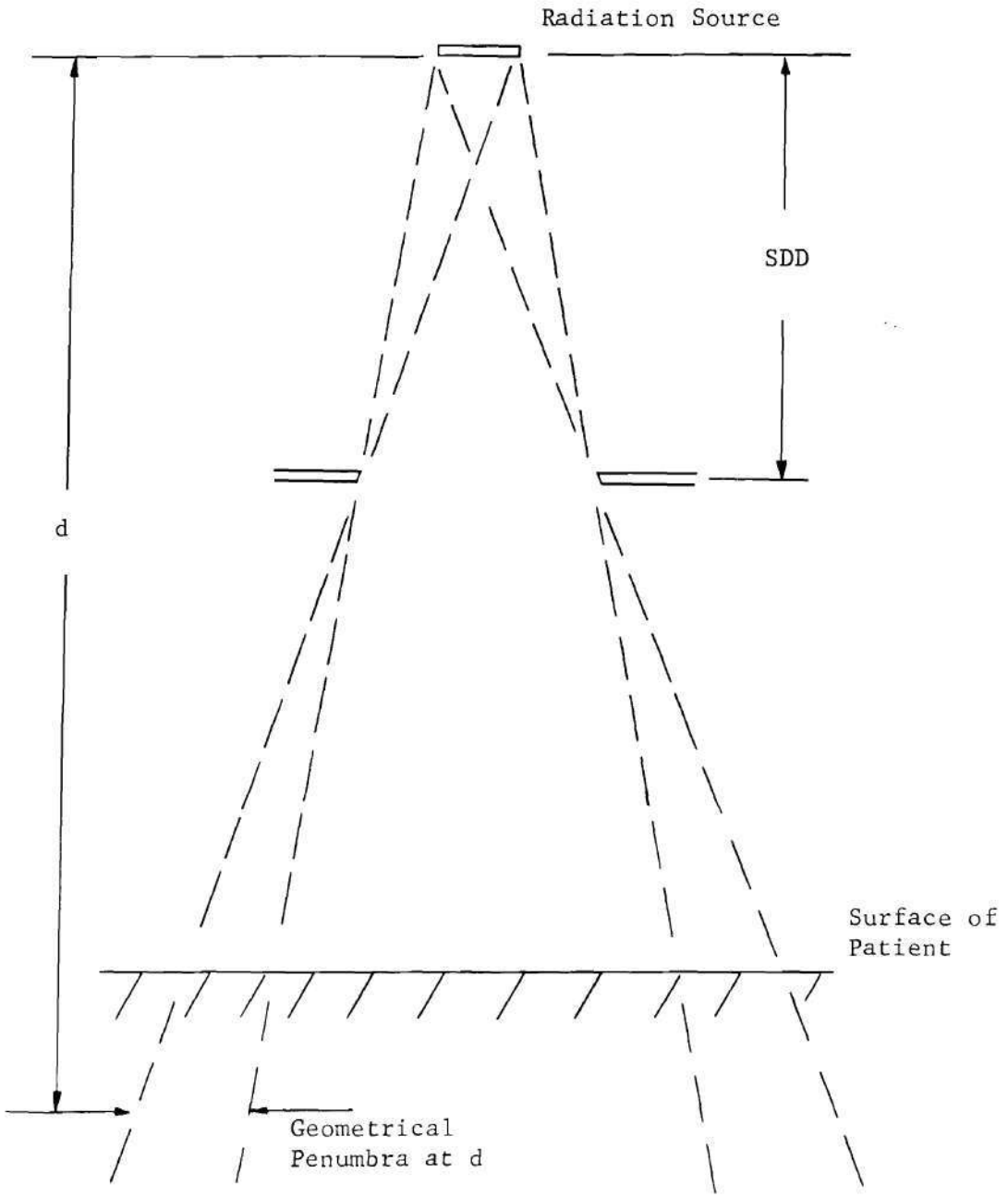

Figure 6. Geometrical Penumbra

radiotherapy purposes the beam sharpness is a more suitable description of the beam since it is based on dose measurements made in tissue or tissue-equivalent material.

In order to obtain a uniform dose in the treatment volume and low dose outside of this region, a radiation beam should have a large beam flatness and low beam sharpness. In addition, the dose level in the area outside of the beam should be low. Typical values of these quantities for a 10 x 10 cm ^{60}Co beam at a depth of one centimeter are 0.5 cm beam sharpness, 85 percent beam flatness, and an F value of 0.01 to 0.02 outside the beam. On the other hand, typical X ray beams have larger beam sharpness and lower beam flatness. For example, values of eight centimeter beam sharpness and 42 percent beam flatness are found for an X ray beam (250 kV, 2.5 mm half value thickness, 10 X 10 cm field size) at a depth of 10 cm in the tissue.

A collimator for use in neutron therapy or a depth dose study should produce a beam that is well defined and that has relatively low contamination by slow neutrons and gamma rays. The desired properties of a fast neutron beam for clinical use are listed below.

1. The beam flatness and sharpness in tissue should be comparable to that obtained for X ray beams used in therapy [32].

2. A beam with 5 to 10 percent gamma dose contamination would be acceptable for radiotherapy [13]. Since gamma rays are used for treatment of cancer and tumors, a 50 percent gamma dose contamination could be tolerated.

3. The beam should have a minimum slow neutron dose component of

a few percent of the total dose [32] to minimize the skin and near surface dose and activation of equipment.

4. The penetration of the neutron beam in tissue should be such that the dose at a depth of 10 cm is at least 50 percent of the dose near the surface [13].

Beam definition similar to that of therapeutic X ray beams is suggested since radiotherapy can be carried out successfully with X ray beams. The requirement for a minimum reduction in dose of 50 percent in 10 cm of tissue is based on treatment planning considerations which are explained in the next section.

Treatment Planning

Treatment planning for radiotherapy aims to optimize treatment procedures so that a maximum dose is delivered to the tumor with a minimum dose deposited in healthy tissue. In general, it is desirable to use an electronic computer for treatment planning since many alternative treatment conditions must be considered. A brief review of the general approach of calculation of dose distribution within the patient is given below.

Radiotherapy planning can be divided into three distinct steps. The first of which is the determination of the percent dose at any point within a given block of soft tissue irradiated by a single stationary beam of radiation. In the second step of treatment planning, corrections are made of the dose distribution obtained in step one to account for patient contour and heterogeneity and for beam modifying filters and penumbra effects. As a last step, depth dose distributions are produced for multi-

field and rotational therapy by systematic summing and interpolation of the distributions for single fields. The radiologist can now determine the suitability of a particular treatment plan by examination of the dose distribution produced in step three. Factors such as the uniformity of the dose distribution in the tumor volume, the amount of healthy tissue irradiated, the extent of the safety margin, and the maximum dose to healthy tissue are used to evaluate a treatment plan.

Multifield and rotational therapy are used to treat tumors that lie at considerable depth below the skin. It has been found that treatment of deep tumors with a single field usually results in excessive damage to healthy tissue. This damage can be avoided by use of the multifield technique in which two or more beams of radiation with different portals of entry are aimed at the tumor volume. Rotational therapy in which the source is revolved about the patient with the beam aimed continually at the tumor is an outgrowth of the multifield technique. For treatment of tumors of the trunk region of the body by the rotational or multifield method, the radiation should have a degree of penetration that will result in the 50 percent depth dose occurring at a depth of at least 10 cm. With this degree of penetration, dose distributions can be obtained for multifield and rotational therapy that have higher tumor dose than the dose to healthy tissue outside the treatment region.

It should be pointed out that the basic problem in computer therapy planning is the generation of a single-field dose distribution. At present, the majority of the methods used to calculate single-field distributions are of the form shown by equation 10.

$$P_{x,y} = P_{o,y} \times F \ , \tag{10}$$

where

$P_{x,y}$ = percent depth dose at point (x,y)

$P_{o,y}$ = percent depth dose at depth y along central axis

x = distance off central axis

y = depth in patient

F = traverse dose function.

Equations fitted directly to percent depth dose values have been used to generate values for $P_{o,y}$. One of the newer and more successful empirical equations was developed by Sterling [38]. This relationship was based on the fact that the percent depth dose was shown to be a simple function of the logarithm of the ratio of the area to perimeter of the field, the depth below the surface, and the source-to-skin distance. For a fixed SSD the expression takes the form

$$\log P_{o,y} = m \log(A/E) + h \ , \tag{11}$$

where

$P_{o,y}$ = percent depth dose at depth y along the central axis

A = area of field

E = perimeter of field

h and m = fitting constants.

It was found that, for ^{60}Co gamma radiation, h and m are linear functions of depth below the surface according to equations 12 and 13

$$h = ay + b \ , \tag{12}$$

$$m = a'y + b' \ , \tag{13}$$

where a, b, a', and b' are experimentally determined constants.

Combining equations 11, 12, and 13 gives equation 14.

$$P_{o,y} = \text{antilog}\,[ay + (a'y + b')\,\log(A/E) + b] \ . \tag{14}$$

Four fitting constants are needed in equation 14 to describe the central axis dose distribution for all field sizes of clinical interest at a fixed SSD. Agreement between observed and calculated percent dose values was found by Sterling [38] to be within 2.0 percent for depths from 1 to 20 cm in tissue.

The function $P_{o,y}$ may also be determined by use of tissue-air ratios (TAR) [39,40]. This ratio relates the dose in air to the percent depth dose in tissue at the same point on the central axis.

To obtain percent dose values at points off the central axis, values of the function F are required. According to Clifton and Gallagher [41] the various methods used to represent the traverse dose function fall into three groups:

1. Specific Cross Plot Data.
2. Representation of Primary and Scatter Contributions.
3. General Empirical Curve Fit.

The first group requires large amounts of computer memory, and interpolation techniques are needed to generate dose values for points not included in the list of data. The decrement line system developed by

Ochard [42] offers an efficient method of obtaining dose values from a minimum number of experimental measurements.

The second group of algorithms has evolved from methods suggested by Clarkson [43] and Meredith and Neary [44] in which the percent dose at a point is obtained by separate calculation of the primary and scattered radiation components. Much use of this system has been made in conjunction with the TAR method for computer-generated depth dose distributions.

Sterling [38] has used empirical curve fitting methods to obtain a simple traverse dose function. It was found that the traverse dose function could be represented by the cumulative probability function shown by equation 15.

$$F = 1 - \int_{-\infty}^{\ell/L} \frac{1}{\sqrt{2\pi}\,\sigma} \exp\left\{-\frac{[(\ell/L) - \mu]^2}{2\sigma^2}\right\} d(\ell/L) \qquad (15)$$

where

F = traverse dose function

ℓ = distance from central axis to the point where the line from source S to point (x,y) intersects the skin of the patient (see Figure 1)

L = half field width

μ, σ = experimentally determined constants.

Computer programs have been written which are based on the algorithms developed by Sterling for the central axis and traverse dose function [45]. Programs of this type can be used to determine three-dimensional dose distributions in which many of the corrections required for treatment planning have been taken into consideration.

To the best of the author's knowledge, only one article has been published on neutron depth dose equations. In this article, Glover [46] has fitted exponential equations to the central axis depth dose data of Lawson et al. [10]. The general form of equation used is shown by equation 16.

$$P_{o,y} = 100(1 - (1 - \exp(-\lambda y))^{n}) \ . \qquad (16)$$

The constants λ and n were determined from experimental data for two field sizes at a source-to-skin distance of 76 cm. It was found that both λ and n depended on the field size.

CHAPTER III

PREVIOUS WORK

This chapter contains a review of the information available for use in planning a study of the dose distribution produced in tissue by 14 MeV neutrons. A summary of the techniques of dosimetry, collimation and shielding suitable for fast neutron therapy is given. This is followed by a review of the available depth dose information related to 14 MeV neutron therapy.

Dosimetry Methods

Several systems have been devised to resolve the absorbed dose into gamma and neutron components. A proportional counter system has been developed by Hurst [47] for the determination of absorbed dose in tissue from fast neutrons while discriminating against gamma rays. This instrument has a lower energy limit of about 200 keV for neutrons; therefore, additional measurements of the slow neutron component and gamma dose must be obtained. Usually the slow neutron dose is determined by use of a calibrated BF_3 detector shielded with a layer of Cd. The dose due to neutrons in the energy range from the cadmium cutoff (0.4 eV) to 200 keV is not determined and the total neutron dose may be considerably underestimated [48].

The total dose due to mixed radiation fields may be obtained by use of small gas-filled tissue-equivalent ionization chambers. The ion-

ization produced in the gas by charged particles originating in the cavity walls can be related to the absorbed dose in the wall material of the chamber by equation 17, which is known as the Bragg-Gray relation.

$$D = JWS/100 , \tag{17}$$

where

D = absorbed dose (rads)

J = number of ion pairs formed per gram of gas

W = average energy in ergs expended per ion pair formed by ionizing particles crossing the chamber

S = effective value of the ratio of the mass stopping power of the wall material to that of the cavity gas for the ionizing particles.

This relationship can be applied only if the following conditions are met.

a. The cavity must be small so that there is a negligible effect on the distribution of secondary charged particles in the medium into which the cavity is introduced. This implies that the linear dimensions of the cavity must be small in comparison to the range of secondary charged particles in the gas.

b. The chamber walls must be thicker than the maximum range of secondary charged particles in the wall material so that all particles crossing the chamber originate in the wall material.

c. The intensity of the primary radiation must be substantially constant over the chamber volume.

It has been demonstrated by Fano [49] that condition (a) may be relaxed if the wall and gas material have similar atomic composition and the value of S in equation 17 then becomes unity. Condition (b) can be satisfied for fast neutrons by making the wall thickness greater than 2.5 mm.

Ionization chambers have been constructed with wall and gas of tissue-equivalent material in order to obtain the total absorbed dose in tissue due to any ionizing radiation. The chamber walls are constructed of a gel-like material which has the same atomic composition as soft tissue. An explosive mixture of hydrogen, oxygen, nitrogen, and methane is used as a filling gas. It is necessary to use this mixture in order to obtain a tissue-equivalent gas which is not soluble in the chamber walls. The composition of the chamber walls is given in Table 2. For obvious reasons this instrument has been used only as a laboratory standard. Practical dosimetry is done with tissue-substitute materials such as tissue-equivalent plastics and gases. This change results in replacing a large part of the oxygen concentration needed to simulate soft tissue by carbon. Since the cross sections of carbon and oxygen are rather similar over a wide neutron energy range, Rossi [23] has pointed out that this approximation of tissue is justified on the basis of theoretical principles.

At neutron energies above 10 MeV non-elastic reactions with oxygen become important, being responsible for about 15 percent of the absorbed dose due to 14 MeV neutrons [50]. Therefore, corrections should be considered for non-tissue composition of ionization chamber dosimeters. Dose values obtained with tissue-substitute chambers and standard tissue-

equivalent chambers have been found to agree within experimental error for neutrons with energy from 0.5 to 14 MeV energy after applying corrections for the difference of atomic composition [23].

Some uncertainty in the absorbed dose determined by tissue-equivalent ionization chambers arises when relating the charge collected to the dose. The energy lost by secondary charged particles in producing an ion pair has been found to vary somewhat with particle velocity [51,52] and particle type [52,53]. The variation with velocity is small. On the other hand, the change with particle type may be significant [47]. In general, W values for charged particles other than electrons and alpha particles are not well known and this introduces error in the value of the absorbed dose. A second problem is the recombination of ion pairs and the subsequent reduction of the measured value of J as a result of the high ion density produced by heavy recoil particles such as carbon and oxygen ions.

The absorbed dose due to gamma rays may be determined by use of a second ionization chamber with low neutron sensitivity such as a graphite chamber filled with CO_2 gas [48].

When the tissue-equivalent and graphite chamber are exposed to a mixed radiation field of neutrons and gamma rays the following relationship may be used to obtain the absorbed dose due to neutrons and gamma rays [54,55].

$$T = aN + b\gamma \ , \tag{18}$$

$$G = kN + b\gamma \ , \tag{19}$$

where

T = response of tissue-equivalent chamber in terms of roentgens of ^{60}Co gamma radiation

G = response of graphite chamber in terms of roentgens of ^{60}Co gamma radiation

N and γ = absorbed dose in tissue due to neutrons and gamma rays, respectively (rads)

a, b, and k = correction terms which are explained below.

To obtain T and G each chamber must be calibrated with a known ^{60}Co gamma ray exposure. The instrument response (current, charge, voltage loss, etc.) to a mixed neutron and gamma ray field is multiplied by the appropriate calibration factor to evaluate T and G.

Equations 18 and 19 contain several correction terms (a, b, and k) that are required due to the fact that T and G are expressed in terms of roentgens of ^{60}Co gamma radiation. The first term (a) in equation 18 is necessary since equal amounts of ionization are not produced in tissue-equivalent gas by equal absorbed doses of neutrons and gamma rays due to a difference in the W values for electrons and protons. Therefore, the portion of the ionization that is caused by neutrons must be adjusted if it is to be reckoned equivalent to that caused by an equal dose of gamma rays. The rad to roentgen factor (b) is also used to obtain consistent units on both sides of equation 18. The correction factor (a) has a value of 0.97 R per rad [54] and is given by

$$a = b \frac{W_e}{W_p} , \qquad (20)$$

where

b = rad to R conversion factor (1.03 R/rad)

W_p = W value for protons

W_e = W value for electrons.

The factor k which appears in equation 19 is the ratio of the response produced by exposing the graphite chamber to a neutron field that would result in the deposition of one rad in tissue to the response produced by exposing the graphite chamber to one R of ^{60}Co gamma radiation.

Values of k have been calculated for various neutron energies for the graphite chamber. At 14 MeV neutron energy this parameter has a value of 0.29 R/rad and decreases to 0.08 R/rad at 2.5 MeV neutron energy [55]. Thus, a reasonable knowledge of the neutron energy spectrum is required for use of this paired chamber system. Hurst [56] has indicated that uncertainties in the value of k result in an error of the order of ± 10 percent or less in the neutron absorbed dose. Considerable error may result in the determination of the gamma dose component for mixed radiation fields with low gamma contamination. This error is a result of the fact that for this case the gamma dose component depends on the difference of two numbers which are about equal size.

Many detector systems have been used for the determination of the gamma dose in the presence of neutrons. A Geiger-Müller gamma-ray dosimeter that is relatively insensitive to neutrons has been developed by Wagner and Hurst [57]. The k value for this instrument due to neutrons in the energy range from 0.68 to 4.2 MeV has been shown to be less than 0.005 R/rad. Values of k due to higher energy neutrons have not been measured, but are estimated to be less than 0.015 R/rad.

Lithium fluoride thermoluminescent dosimeters may be used in place of a graphite chamber for mixed field dosimetry. Harshaw Chemical Company has developed LiF thermoluminescent dosimeters (TLD) which have the isotopic composition shown in Table 4.

Table 4. Isotopic Composition of TLD-100 and TLD-700

Type	^{6}Li (%)*	^{7}Li (%)*
TLD-100	7.5	92.5
TLD-700	0.01	99.99

*percent by weight

The first dosimeter in Table 4, TLD-100, responds to both thermal neutrons and gamma rays. A strong thermal neutron response is produced by the $^{6}Li(n,\alpha)^{3}H$ reaction which has a cross section of 950 barns for pure ^{6}Li. The cross section for this reaction has an average value of one barn for neutrons in the energy range from 10 keV to 15 MeV [58]. Due to the reduced concentration of ^{6}Li in TLD-700 little response is produced by thermal neutrons and the dosimeter is sensitive primarily to gamma rays.

Values of k have been determined for TLD-700 for neutrons with energy from 0.26 to 14.1 MeV [59,60,61]. An increase in k from 0.005 at 0.26 MeV neutron energy to 0.17 at 14.1 MeV neutron energy was reported [60]. Davy and O'Brien [62] observed changes in the ^{6}Li content of TLD-

700 (from 0.01 to 0.6 percent by weight) resulted in variations in the value of k. The range of ^{6}Li percentage given above was obtained by mass analysis of TLD-700.

The author of this thesis found that a plot of the k values given in reference 60 indicates a linear relationship between k for TLD-700 and the energy of the neutrons as shown by equation 21.

$$k(E) = mE + C \ , \tag{21}$$

where

$$k(E) = \frac{\text{Response of TLD-700 produced by exposure to a neutron field which will deposit one rad in tissue}}{\text{Response of TLD-700 produced by an exposure of one R of } ^{60}\text{Co gamma radiation}}$$

E = energy of neutrons (MeV)

m and c = slope and intercept constants.

Davy and O'Brien [62] also presented theoretical values from which k can be obtained for neutrons with energy from 0.01 to 15 MeV. These calculations were based on the activation saturation model developed for scintillation detectors [63]. Theoretical curves were reported that relate the response of LiF thermoluminescent dosimeters produced by an exposure of unit fluence of neutrons to the response produced by an irradiation which would result in the deposition of one rad in tissue.

The present author has converted these data to k values for TLD-700 and TLD-100 by use of fluence to dose conversion values given in ICRU Report 13 [64] and a rad to roentgen conversion factor of 1.03. A linear relationship similar to equation 21 was obtained between k(E) and

the neutron energy for both TLD-100 and TLD-700.

In none of these studies was an attempt made to shield the LiF dosimeters from stray thermal neutrons. Slight thermal neutron contamination of the fast neutron beam could cause uncertainty in the fast neutron response values. This uncertainty could be quite large for TLD-100 due to the higher concentration of ^{6}Li in this dosimeter [65].

It has been found that ^{6}LiF makes an excellent thermal neutron shield for TLD dosimeters [66,67]. This material has a high thermal neutron cross section and does not emit secondary gamma rays upon neutron capture. There is only one other material with these properties (^{3}He) and being a gas, it is not suitable for neutron shielding [66].

Lithium fluoride thermoluminescent detectors have many properties that make them ideal for use as gamma ray dosimeters in depth dose studies for neutron therapy. Some of these properties are listed below:

1. Low fast-neutron sensitivity.

2. Simple linear response function for neutron energies from 0.30 MeV to 15 MeV.

3. Compact size.

4. Response that is independent of gamma ray energy over wide range (0.100 to 10 MeV).

5. Approximately tissue-equivalent for gamma rays and X rays.

6. Not affected by humidity, atmospheric pressure changes, and normal room temperature change.

7. Very low dose fade with time (5.0 percent per year).

8. Dose rate-independent to more than 10^{11} R/sec.

9. Wide dose range (few mR to 10^5R).

10. Low thermal neutron sensitivity of TLD-700 and high sensitivity of TLD-100 permits determination of thermal neutron flux density.

It was for these reasons that LiF dosimeters were chosen for use in this depth dose study. Probably the most accurate method for measurement of the total dose due to neutrons and gamma rays is by use of tissue-equivalent ionization chambers. For clinical trials of fast neutron therapy, long-term consistency and repeatability of measurements may be more important than absolute accuracy of the dosimetry system. It has been estimated by Bewley et al. [68] that the systematic error in the dosimetry system mentioned above is less than ± 20 percent while the error in relative dose levels is unlikely to be more than 5.0 percent.

Shielding and Collimation

Several fast neutron collimators and shields have been constructed for use in tumor therapy with neutrons produced in cyclotrons using the $^{9}Be(d,n)^{10}B$ reaction [68,69,70]. Large thicknesses of hydrogenous materials were employed to attenuate the neutron flux. Only stationary horizontal beams were produced and no attempt was made to provide beam directional control due to the weight of the source and shield.

A lower weight and more compact shield can be produced by use of a composite shield [16,34,71]. An inner layer of iron or mild steel is used to degrade the energy of fast neutrons emitted by the source. Iron has a large cross-section for inelastic scattering of 14 MeV neutrons and on the average the neutron energy is reduced to below one MeV per reaction.

A relaxation length of about 8.5 cm has been reported [16,32] for this mechanism of removal of fast neutrons. Therefore, a 26 cm layer of iron would reduce the 14 MeV neutron flux by a factor of 95 percent. Iron is relatively ineffective as a shielding material for slower neutrons so a second layer of hydrogenous material, for examply polyethylene, is used to slow and capture the degraded neutrons. The neutrons now have a relaxation length of about five centimeters with respect to dose attenuation in polyethylene. A thin outer layer of gamma shielding material may be necessary to reduce the capture gamma dose outside of the shield.

Penetration of fast neutrons through various combinations of iron and polyethylene slabs and iron and water has been investigated [16,72]. Greene and Thomas [72] indicated that a combination of 20 cm of iron and 20 cm of polyethylene produced optimum attenuation of 14 MeV neutrons in terms of the dose reduction produced by a shield of 40 cm total thickness. An attenuation of the neutron dose of 96 percent was obtained by this shield.

Little information on the design of 14 MeV beam collimators exists. Lanfsdorf [73] has developed ray optics methods for collimation of one to three MeV neutrons. Application of this method to 14 MeV neutrons may be difficult since some of Langsdorf's arguments were based on isotropic scattering of neutrons in the laboratory system. The design of a collimator system for 14 MeV neutron scattering experiments has been investigated by Lent [16]. Scattering from the walls of the collimator was analyzed in order to determine the intensity of scattered and 14 MeV neutrons in the beam. Collimator designs were reported for systems con-

siderably larger than those envisioned for neutron therapy. For example, the total distance from the neutron source to the point where the beam emerged from the collimator (SDD) was 60 ft.

A number of collimators have been constructed for use in depth dose studies of 14 MeV neutrons. Greene and Thomas [34] used tapered steel collimator inserts to produce various beam sizes. A homogeneous iron shield of 35.5 cm thickness was utilized to produce an attenuation of the neutron dose by a factor of 99 percent. A beam contamination of 8.0 percent and 2.0 percent of the total dose was found for gamma rays and slow neutrons, respectively.

Lawson, Clare, and Watt [10] utilized a polyethylene and lead shield to obtain depth dose measurements in tissue-equivalent phantoms for 14 MeV neutrons. Poor collimation resulted from this arrangement. At two centimeters depth the dose value changed only by a factor of 50 percent when one moved from the geometrical edge of the beam laterally a distance of one centimeter. On the other hand, a change of 90 percent is seen for Greene's collimator for the same depth and lateral distance change.

A shadow shield and collimator constructed of pressed hardwood has been used to obtain collimated beams of 14 MeV neutrons at the Lawrence Radiation Laboratory neutron generator [12,19]. This shield was in the form of a cube 60 cm on edge and was equipped with a removable collimator insert.

Field sizes of 5 X 5 cm and 15 X 15 cm were investigated in a source study for neutron radiation therapy using this collimator. A

gamma contamination of 2.5 percent of the total absorbed dose was found for the smaller field and 8.2 percent for the larger field.

A composite iron-polyethylene collimator and shield is being considered for use in a clinical trial of 14 MeV neutron therapy by Brennan [74]. The shield is designed to give one percent dose transmission and will have a total weight of less than 500 lb. The target housing is 80 cm thick of which 20 cm is steel. To the best of the author's knowledge a test of the collimation properties of this proposed system or a similar one have not been made.

Depth Dose Data

Only meager depth dose information exists for collimated 14 MeV neutrons. Greene and Thomas [34] have obtained central-axis depth-dose values by use of small tissue-equivalent ionization chambers and a Hurst proportional counter. The portion of the total dose due to gamma rays was measured roughly by use of LiF dosimeters. It was not indicated that corrections were made for the fast neutron response of the LiF dosimeters. The phantom used for these measurements was made of Lucite with a 3.0 mm thick front wall. Its dimensions were 30 X 30 X 30 cm and it was filled with water [75]. Central-axis depth-dose data were acquired for four field sizes at 50, 75, and 100 cm source-to-skin distance. All fields were square and the size ranged from 5 x 5 cm to 40 x 40 cm.

For treatment of deep abdominal and chest tumors, the 50 percent depth dose along the central axis should occur at about 10 cm or deeper [13]. With this depth dose distribution, it is possible to obtain a lower skin dose than the dose to the treatment volume. None of the depth

dose curves obtained by Greene at a target-to-skin distance of 50 cm met this requirement since the 50 percent depth dose occurred at 8.0 cm. Increasing the target-to-skin distance to 75 cm results in a 50 percent depth dose at 10 cm for field sizes of 7.5 x 7.5 cm and larger.

Lawson, Clare, and Watt [10] produced isodose plots for a 5.6 cm diameter field and a 16.4 cm square beam for an elliptical tissue-equivalent phantom. Beam definition for these experiments appears to have been poor. It is difficult to detect the geometrical limit of the beam by examination of the isodose curves. Reasonable agreement was obtained [76] between the central-axis depth-dose values of Greene and Thomas and the data of Lawson et al.

Goodman and Koch [12] have obtained isodose distributions due to 14 MeV neutrons for a 5 x 5 cm and 15 x 15 cm field at a target-to-skin distance of 125 cm. A 35 x 35 x 35 cm cubical phantom filled with tissue-equivalent fluid was utilized. The 50 percent depth dose occurred at 10 cm for the small field and 12.6 cm for the large field. Calcium fluoride thermoluminescent dosimeters were used in conjunction with tissue-equivalent ionization chambers to obtain the absorbed dose due to gamma rays and neutrons.

Jones, Snyder, and Auxier [77] have used Monte Carlo techniques to calculate depth dose distributions in standard man tissue for a 14 MeV neutron beam of 5.0 cm diameter. The phantom assumed for this study was a right circular cylinder of diameter 30 cm and height 60 cm with the neutron beam incident perpendicular to the axis of the cylinder. It was found that the depth dose distribution for this beam was similar to the

broad beam case, but showed a more rapid decrease of dose with depth.

Wilkie [20] has also calculated dose distributions in tissue by use of the Monte Carlo method for 14 MeV neutrons. Only the dose due to recoil nuclei was considered in his study. Isodose data were presented for neutron beams of size 5.0 cm and 10.0 cm diameter at a source-to-skin distance of 125 cm. Perfect beam collimation was assumed. An elliptical phantom having dimensions of 30 cm major axis and 20 cm minor axis and height of 60 cm was assumed. Broad beam depth dose distributions were reported for homogeneous and heterogeneous phantoms.

Dose values at the air-tissue interface of a tissue-equivalent phantom were obtained by Goodman and Koch [12] by use of ionization chambers. Figure 7 is a plot of the ionization current measured at points near the surface of the phantom. As can be seen from equation 17, the degree of ionization produced by radiation is directly proportional to the dose. Therefore, a plot of the dose values near the surface of the phantom will have the same form as the curve shown in Figure 7. It has been concluded that the superficial layer of skin (to a depth of 0.5 mm) is the most important as far as the skin reaction to radiation is concerned [78]. Thus, a skin sparing effect was observed for 14 MeV neutrons in the sense that the first few mm of skin received a lower dose than deeper layers.

The position of maximum dose was found to be at 2.7 mm and the dose decreased by a few percent in going from a depth of 2.7 mm to the depth (2.0 cm) which was used in this study as the 100 percent point for dose distributions.

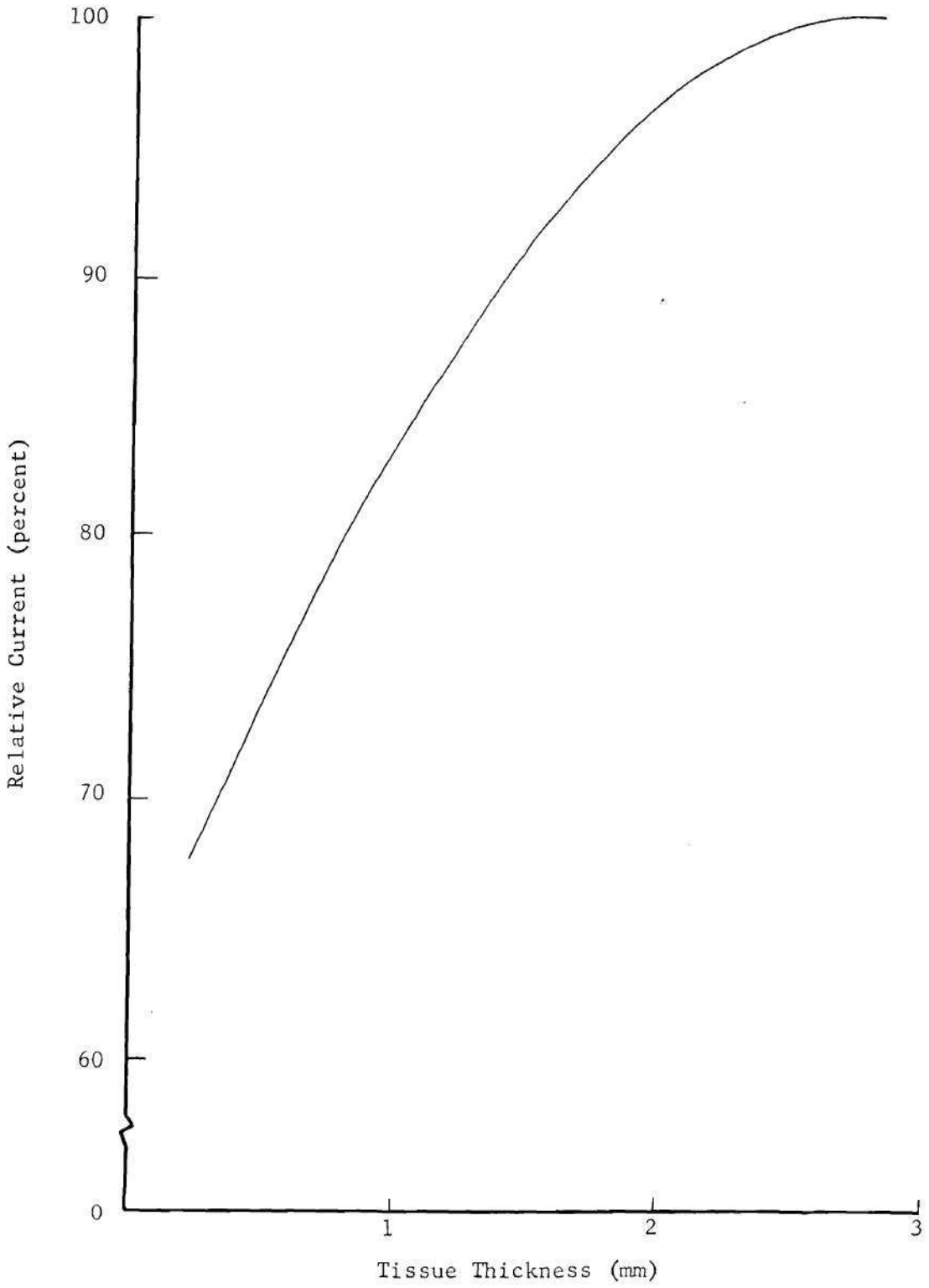

Figure 7. Build-up Curve for 14 MeV Neutrons (from reference 12)

Dose distributions for 14 MeV neutrons have been obtained experimentally by Poston [79] at the bone-tissue interface. Percent dose values were determined in tissue and bone for points near the interface to a distance of two centimeters from the interface.

Summary

Depth dose information has been determined for only two field sizes at the SSD which has been recommended for 14 MeV neutron therapy. These distributions were based on the total dose in a cubical phantom and the gamma dose component was not determined for points off the central axis. Dose distributions due to collimated beams of 14 MeV neutrons at a SSD of 125 cm have not been obtained by measurements in phantoms similar to a human in size and shape. No corrections for bone and lung tissue have been reported for collimated beams of 14 MeV neutrons.

One attempt [46] has been made to express the percent dose along the central axis as a function of the irradiation conditions such as field size and depth. The empirical equation was fitted to data obtained at a SSD smaller than that which may be used for fast neutron therapy. No attempt was made to establish a depth dose equation for points off the central axis. The use of a composite iron-hydrogenous material shield and collimator has been suggested for neutron radiotherapy, but no test of the degree of collimation produced by such a system has been made.

Based on this lack of information, needed for 14 MeV neutron therapy planning, the objectives listed at the end of Chapter I were adopted for this study.

CHAPTER IV

INSTRUMENTATION AND EQUIPMENT

From the information presented in Chapters II and III it was concluded that the objectives listed at the end of Chapter I could best be accomplished by utilization of the following instruments and equipment. An iron-paraffin shield and collimation system was employed in conjunction with a commercial neutron generator to produce beams of 14 MeV neutrons. Dose distributions were obtained for both homogeneous and heterogeneous phantoms by the use of a paired dosimeter system consisting of small ion chambers and LiF thermoluminescent dosimeters. The performance of this paired dosimeter system was evaluated by the utilization of a paired ionization chamber system and miniature tissue-equivalent ionization chambers. A description of the instruments and equipment used in this study occupies the remainder of this chapter.

Ionization Chambers

The dosimeters used to obtain the total dose due to neutrons and gamma rays for this depth dose study were tissue-equivalent ionization chambers. Small cylindrical chambers fabricated of conducting tissue-equivalent plastic were utilized for the majority of the depth dose measurements and miniature Sievert type chambers [80] were employed to investigate wall-gas corrections for the cylindrical chambers. The cylindrical chambers will be referred to as "Type A chamber" and the

miniature Sievert chamber will be designated "Type B" in the discussion that follows.

Figure 8 shows the general form of the Type A chamber and the holder used with this chamber. The sensitive volume of this chamber was 0.53 cm^3 and it was filled with air at atmospheric pressure for depth dose measurements. Since it was necessary to submerse the chambers in tissue-equivalent liquid for dose measurements, water-tight containers were constructed of tissue-equivalent plastic to protect the chambers. A combined chamber-wall plus holder-wall thickness of 3.0 mm resulted from this arrangement. Thus, an equilibrium thickness of tissue-equivalent plastic surrounded the gas volume of each chamber [6,78].

Total dose values were determined by measuring the voltage change produced by ionizing events in the sensitive volume of the chamber. Voltage measurements were obtained with a standard deviation of ± 1.0 percent by use of a Keithley 610 B electrometer. The voltage change (ΔV) produced by exposing the chamber to radiation was determined by use of equation 22.

$$\Delta V = ((V_1 + V_3)/2) - V_2 \ , \tag{22}$$

where

V_1 = voltage of fully charged chamber before exposure

V_2 = voltage of chamber after exposure to radiation

V_3 = voltage of fully charged chamber after exposure.

The voltage of the fully charged chamber was determined before and after the irradiation for the following reasons. First, these voltage

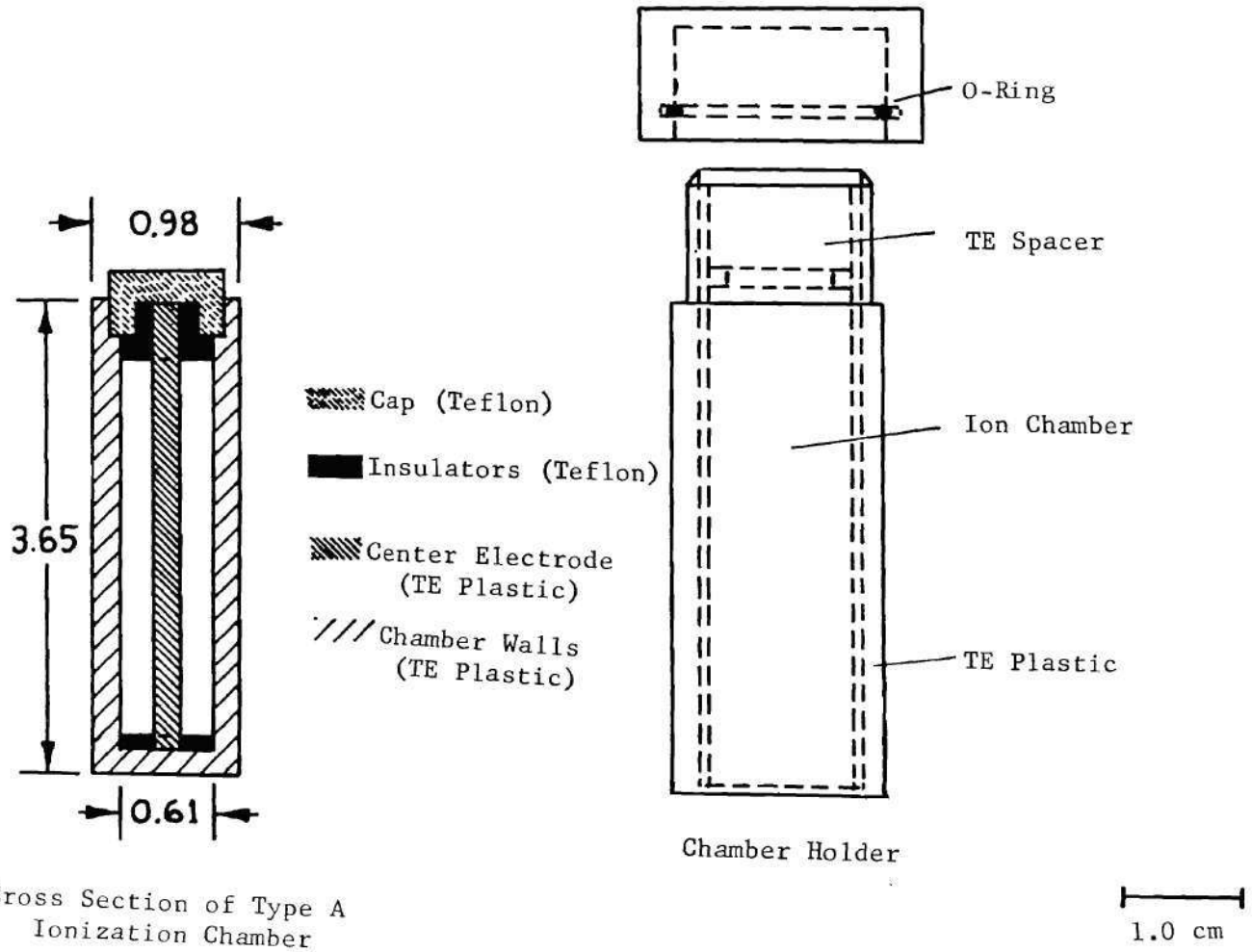

Cross Section of Type A
Ionization Chamber

Figure 8. Type A Chamber and Waterproof Holder

values can be used to establish the average voltage of the fully charged chamber. Second, any change in the capacitance of the chamber due to breakage or movement of the insulators can be detected by a change of V_1 or V_3. Third, gross leakage due to contamination of the insulators by moisture or dirt can readily be detected by failure of the chamber to recharge.

Calibration factors were determined for each chamber by exposing the chamber and a Victoreen "R chamber" to a 70 millicurie ^{60}Co source. The source was in the form of a small cylinder 0.63 cm in diameter and 1.89 cm long. A light weight Styrofoam frame was used to position the source and chambers at a height of one meter above the floor of the calibration room. All exposures were made in air with the chambers placed at a distance of 30.5 cm from the source. Figure 9 is a calibration curve obtained for a Type A chamber using the procedure outlined above. As can be seen from this curve, the voltage loss is directly proportional to the exposure in the range 0.0 to 1.0 R. All depth dose measurements were obtained on this portion of the curve. The Type A chambers all had calibration factors of about 0.550 R/volt.

The reproducibility of dose measurement was determined for each chamber by exposing the chamber repeatedly to a known dose of gamma radiation. Twenty separate irradiations produced the results shown in Table 5 for a Type A chamber. None of the chambers exhibited a standard deviation exceeding ± 4.0 percent for an exposure of 0.36 R and the majority of the chambers had a standard deviation of ± 3.0 percent or less. Similar results were obtained using 14 MeV neutrons and repeating the

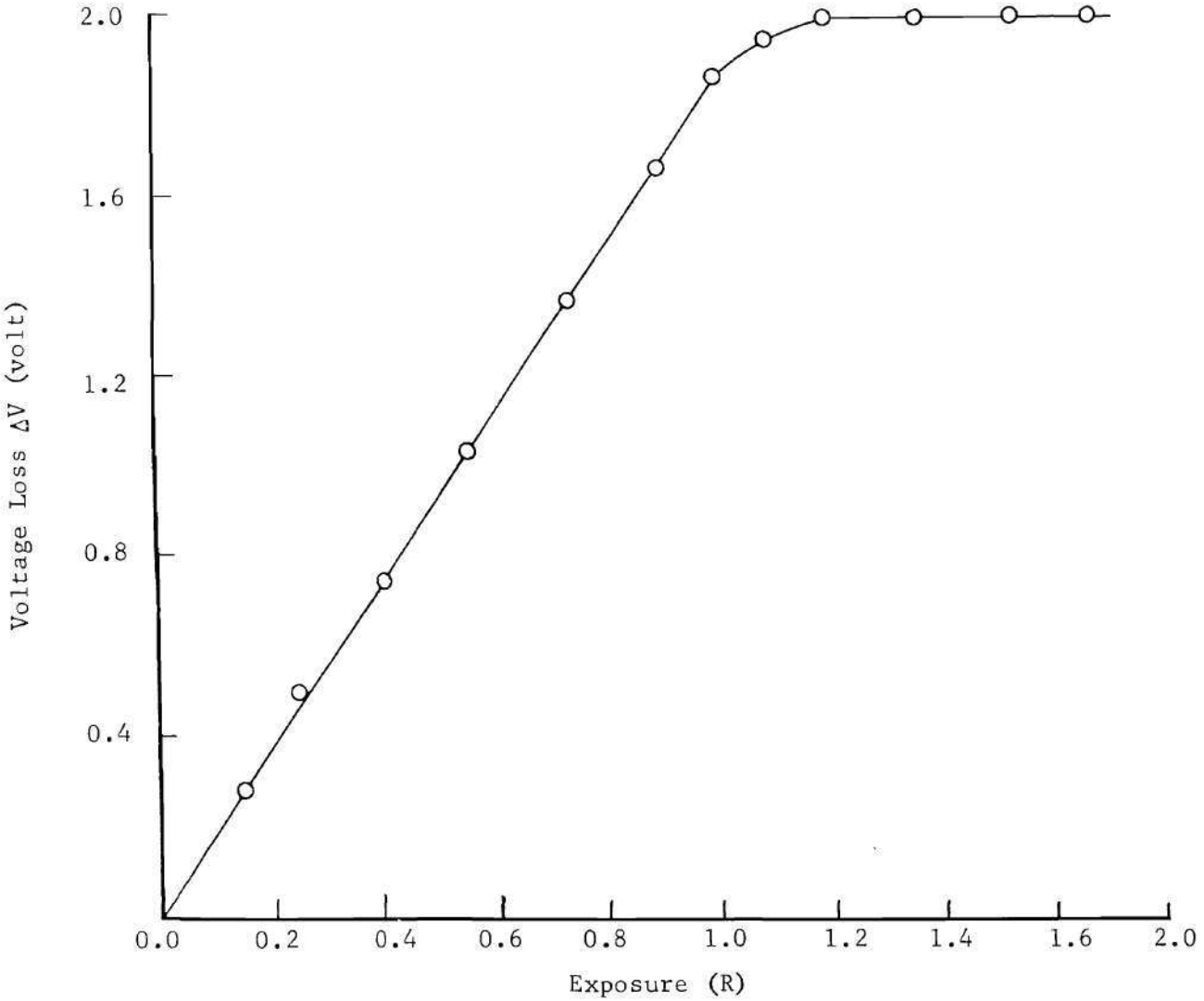

Figure 9. Response Curve for Type A Chamber

irradiation ten times. No dose rate effect was noted for the Type A chambers when the gamma exposure rate was varied by a factor of 20 nor were any dose rate effects observed for 14 MeV neutrons over the range of dose rates used.

Table 5. Reproducibility of Type A Chamber

Run	ΔV (volt)	$\Delta V - \overline{\Delta V}^*$ (volt)	$[\Delta V - \overline{\Delta V}]^2$ $(volt)^2$
1	0.66	-0.006	0.000036
2	0.67	0.003	0.000009
3	0.68	0.014	0.000196
4	0.69	0.024	0.000576
5	0.66	-0.006	0.000036
6	0.66	-0.006	0.000036
7	0.67	0.003	0.000009
8	0.65	-0.016	0.000256
9	0.65	-0.016	0.000256
10	0.66	-0.006	0.000036
11	0.68	0.014	0.000196
12	0.66	-0.006	0.000036
13	0.67	0.003	0.000009
14	0.65	-0.016	0.000256
15	0.65	-0.016	0.000256
16	0.66	-0.006	0.000036
17	0.68	0.014	0.000196
18	0.67	0.003	0.000009
19	0.66	-0.006	0.000036
20	0.66	-0.006	0.000036

*$\overline{\Delta V}$ = 0.666 volts

NOTE: Dose = 0.36 roentgens.

The standard deviation as derived from Table 5 is given by

$$\sigma = \sqrt{\frac{[\overline{\Delta V} - \Delta V]^2}{N - 1}} = \pm \frac{0.002452}{19} = \pm 0.011 \text{ volts} , \qquad (23)$$

where

ΔV = voltage loss of ionization chamber in each run and

$\overline{\Delta V}$ = average voltage loss of ionization chamber.

The directional dependence of Type A chambers was investigated by irradiation of several chambers enclosed in waterproof containers at various angles to the incident beam. Figure 10 is a polar diagram of the result of this test. Slightly less directional dependence was noted when several of the chambers were exposed in a water phantom. The in-phantom results are shown in Figure 10 by dotted lines. Similar results were obtained for the directional response to fast neutrons.

All Type A chambers exhibited small voltage losses due to insulator leakage. As many as 15 chambers were exposed to radiation at the same time when depth dose data were obtained. In general, a time of one hour was required between the exposure and the voltage measurement of the last chamber. No detectable leakage losses were observed for a one hour period. A 24 hour leakage loss of 3.0 percent was typical of all Type A chambers.

Miniature Sievert ionization chambers were used to investigate corrections for the wall-gas mismatch of the Type A chamber. Each of these Type B chambers was 5.0 mm in diameter and 20.0 mm in length and had a sensitive volume of 20 mm^3. The sensitive volume of the chamber was filled with tissue-equivalent gas and the chamber was placed in a gas-tight holder. A total thickness of 3.0 mm tissue-equivalent plastic surrounded the gas volume, resulting in charged particle equilibrium for 14 MeV neutrons.

Table 6 shows the results of irradiation of Type A and Type B chambers with 14 MeV neutrons. A Plexiglas cubical contained filled with

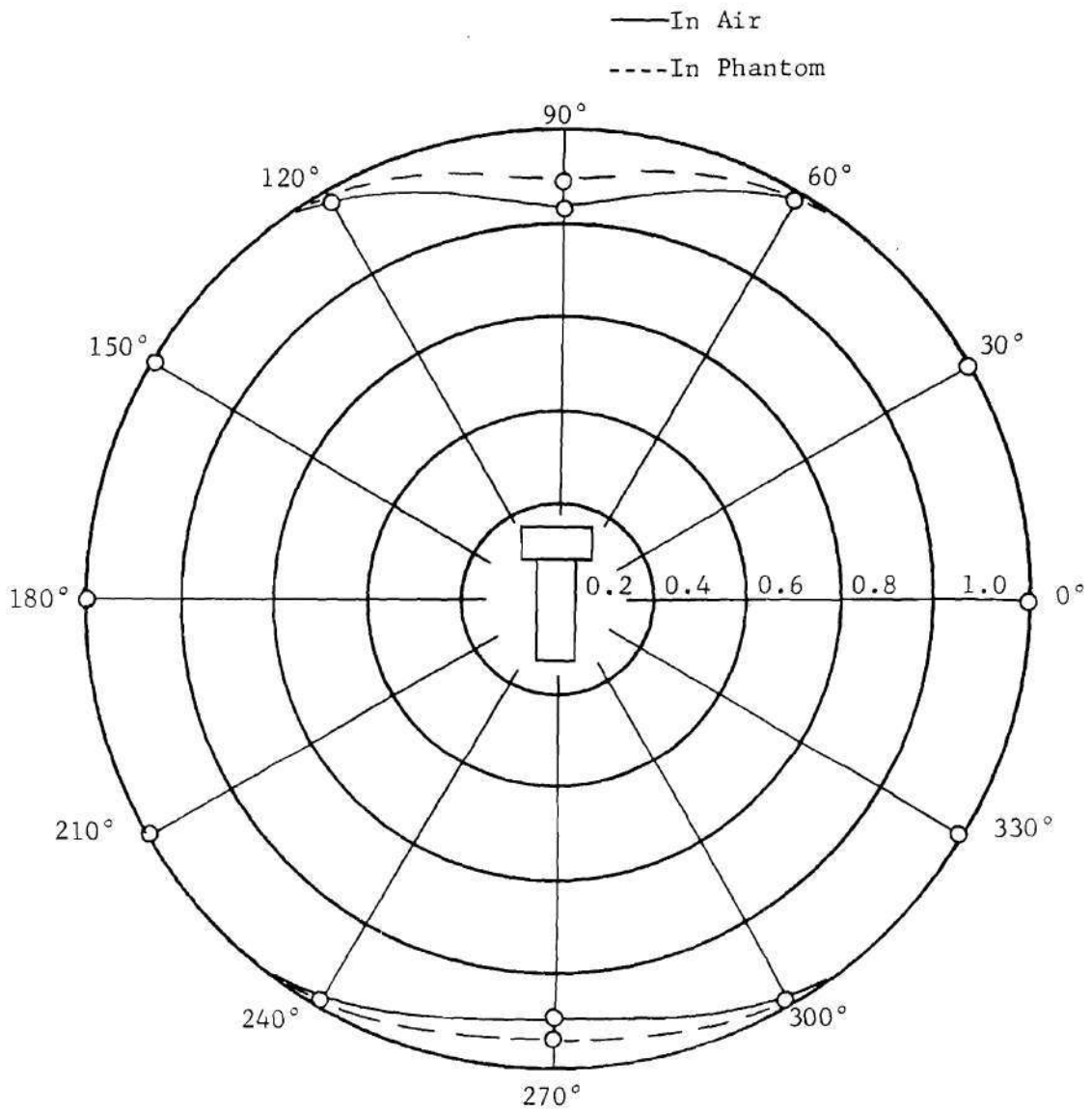

Figure 10. Directional Response of Type A Chamber in Waterproof Container

tissue-equivalent liquid was used at a source-to-skin distance of 20.0 cm for these measurements. The agreement between the air filled Type A chamber and the tissue-equivalent was that expected from the experimental errors involved. Therefore, wall-gas corrections were neglected subsequently for the Type A chambers.

Table 6. Response of Type A and B Chambers to 14 MeV Neutrons in Terms of ^{60}Co Gamma Ray Calibration

Depth (cm)	Dose Type A Chamber (equivalent ^{60}Co R)	Dose Type B Chamber (equivalent ^{60}Co R)
1.5	0.81	0.83
7.5	0.48	0.45
12.5	0.35	0.35
22.5	0.13	0.12

A second test was initiated to determine if a significant correction was needed for the air filling of the Type A chamber. A 50.0 cc spherical tissue-equivalent ionization chamber flushed with tissue-equivalent gas at a flow rate of six cubic feet per hour was used for this test. The spherical chamber and Type A chambers were exposed in air to a broad beam of 14 MeV neutrons. Once again no detectable difference in the response of the two chambers was noted.

Paired Chamber

A paired system of a tissue-equivalent and a graphite ionization chamber was employed for fast neutron calibration of the LiF dosimeters

and evaluation of the Type A chambers. With this system it is possible to obtain the gamma ray dose and the neutron dose in a mixed radiation field by use of the method outlined in Chapter III.

Each of these chambers had a 50.0 cc spherical sensitive volume and a wall thickness of 0.6 mm. Tissue-equivalent gas or CO_2 was used to flush the chambers during measurements at a flow rate of six cubic feet per hour. To obtain saturation conditions, a voltage of 1350 volts was applied to the center electrode of each chamber. Two Keithley 410 Micro-Microammeters were used to measure the current produced by ionizing events in each chamber.

Calibration factors were obtained for the chambers by exposing the chambers to ^{60}Co gamma radiation in a manner similar to that described for the Type A chambers. A response of 3.42×10^{-9} R/min/amp was found for the tissue-equivalent chamber and 2.46×10^{-9} R/min/amp for the graphite chamber. The performance of the paired chamber system is shown in Table 7 for two fast neutron sources. The same neutron generator was used to obtain the reported [81] and observed values shown in Table 7. A five-curie PuBe neutron source was employed to obtain the observed value and a one-curie PuBe source was utilized in obtaining the reported values [82] shown in Table 7. The reported neutron dose for the PuBe source was obtained by multiplication of the value given in reference 82 by a factor of five.

Table 7. Dose Measurements with Paired Chambers

Neutron Source	Observed		Reported		Ref.
	γ Dose* (%)	Neutron Dose (rad)	γ Dose* (%)	Neutron Dose (rad)	
14 MeV Neutron Generator	4	1.08	7	0.935	81
PuBe 5 Ci	8	0.0930	10	0.0887	82

*Percent of total dose

Thermoluminescent Dosimeters

Tissue-equivalent ionization chambers respond to both neutrons and gamma rays. It is desirable to resolve the total dose indicated by ionization chambers into gamma and neutron components. This allocation of the total dose can be facilitated by use of thermoluminescent dosimeters.

Extruded lithium fluoride dosimeters (TLD-700) purchased from the Harshaw Chemical Company were used with the Type A ionization chambers to determine the neutron and gamma ray dose in liquid tissue-equivalent phantoms. Lithium fluoride TLD-100 obtained from the same supplier was used to obtain the thermal neutron dose. Both types of dosimeters were in the form of 1/8" × 1/8" × 0.035" chips. The ^{60}Co gamma ray response of TLD-100 and TLD-700 was determined using the same procedure as that used for the calibration of the Type A chambers. These gamma ray calibration factors were measured with a standard deviation of ± 6 percent using a commercially available (Harshaw Model 2000) thermoluminescence analyzer. The magnitude of the radiation-induced response of the LiF dosimeters was

obtained by integrating the output from the photomultiplier tube of the analyzer. Glow curves of time versus luminescence were also recorded for each dose measurement. A 30 second heating cycle in which the dosimeter was heated to 240°C was utilized to stimulate the emission of light from the dosimeter.

Dry nitrogen flowed through the heating chamber at a rate of five cubic feet per hour to eliminate light produced by heating the dosimeters in the presence of oxygen. The dosimeters were annealed by heating to 400°C for 15 minutes followed by two hours at 100°C to suppress the low temperature traps.

Depth dose measurements and calibration determinations were made with the dosimeter enclosed in ^{6}LiF shields of wall thickness of 0.4 cm. These shields were used to eliminate the strong response of TLD-100 to slow neutrons and to reduce the slight response of TLD-700 to slow neutrons. An attenuation of the thermal neutron flux of about 1000 times was obtained with this thickness of ^{6}LiF.

Thermal neutron response curves were established for TLD-100 by using a calibrated five-curie PuBe neutron source surrounded by 10.2 cm of paraffin. This arrangement produced a thermal neutron flux of 2.20 $\times 10^{3}$ n/cm^{2}/sec at the surface of the moderator. Gold foils with and without cadmium shields were used to establish the thermal neutron flux. A cadmium ratio of 5.9 was established from the foil measurements. For calibration, the dosimeters were irradiated with and without ^{6}LiF shields for periods ranging from 2.0 hours to 16.5 hours.

In order to evaluate the absorbed dose due to neutrons and gamma

rays, values for k are needed for the LiF dosimeters. These values were established for a number of neutron energies. Table 8 presents the results obtained and the various neutron sources used for this measurement. The paired chamber system described in this chapter was used to establish the total dose, neutron dose, and gamma dose for all neutron sources but the cyclotron sources. Neutron and gamma absorbed dose values were supplied by the Radiological Physics Group at each location. The neutron and gamma doses were obtained by the use of paired ionization chambers. The gamma dose was also verified by LET spectrum measurements at the Texas A & M Cyclotron and by the use of film at the Hammersmith Cyclotron.

Each response value represents the average of at least six dosimeter readings. The dosimeters were exposed to a neutron dose of two to five tissue rads of fast neutrons. All dosimeters were shielded with one-eighth inch of ^{6}LiF in order to eliminate thermal neutrons.

Response values obtained for the LiF dosimeters used in this study were of the same magnitude as values reported in the literature. Figure 11 is a comparison of reported and observed values of the fast neutron response of TLD-100 and TLD-700. The experimental uncertainty indicated for the values obtained from this work was based on the precision of the TLD reader system and error due to statistical variations in the current values obtained from the paired chamber system. The lines shown in Figure 11 were based on a least-square analysis of the k values obtained in this study.

Table 8. Values of k for TLD-100 and TLD-700 Obtained in This Study

Neutron Source	Location	Neutron Energy (Mev)	Gamma Contamination (% total dose)	k TLD-700 (R/rad)	k TLD-100 (R/rad)
Neutron Generator $^{2}H(d,n)^{3}He$	ORNL, Oak Ridge, Tennessee	2.2 [29]	1	0.038	0.090
		2.9 [29]	1	0.050	0.088
^{252}Cf	Georgia Institute of Technology	2.3* [83]	25	0.033	0.075
PuBe (α,n)	Georgia Institute of Technology	4.1* [84]	8	0.060	0.11
Cyclotron $^{9}Be(d,n)^{10}B$	Texas A & M University	~7 * [85]	5	0.091	0.155
Cyclotron $^{9}Be(d,n)^{10}B$	Hammersmith Hospital, London	7.65* [86]	3-4	0.117	0.131
Neutron Generator $^{3}H(d,n)^{4}He$	ORNL, Oak Ridge, Tennessee	14.7 [29]	4	0.186	0.220

*Mean Neutron Energy

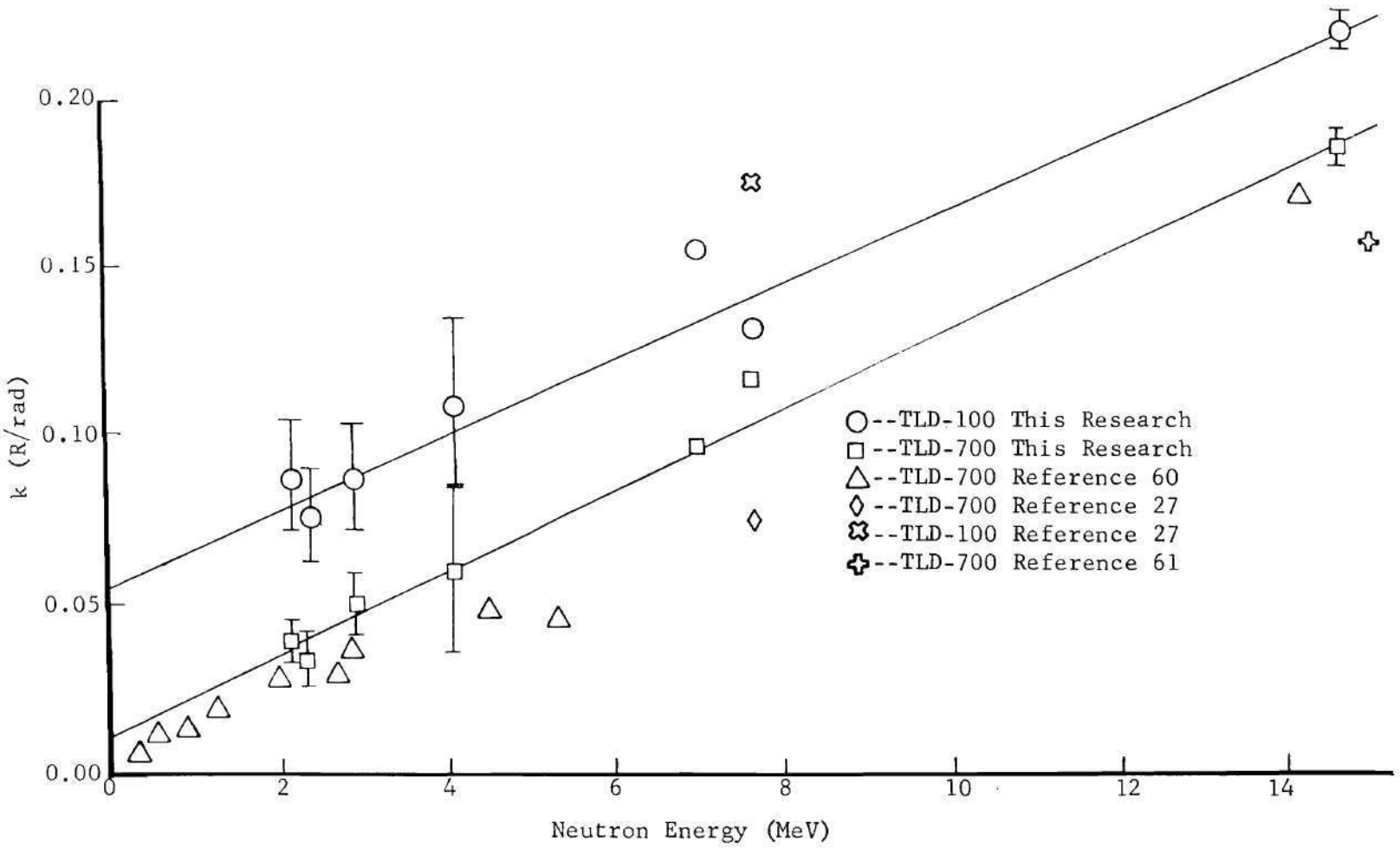

Figure 11. Comparison of k Values for TLD-100 and TLD-700

All values cited from the literature were converted from R per neutron/cm^2 to R/rad using values obtained from reference 64, except the values given by Wingate and co-workers [60] and Bewley and Parnell [27]. Based on values obtained from this study, the value of k for TLD-700 was expressed as a linear function of the neutron energy (E) as shown by equation 24.

$$k(E) = 0.012\ E + 0.010\ , \qquad (24)$$

where

E = neutron energy in MeV.

Neutron Source

Neutrons were produced by a Texas Nuclear Corporation Model 9999 generator located at the DOSAR facility at the Oak Ridge National Laboratory. Depth-dose measurements and a portion of the calibration of the LiF dosimeters were performed using this neutron source. Accelerating voltages up to 200 kilovolts and beam currents greater than 1.5 mA were employed to produce neutrons.

Neutrons of approximately 14.7 MeV energy were generated by the $^{3}H(d,n)^{4}He$ reaction by bombarding a thin tritium target with deuterons. A thickness of 0.470 cm of brass and 0.80 cm of water must be traversed by neutrons emerging from the target holder. The target contained 1.86 Ci/cm^2 of tritium deposited in a thin layer (5.0 mg/cm^2) of titanium evaporated onto a copper disc 0.025 cm thick. The active area of the target was about 2.54 cm in diameter. The deuteron beam was focused on a spot 1.0 cm in diameter near the center of the target. Target cooling

was achieved by a flow of water behind the copper backing.

Neutrons of energy from two to three MeV were also obtained from this generator employing the $^{2}H(d,n)^{3}H$ reaction. Accelerating voltage and beam currents similar to those indicated for the DT reaction were used. Targets were prepared for the $^{2}H(d,n)^{3}H$ reaction by bombardment of a thin aluminum foil with a beam of deuterons.

A modified Hansen-McKibben long counter [87] located 7.0 meters from the target of the neutron generator was used for normalization of the depth dose measurements. Neutrons were detected by a BF_3 proportional counter 1.5 cm in diameter and 37 cm long. The BF_3 tube was mounted axially in a cylindrical paraffin moderator 22.5 cm in diameter and 37 cm long. It has been found by Auxier and co-workers [88] that this modified long counter is relatively insensitive to changes in neutron energy. It was reported that the counts produced per neutron changed by a factor of about 18 percent over the neutron energy range 0.5 to 4.0 MeV. The standard deviation produced by random variation of the neutron monitor was estimated by exposing several Type A chambers in a fixed position to repeated neutron exposures and comparing the readings of the long counter with the chamber voltage changes. An increase of the standard deviation of ± 0.5 percent over that expected for the Type A chambers (± 3.0 percent) was attributed to variations in the long counter readings.

Collimator

A collimator and shield somewhat similar to the ones suggested for neutron therapy were used to produce neutron beams of various sizes. The

major difference between the proposed collimator and the one utilized in this study was the fact that, in this study due to space limitations near the neutron generator, shielding material could not be placed completely around the target. The shadow shield system shown in Figure 12 was employed to produce beams of field size from 7.5 x 7.5 to 18.4 x 18.4 cm at a source-to-skin distance of 125 cm. The shield was designed so that the target of the neutron generator could be placed 8.0 cm within the paraffin cube. This arrangement provided shielding for neutrons leaving the target at angles greater than 90° and tended to reduce room scatter. The shield was equipped with a removable collimator insert and the collimator opening had tapered sides which projected on the edges of the 2.54 cm diameter target. A cast iron cylinder of 19 cm diameter and 16.4 cm length was placed adjacent to the target holder. The iron cylinder was imbedded in a paraffin parallelepiped 75 cm long, 75 cm wide, and 70 cm high. The center line of the collimator was located 0.96 meter above the floor of the accelerator room.

Phantoms

Two phantoms were constructed for the depth-dose study. One of these was a Plexiglas cube 35 x 35 x 35 cm with 6.0 mm walls. A rigid plastic frame was used to position the ionization chambers and LiF dosimeters for dose measurements. This phantom was filled with tissue-equivalent liquid suggested by Goodman [25].

The other phantom was an elliptical cylinder with a major axis of 32 cm and a minor axis of 21 cm and a height of 35 cm. Polyethylene 4.0 mm thick was used to fabricate the walls of this phantom. Tissue-

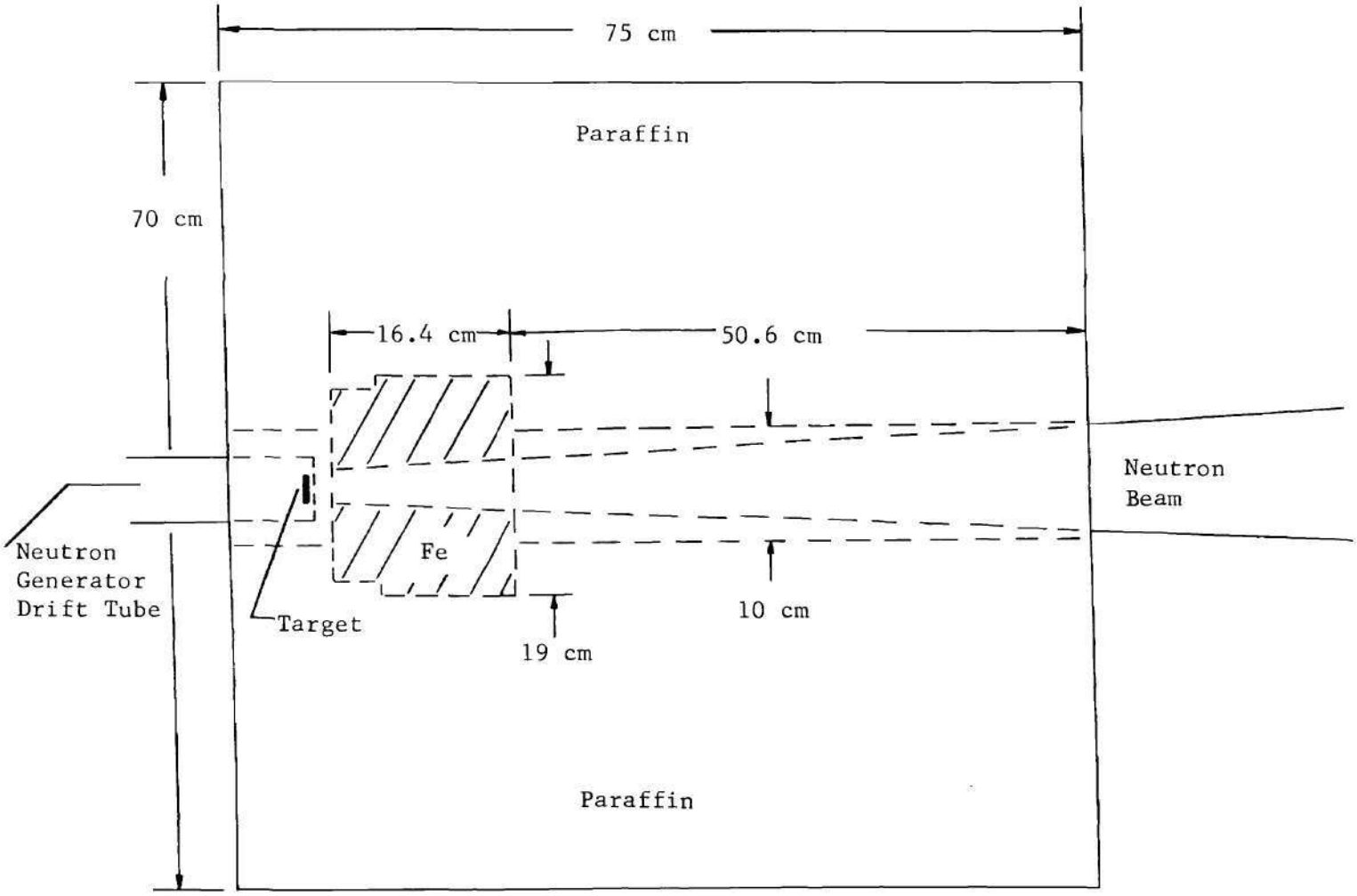

Figure 12. Shadow Shield and Collimator

equivalent liquid was added to the phantom for depth-dose measurements. No bowing or distortion of either phantom was observed when they were filled with liquid.

The effect of bone and lung on the dose distribution produced in soft tissue by neutrons was investigated by use of a cylinder of bone-equivalent plastic (B-100) and a model of the lung constructed of granulated tissue-equivalent plastic (A-150). The bone model was in the form of a cylinder 20 cm long and 4.0 cm in diameter. Figure 13 shows the outline of the lung phantom in a plane through the center of the beam. The dimensions used for the lung phantom were similar to those suggested by Fisher and Snyder [89]. Thin plastic sheets of thickness 0.01 mm were used to fabricate the sides of the lung shaped container. The top and bottom of the container were closed with 0.6 cm thick plastic sheets. It was found that a density of 0.38 g/cm^3 could be obtained by filling the container with granulated tissue-equivalent plastic.

A thin Plexiglas frame was used to position the dosimeters and to also anchor the lung models in the elliptical phantom. Thin plastic tubes allowed the introduction of ionization chambers at three points within one of the lung models.

Dosimeters could be placed at two centimeter intervals on a grid in a horizontal plane through the center of the neutron beam. The position of the dosimeter frame was controlled by a row of nylon pins in the bottom and along the sides of each phantom. With this system, the position of each dosimeter could be established to within 0.5 mm.

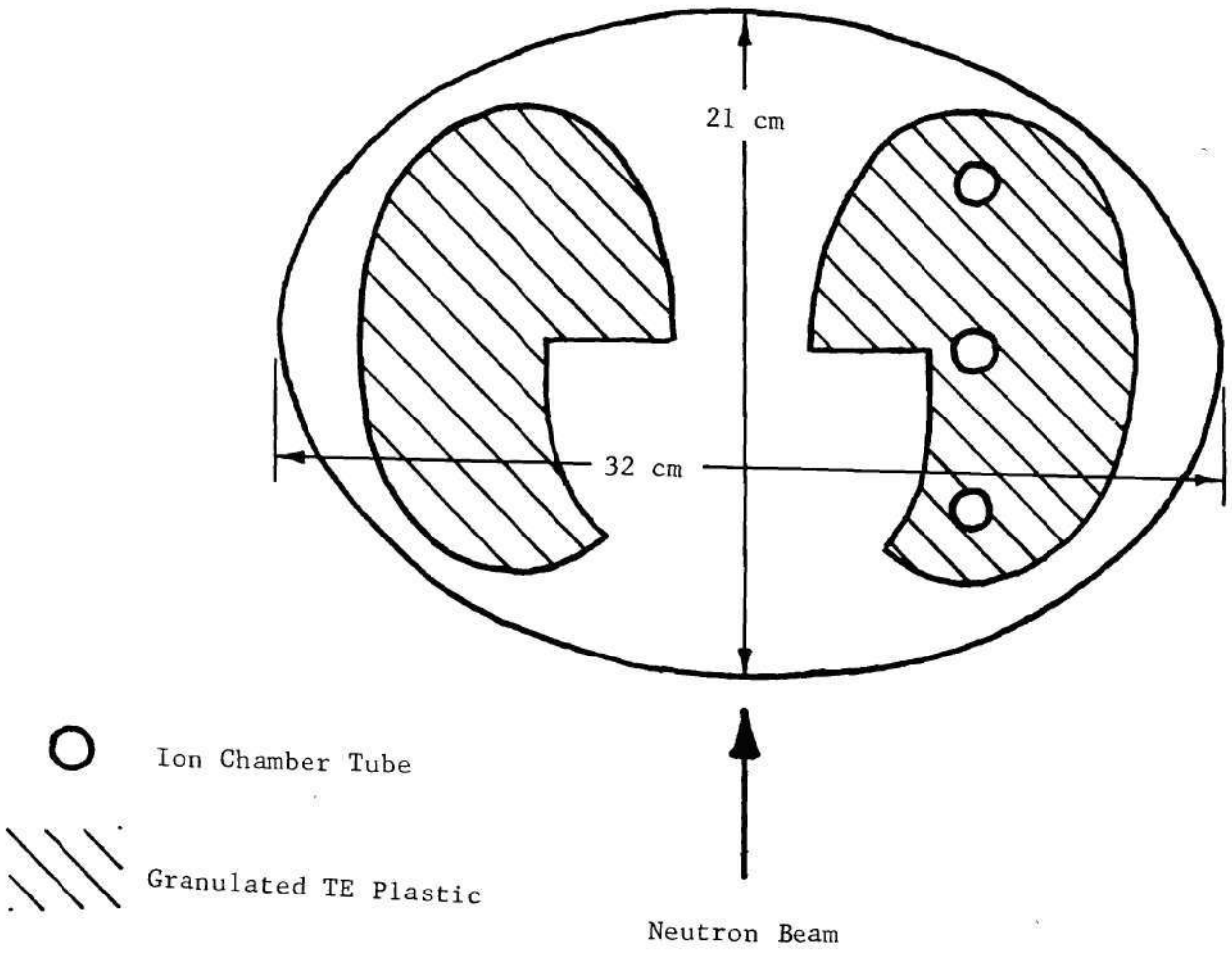

Figure 13. Lung Phantom

CHAPTER V

EXPERIMENTAL METHODS

The procedure used to obtain depth dose data and the method employed to reduce these data to percent dose values is outlined in this chapter.

Beam Alignment

Accurate alignment of the center of the neutron beam with the central axis of the phantom was achieved by measurement of the dose distributions with Type A chambers. Vertical and horizontal lines of detectors were placed on the front and rear of the phantom to determine the location of the beam center with respect to the center of the phantom. It was usually necessary to make three or more beam traverse measurements for positioning of the phantom.

Total Dose

Total dose due to neutrons and gamma radiation was measured by exposing a horizontal row of Type A chambers at a given depth in the phantom. As many as 15 Type A chambers spaced two centimeters apart were used for a single beam traverse. Traverse beam distributions were made at 2.0 cm depth intervals from 0.0 to 20.0 cm depth at a SSD of 125 cm.

An investigation was made of the effect of placing 15 ionization chambers adjacent to each other. When dose values were compared for a

line of 15 detectors and a single detector, no difference was noted for the dose values at a given point in the phantom, indicating negligible perturbation of the radiation field.

Central axis depth dose values were determined by use of Type A chambers that exhibited a standard deviation of 3.0 percent or less. The output of the neutron generator was determined for each exposure using the long counter described in Chapter IV. All dose values were corrected for temperature and pressure and normalized to a neutron output which would result in 1×10^5 long counter counts as shown by equation 25.

$$D_t = (\Delta V)(C)\left(\frac{T + 273}{273}\right)(760/P)(10^5/LC) \quad , \tag{25}$$

where

D_t = total dose expressed in terms of ^{60}Co calibration

ΔV = voltage loss caused by exposure

C = calibration factor for chamber in R/volt

T = temperature ($^{\circ}C$)

P = pressure (Torr)

LC = long counter counts for given irradiation.

The performance of each Type A chamber was evaluated at intervals of about two weeks by exposing the chambers to three dose levels with a ^{60}Co source. This procedure was adhered to for a period of about nine months during which depth dose data was taken. Leak tests were conducted on a daily basis when the chambers were being used for measurements. A

third factor, the voltage of a fully charged chamber, was also utilized to detect any change in the performance of the ionization chambers.

Gamma Ray and Neutron Dose

Lithium fluoride thermoluminescent dosimeters (TLD-700) and Type A ionization chambers were used as a paired dosimeter system to obtain the gamma ray and neutron absorbed dose. Horizontal traverse runs were made with the dosimeters exposed at several points in the beam and outside. All TLD dosimeters were shielded with 0.3 cm of ^{6}LiF to eliminate response due to thermal neutrons. The dose indicated by the TLD-700 dosimeters (D_{TLD}) was expressed in terms of the ^{60}Co calibration factor as shown below.

$$D_{TLD} = (C_{TLD})(NC)(10^{5}/LC) \quad , \tag{26}$$

where

NC = response of TLD-700 obtained with TLD analyzer (nanocoul)

C_{TLD} = ^{60}Co gamma ray calibration factor for TLD-700 (R/nanocoul)

LC = long counter counts.

The neutron and gamma ray dose was then determined using the paired dosimeter concept.

$$D_{t} = 0.97\ N + 1.03\ \gamma \quad , \tag{27}$$

$$D_{TLD} = \bar{k}N + 1.03\ \gamma \quad , \tag{28}$$

where

N = neutron absorbed dose (rads/10^5 long counter counts)

γ = gamma absorbed dose (rads/10^5 long counter counts)

$\bar{k}$ = average value of k (explained below).

The average value of k was determined for TLD-700 based on the neutron spectrum measurements of Lucas and Quam [19] for a 5 x 5 cm and a 15 x 15 cm beam of 14 MeV neutrons in tissue and in air. This correction factor was calculated as

$$\bar{k} = \int_{E_1}^{E_2} f(E)k(E)dE \ , \tag{29}$$

where

$f(E)$ = fraction of fast neutrons with energy between E and E + dE per unit energy interval

E_2 = maximum energy of neutron spectrum (15 MeV)

E_1 = minimum energy of neutron spectrum (2 MeV)

$k(E)$ = k value for TLD-700 at neutron energy E (given by equation 24).

It was found that at most the value of $\bar{k}$ was 2.2 percent less than k(15 MeV). This small difference between $\bar{k}$ and k(15 MeV) is a result of the low fraction of degraded neutrons and the decrease in neutron response of TLD-700 with neutron energy. A value of 0.18 R/rad was found for $\bar{k}$ using this method. Solving equation 27 and equation 28 for the neutron and gamma ray dose gives equation 30 and equation 31.

$$N = \frac{D_t - D_{TLD}}{0.79} \tag{30}$$

$$\gamma = \frac{0.18D_t - 0.97D_{TLD}}{1.03} \tag{31}$$

Thermal Neutron Dose

Due to the strong absorption of thermal neutrons in tissue, a large skin or near-skin dose may be deposited by a fast neutron beam that is contaminated with thermal neutrons. Therefore, thermal neutron fluence measurements were made for each neutron beam in air and at several points within the phantom. The fluence values were then converted to dose due to thermal neutrons as explained below.

Thermal neutrons were detected by use of TLD-100 with and without ^{6}LiF shields. The thermal neutron fluence Φ was calculated from the difference in the response of the shielded and unshielded dosimeters and normalized to 1×10^5 long counter counts.

$$\Phi = C_{th}(NC_u - NC_s)(LC/10^5) \ , \tag{32}$$

where

C_{th} = thermal neutron calibration factor (7.15×10^7 (n/cm^2)/ nanocoul)

NC_u = unshielded response of TLD-100 (nanocoul)

NC_s = shielded response of TLD-100 (nanocoul)

LC = long counter counts for given exposure.

Fluence-to-dose conversion factors obtained by Auxier and co-workers [90] for thermal neutrons were used to obtain the dose deposited by thermal neutrons in tissue D_{th}.

$$D_{th} = K\Phi \, , \tag{33}$$

where

K = fluence-to-dose conversion factor (rads/(n/cm^2))

D_{th} = dose deposited in tissue due to thermal neutrons (rads/10^5 long counter counts).

Corrections for Patient Heterogeneity

Several dose distributions were obtained for the purpose of establishing order of magnitude corrections for bone, lung and curvature of the patient. Dose distributions in soft tissue near bone were investigated by use of a four centimeter diameter cylinder of bone equivalent plastic (B-100). The cylinder was located on the central axis of the cubical phantom at a depth of five centimeters with the axis of the cylinder in a vertical position. Traverse dose measurements were made in a horizontal plane at 0, 2, 10, 14, and 20 cm depth for a 18.4 × 18.4 cm beam. The central axis depth dose was measured at two centimeters depth intervals for the elliptical phantom filled with tissue-equivalent fluid. The phantom was irradiated with an 18.4 × 18.4 cm neutron beam. The depth dose values were compared with the central axis data obtained for the cubical phantom in order to determine the change in the dose distribution produced by the shape of the patient.

The lung models were then added to the elliptical phantom and depth dose data were obtained with the 18.4 × 18.4 cm beam centered on one of the lungs.

Percent Dose, Gamma Dose Component, and Traverse Function

For treatment planning the dose values are usually expressed as percentage of the dose at some reference point. These values are used to obtain percent dose values for complex treatment plans such as those based on the multifield technique. The actual dose delivered to various points in the patient can then be established by use of this dose distribution and a single dose measurement made at the reference point. The percent total dose P_y^t at depth y along the central axis was calculated as

$$P_y^t = \frac{D_y^t}{D_2^t} \quad 100 \ , \tag{34}$$

where

D_y^t = dose due to total radiation (neutron + gamma) at depth y along central axis

D_2^t = total dose at depth of two centimeters along central axis.

A discussion of the error involved in the determination of P_y^t is given in Appendix A.

The gamma dose component which represents the portion of the total dose at a given point due to gamma radiation was obtained by use of equation 35.

$$P^{\gamma}_{x,y} = \frac{D^{\gamma}_{x,y}}{D^{t}_{x,y}} \times 100 \ , \tag{35}$$

where

$P^{\gamma}_{x,y}$ = percent of total dose at point (x,y) due to gamma radiation

$D^{\gamma}_{x,y}$ = dose due to gamma radiation at location (x,y)

$D^{t}_{x,y}$ = dose due to neutron plus gamma radiation at (x,y).

Equation 36 was utilized to calculate the traverse dose function F.

$$F = \frac{D^{t}_{x,y}}{D^{t}_{o,y}} \ , \tag{36}$$

where

x = distance off central axis

y = depth in phantom (constant for a traverse).

A summary of the sources of error in the gamma dose component and the traverse dose function is given in Appendix A.

CHAPTER VI

RESULTS

Collimation and Shielding

In order to determine the properties of each beam used in this study, beam profiles were obtained at the position of the surface of the phantom. Figure 14 shows a beam profile for the 13 x 13 cm field at a source-to-skin distance of 125 cm. The traverse run made without the phantom in place will be referred to as an air traverse and is shown in Figure 14 by the dotted curve. The traverse dose distributions made with and without the phantom in place are of similar shape. On the other hand, the magnitude of the dose values measured with the phantom in place was about 10 percent greater than that obtained in air. It was found from TLD and Type A ionization chamber measurements that the majority of the radiation "backscattered" by the phantom was gamma radiation. The gamma dose component at the central axis increased from 4.0 percent in air to approximately 10 percent with the phantom in place. This increased gamma dose was due to neutron capture and inelastic scattering reactions in the volume of the phantom irradiated.

Table 9 is a summary of the beam properties of each field utilized in this study. As can be seen from this table, a beam sharpness of two to three centimeters was found for each beam and accounted for up to 30 percent of the nominal beam size. Similar values were obtained from beam profiles reported by Bewley and co-worker [27] for fast neutrons with a

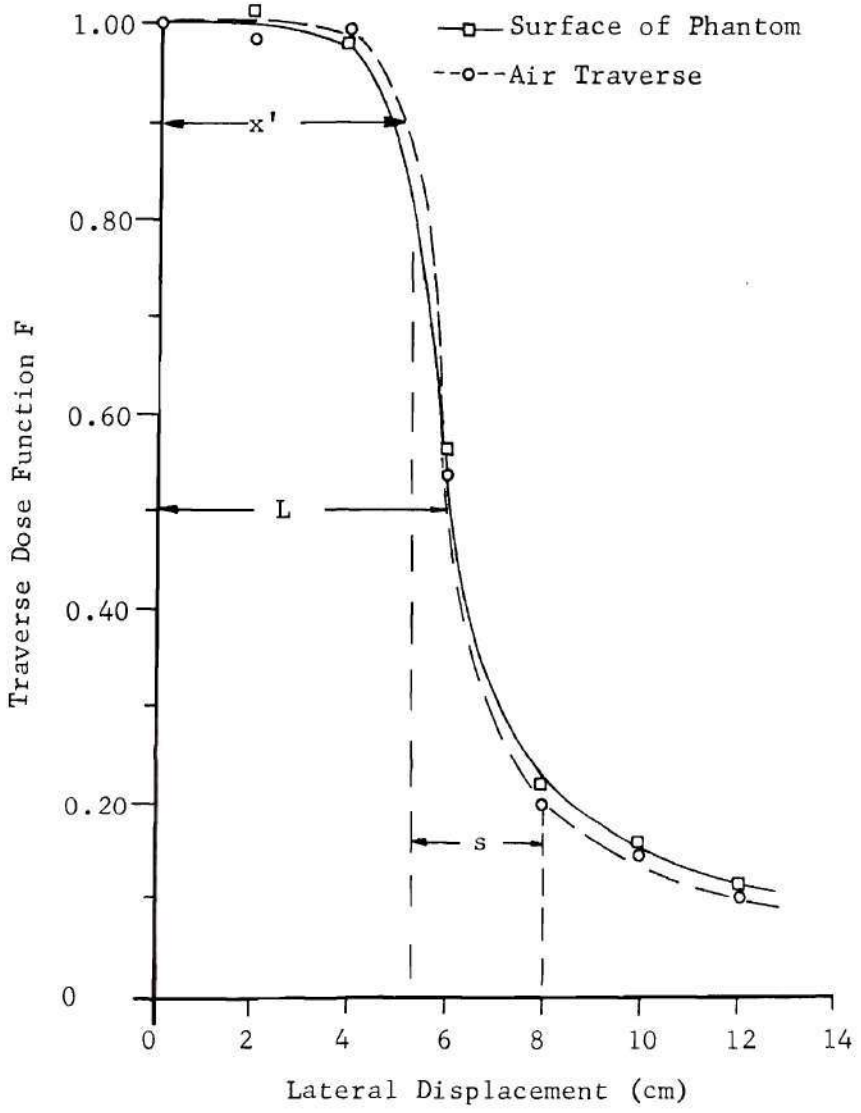

Figure 14. Traverse Dose Functions in Air and at the Surface of the Phantom for the 13 × 13 cm Field

mean energy of 7.65 MeV and by Greene and Thomas [34] for 14 MeV neutrons. These values of beam sharpness were found to be quite large when compared to those obtained from traverse dose functions for ^{60}Co radiotherapy beams. Values of the order of 0.5 cm or less were obtained for ^{60}Co beams and accounted for 10 percent of the beam size. The neutron beams were found to be flat over approximately 70 percent of the beam width in air and then decreased to 10 to 15 percent of the central axis value a few centimeters outside of the beam. The fraction of the total dose due to thermal neutron contamination of the beam is quite low, being of the order of about one percent.

Table 9. Properties of Neutron Beams in Air

Field Size (cm)	f Flatness	s Sharpness (cm)	p Geometrical Penumbra (cm)	p^{γ} Percent of Total Dose Due to γ	p^{th} Percent of Total Dose Due to Th. Neutrons
7.5 x 7.5	0.65	2.5	0.87	4.4	1.2
11.5 x 11.5	0.70	3.0	0.87	4.3	0.86
13 x 13	0.70	2.4	0.87	5.1	1.3
18.4 x 18.4	0.71	2.8	0.87	4.9	1.0

The presence of the collimator and shield resulted in little increase of the gamma ray dose component. A gamma contamination of approximately four percent of the total dose was obtained without the shield and values ranging from 4.4 to 5.1 percent were obtained with the shield in place.

A measurement of the radiation reaching the phantom area due to room scatter and penetration through the shield was obtained by blocking the collimator opening with paraffin and exposing the ionization chambers. Dose levels of approximately eight percent of the open beam dose were found. Therefore, most of the radiation reaching points outside of the neutron beam did so by direct penetration through the shield and by room scatter. Measurements of room scatter have been made for the neutron generator used in this study by Stone and Thorngate [91]. It was concluded that about five percent of the total dose was due to scatter of neutrons in the accelerator room. Based on these figures, the reduction in total dose produced by the shield was approximately 97 percent.

Central Axis Depth Dose

Central axis dose values were established by making measurements at two centimeter intervals along the center of the cubical phantom. Table 10 is a summary of the results of this series of measurements. Each total dose value represents the average of three measurements and, as shown in Appendix A, a standard deviation of ± 4.5 percent can be assigned to these values due to experimental error. The gamma dose components may have a larger error due to the inherent inaccuracy of the paired dosimeter method. These gamma dose components could be a factor of two larger than the values shown in Table 10.

All of the neutron beams investigated met the requirement for a 50 percent depth dose at a depth of 10 centimeters or greater. This condition was met in terms of both total dose and neutron dose. As can be seen from Table 10, the dose at a given depth increased with field size as a

Table 10. Central Axis Depth Dose Percentages for 14 MeV Neutrons at an SSD of 125 cm

Depth (cm) y	Field Size (cm × cm) / Percent Dose	7.5 × 7.5		11.4 × 11.4		13 × 13		18.4 × 18.4	
		$P^{t}_{o,y}$	$P^{Y}_{o,y}$	$P^{t}_{o,y}$	$P^{Y}_{o,y}$	$P^{t}_{o,y}$	$P^{Y}_{o,y}$	$P^{t}_{o,y}$	$P^{Y}_{o,y}$
2		100	8	100	9	100	8	100	12
4		88.0		90.7		90.3		91.2	
6		77.6	8	79.8	7	84.3	9	84.5	14
8		65.5		67.9		70.8		72.4	
10		55.4	9	59.5	9	61.5	10	66.7	13
12		45.7		49.1		52.0		56.0	
14		38.0	10	42.2	10	44.0	12	48.0	14
16		30.5		34.5		39.3		39.2	
18		26.0	12	30.0	11	31.5	14	35.2	16
20		22.1		26.3		27.0		29.4	

result of more scattered radiation reaching the central axis. Figure 15 shows the effect quite clearly and can be used to compare some of the Monte Carlo calculations with values obtained from this study. The broad beam dose distribution reported by Auxier and co-workers [90] for 14 MeV neutrons was converted to percent total dose normalized to 100 percent at two centimeters depth. The same procedure was applied to values given by Jones and co-workers [77] to obtain the depth dose curve for a five centimeter beam. It is worth noting that both of the curves produced by the Monte Carlo technique have an infinite value for the source-to-skin distance.

The broad beam depth dose values are considerably larger than the values found for the 18.4 x 18.4 cm field due to two factors. First, an infinite SSD would result in larger depth dose values because there is no reduction of dose due to inverse square attenuation. Secondly, the whole phantom was assumed to be irradiated for the Monte Carlo calculation and as a result more scattered radiation would reach the central axis causing the dose to be greater than that obtained for small beams.

Wilkie [20] has reported neutron dose components based on Monte Carlo calculations for 14 MeV neutrons at an SSD of 125 cm. Figure 16 can be used to compare Wilkie's neutron dose distributions with values obtained from this investigation. There is good agreement between the three dose distributions shown in Figure 16 in the sense that larger percent dose values were obtained at a given depth as the field area was increased from 25 cm^2 to 225 cm^2.

It was found that the portion of the total dose due to gamma rays

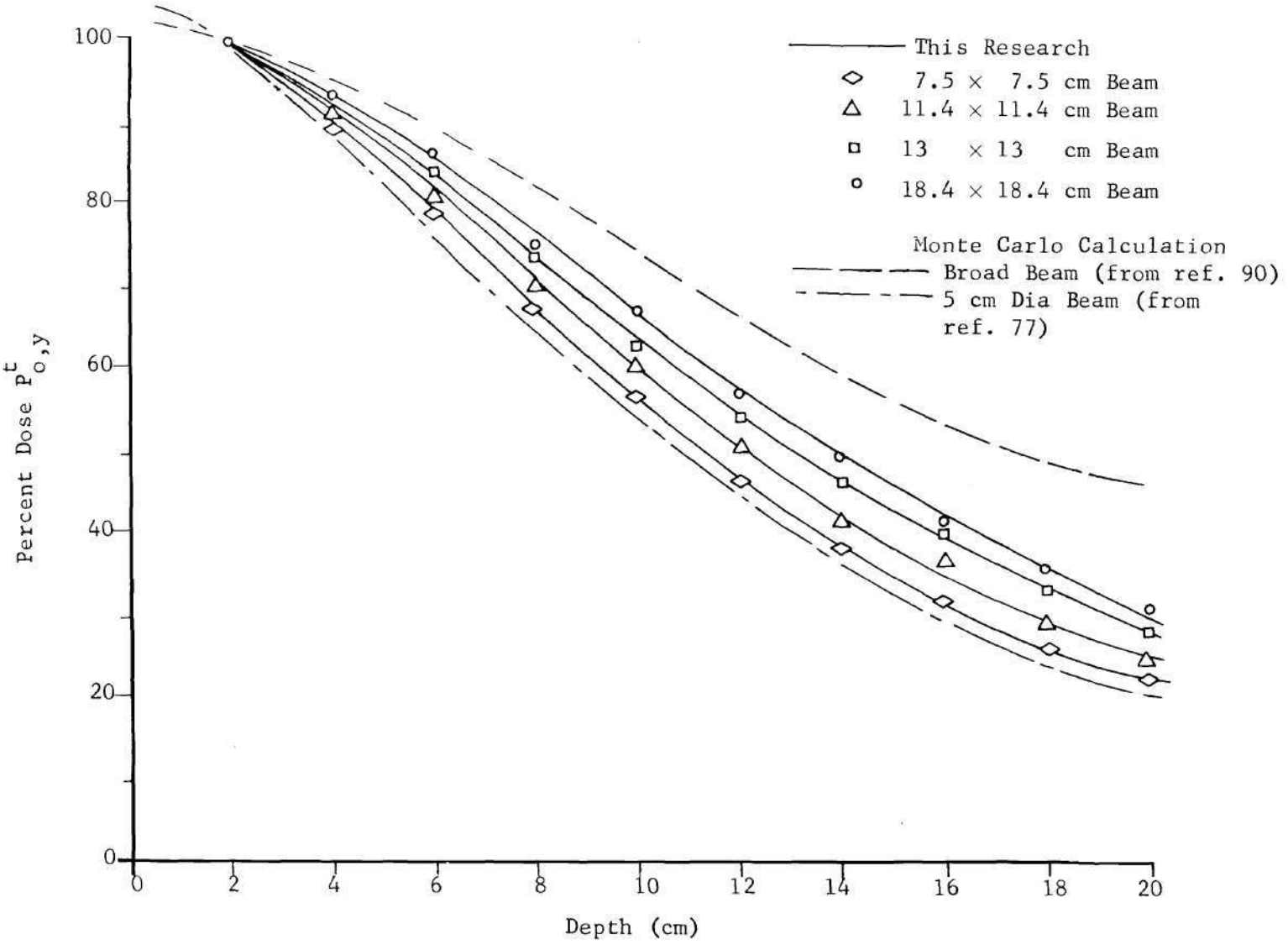

Figure 15. Central Axis Depth Dose Percentages for 14 MeV Neutrons

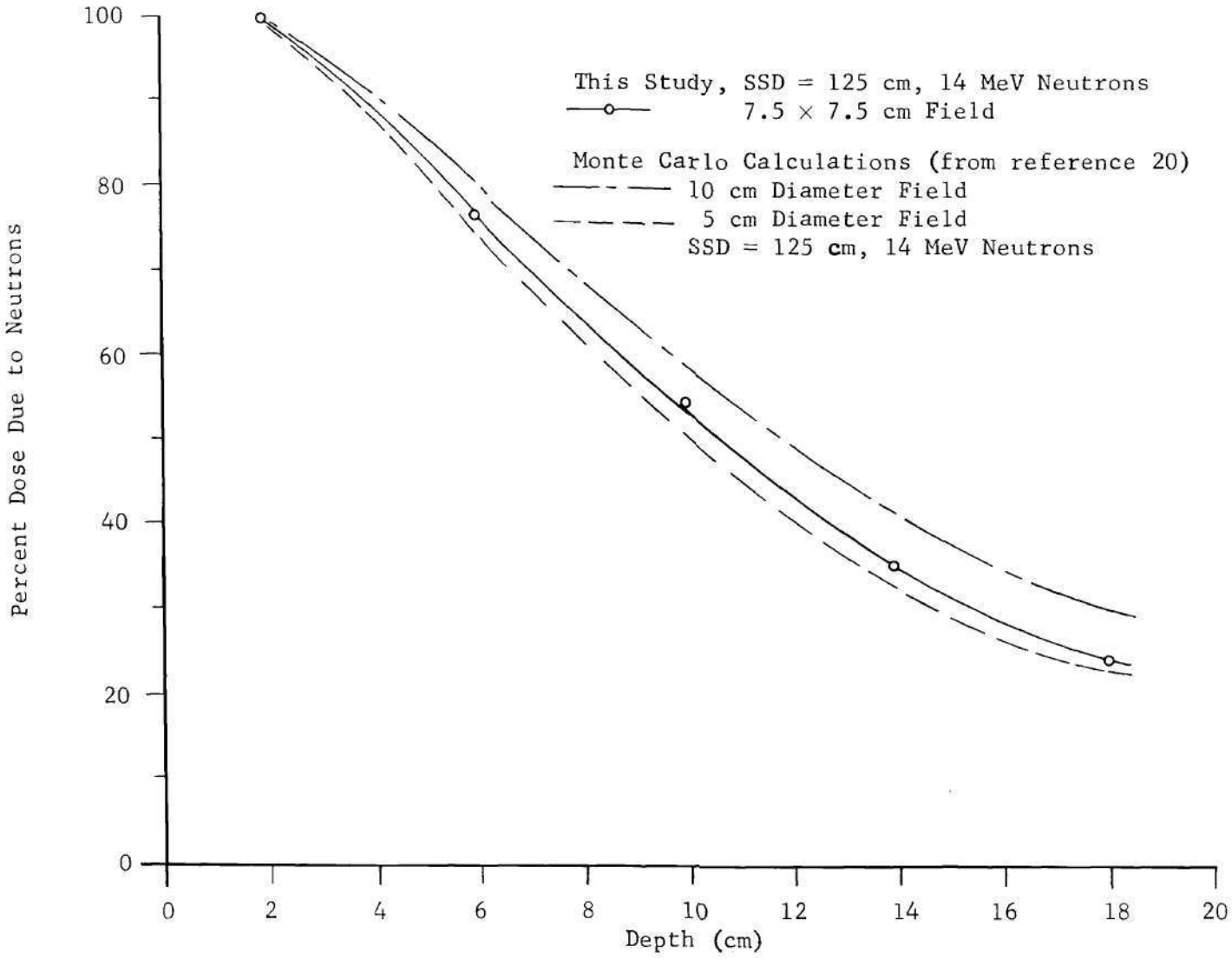

Figure 16. Central Axis Dose Due to Neutrons

was relatively small (< 16 percent). Expressing the dose components in terms of the RBE dose as outlined below results in gamma dose components that are considerably smaller than those shown in Table 10.

The neutron and gamma ray absorbed dose values determined in this study were converted to RBE dose by use of an RBE factor of three [4,13, 15] for 14 MeV neutrons and one for gamma rays. Figure 17 shows the RBE dose obtained for neutrons and gamma radiation for a 13 x 13 cm field. Similar curves were found for the other field sizes utilized in this study. As can be seen, only a small portion of the total RBE dose is due to gamma rays.

Traverse Dose Distribution

Traverse dose distributions based on total dose due to 14 MeV neutrons are shown in Figures 18 and 19. Measurements supplied by Goodman [92] for a 15 x 15 cm field are also shown in Figure 19 by dotted lines. A complete summary of all traverse measurements is given in Appendix B. A beam sharpness of 2.8 cm was obtained from Goodman's data at 10 centimeters depth and 5.0 cm for the 13 x 13 cm field utilized in this study. As expected, the beam width and beam sharpness increased with depth in the phantom for all fields. Figure 18 shows traverse dose distributions for several depths. As can be seen from these curves, there was also considerable increase in the dose outside of the beam as one goes from points near the surface to a depth of 20 cm.

Figure 20 can be used to compare the traverse functions for 14 MeV neutrons and ^{60}Co gamma radiation. The ^{60}Co curves are from reference 40

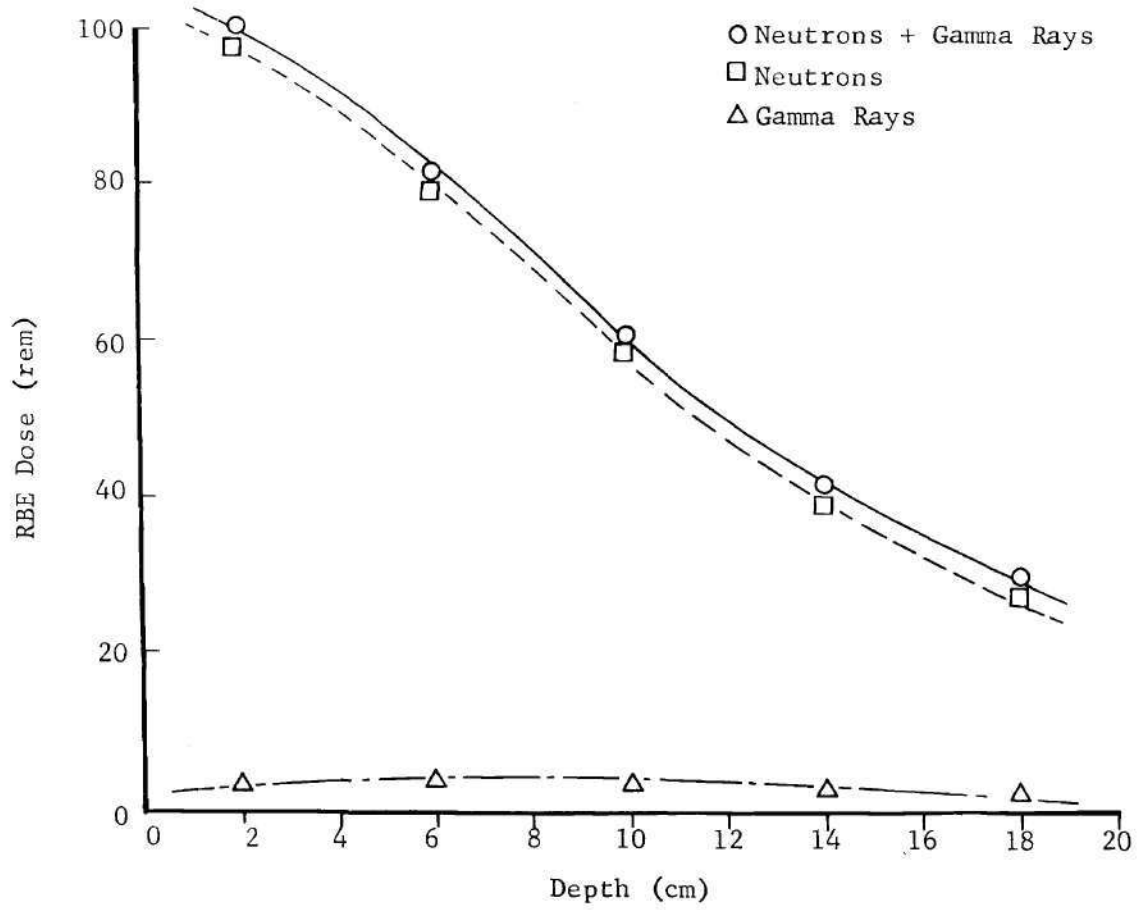

Figure 17. RBE Dose for Neutrons and Gamma Rays (14 MeV Neutrons, 125 cm SSD, and 13 x 13 cm Field)

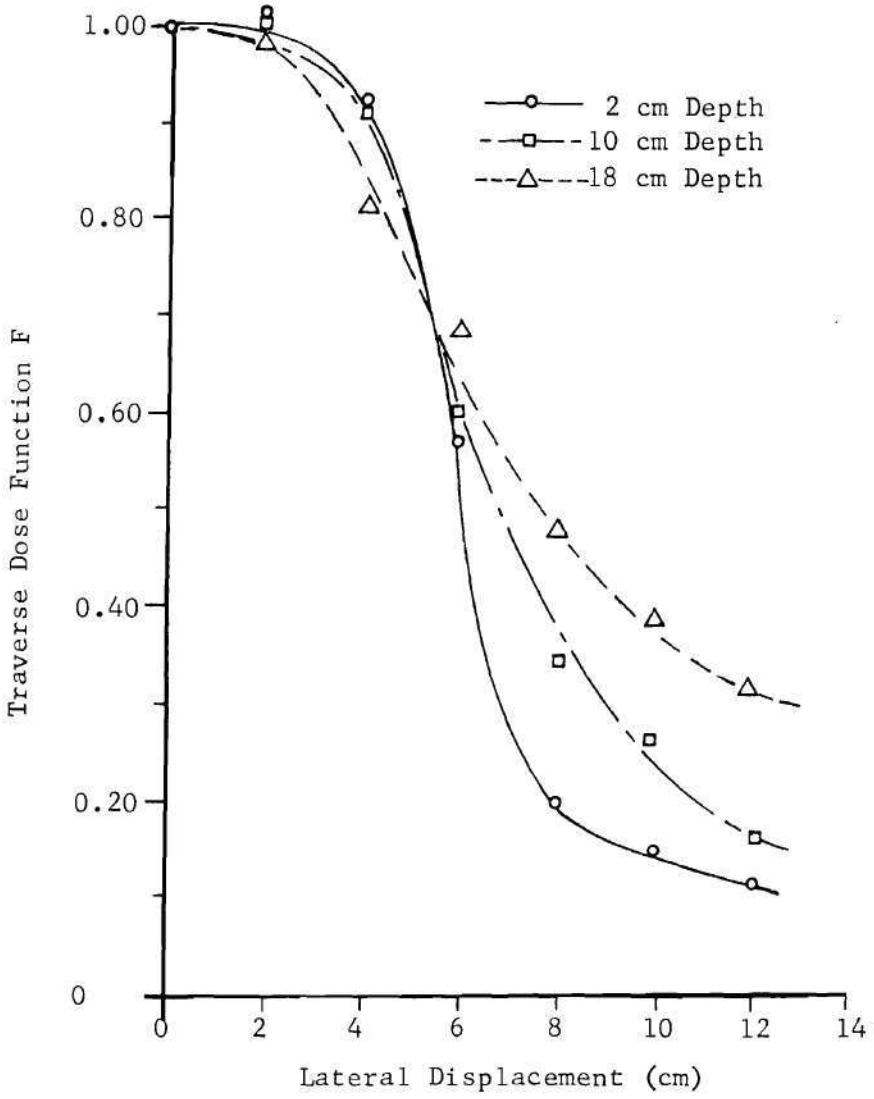

Figure 18. Traverse Dose Functions for 11.4 x 11.4 cm Field (14 MeV Neutrons, 125 cm SSD)

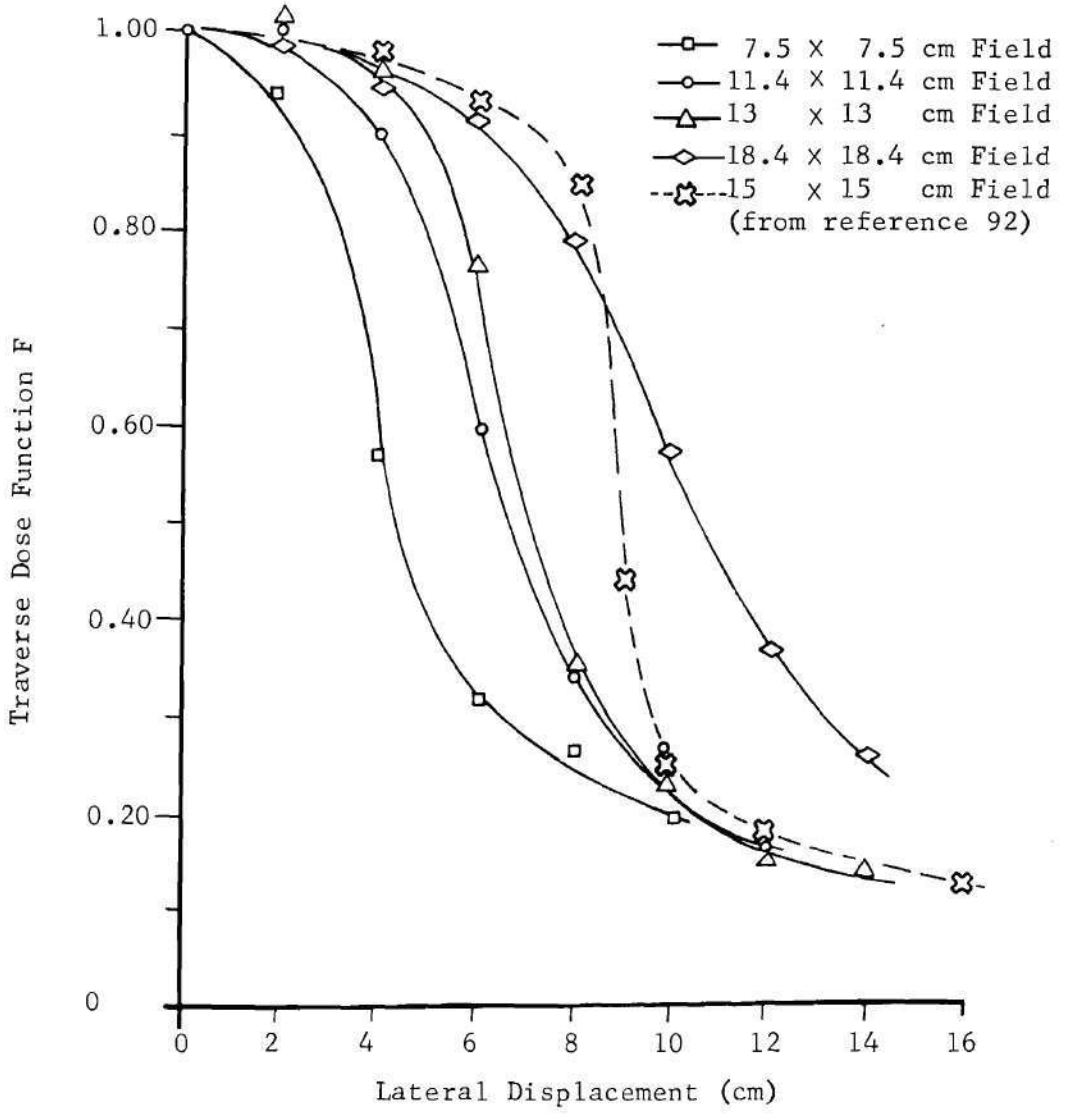

Figure 19. Traverse Dose Functions for Various Field Sizes at 10 cm Depth

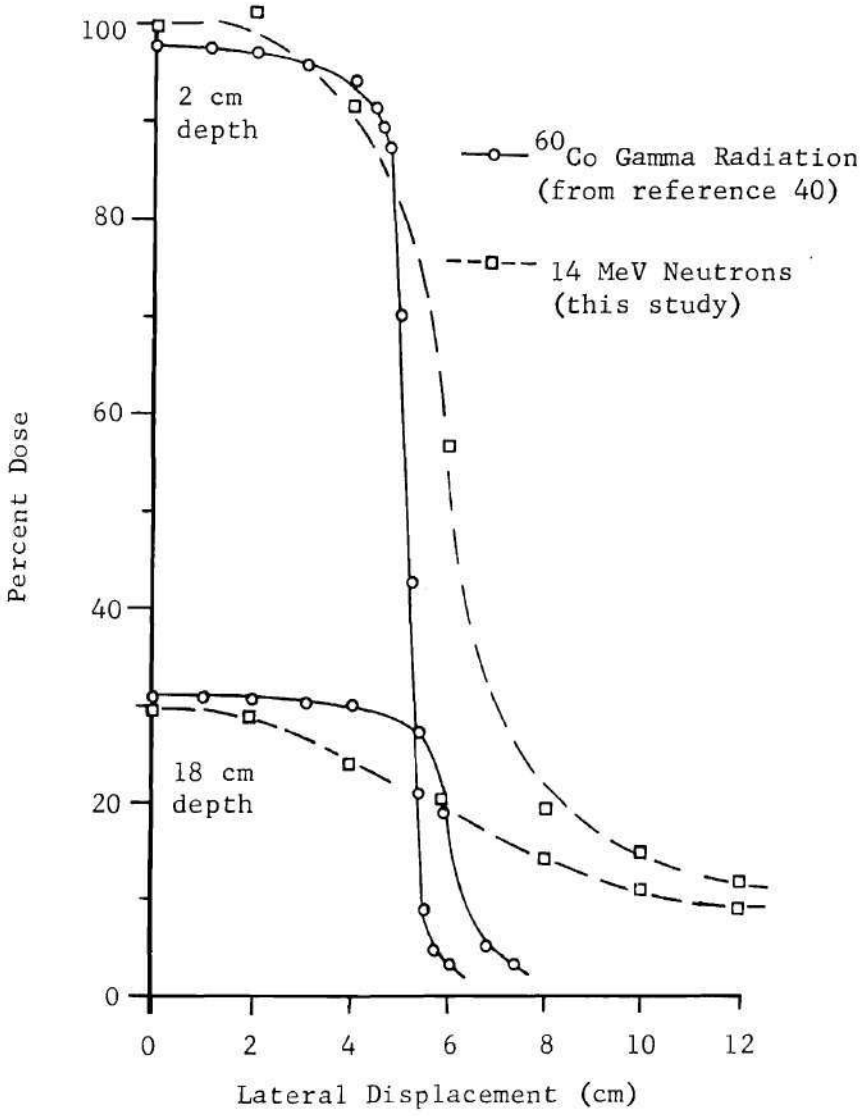

Figure 20. Traverse Dose Functions for ^{60}Co Gamma Radiation and 14 MeV Neutrons

and are for a typical 10 × 10 cm field at 80 cm source-to-skin distance. All curves are normalized to 100 percent near the surface of the phantom. Smaller penumbra width and lower dose level outside the beam are exhibited by the curves for gamma radiation at all depths.

A traverse function for an X ray beam [34] of common clinical use is shown in Figure 21 for a depth of 10 cm in tissue. The neutron beam for the same depth exhibits superior beam flatness, penumbra width, and dose level outside of the beam.

The gamma dose component was determined at several depths for points off the central axis. It was found that the gamma dose component ($P^{\gamma}_{x,y}$) was approximately constant in the beam area and increased as one moves away from the edge of the beam. Values of the gamma dose component are given in Appendix B. It should be pointed out that the neutron response values used for the LiF dosimeters outside the beam were too large since they were based on the average response in the beam. The average energy of the neutron field outside of the beam would be approximately seven MeV or less as a result of energy degradation by scattering. Therefore, the values shown in Appendix B for the gamma component outside of the neutron beam have been over-corrected for neutron response.

The only available data with which a comparison of the gamma dose component can be made are those reported by Jones et al. [77] for a five centimeter diameter beam. The gamma component for this beam was based on the dose due to (n,γ) reactions. Gamma rays generated by inelastic scattering were not taken into consideration by Jones. In general, Jones' data showed an increase in the gamma contamination from about one to two

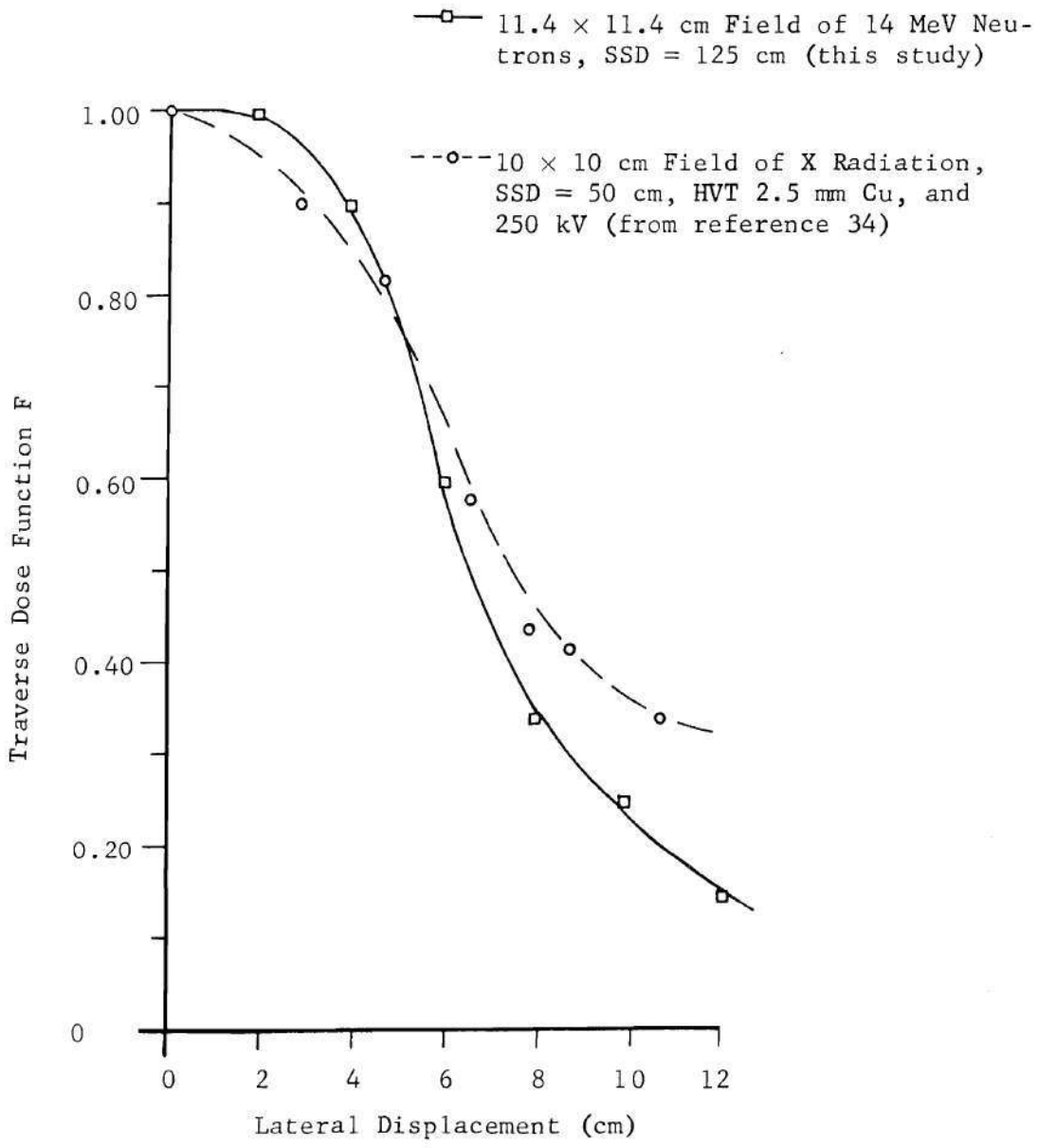

Figure 21. Traverse Dose Function for X Ray and 14 MeV Neutrons at a Depth of 10 cm

percent in the beam to approximately 25 percent for points 11.5 cm off the central axis. The fraction of the total dose due to gamma rays obtained from Jones' data showed little change with the depth at which the traverse distribution was determined.

The gamma dose component obtained for the 7.5 × 7.5 cm field showed an increase from approximately 9.0 percent to 30 percent in going from points on the central axis to points well outside of the beam. This larger gamma dose component could be due to a number of factors such as the presence of gamma radiation generated in the accelerator room by capture and inelastic scattering of neutrons. The wide penumbra of the 7.5 × 7.5 cm field would contribute to an increased gamma dose. On the other hand, perfect collimation was assumed for the five centimeter beam. Uncertainty in the calibration of the TLD dosimeters for neutrons and gamma rays could easily lead to a large positive systematic error. It has been indicated by Ritts [93] that inclusion of gamma rays produced by inelastic scatter can result in an increase of the gamma dose in tissue by a factor of two for the broad beam case.

Depth dose data may be presented in a diagrammatic form by isodose plots. These diagrams are contours of equal dose values for points in a plane through the center of the beam. The dose distributions given in Appendix B were used to establish the isodose charts shown in Figures 22, 23, 24, and 25. A falling-off of dose near the edge of the beam can be seen as can scattered radiation beyond the geometrical confines of the beam. The relatively high dose level of 10 to 20 percent of the central axis value at two centimeters depth for points approximately five centi-

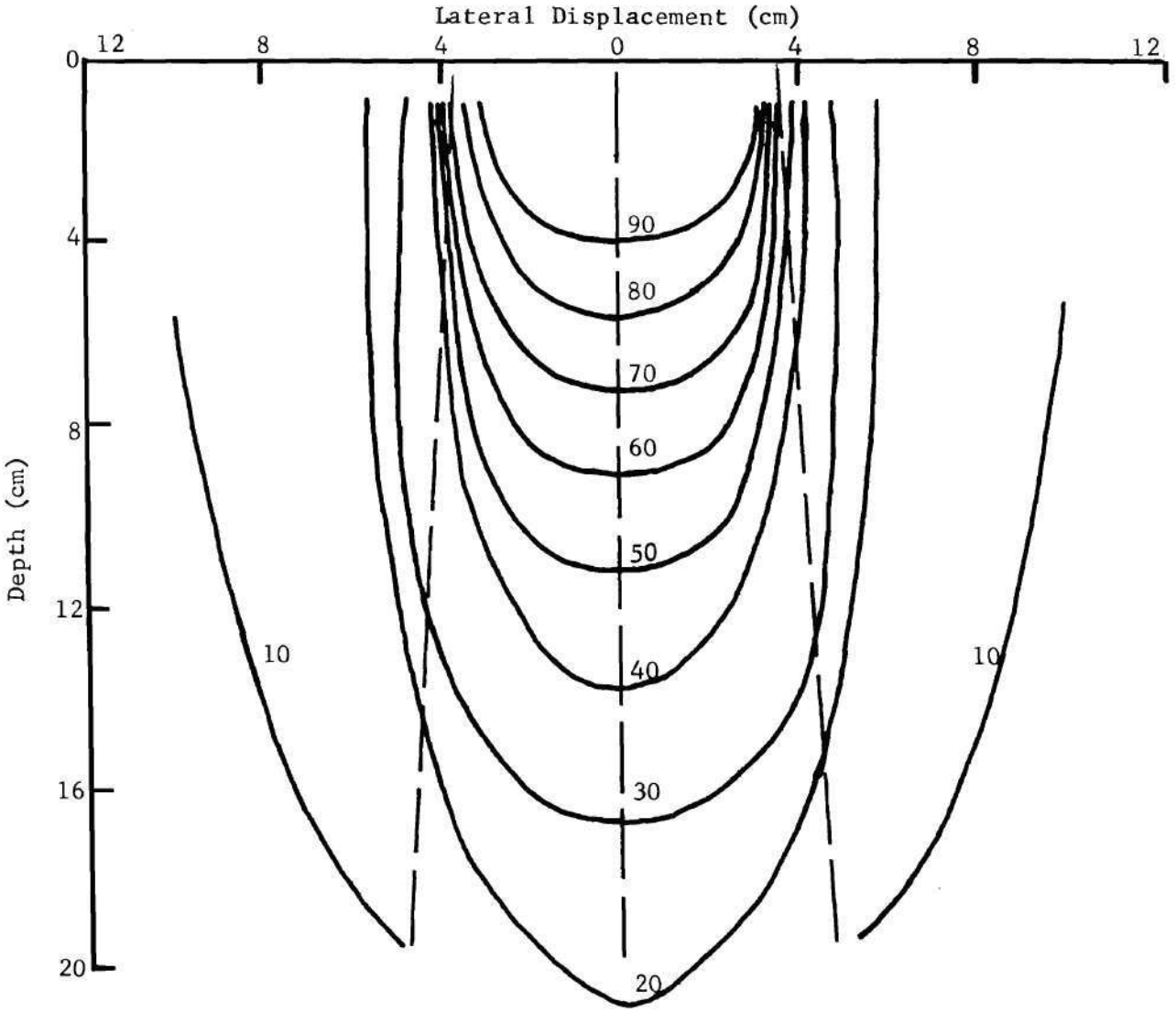

Figure 22. Isodose Contours Derived from Experimental Data in Table 14 for 7.5 × 7.5 cm Field of 14 MeV Neutrons at an SSD of 125 cm

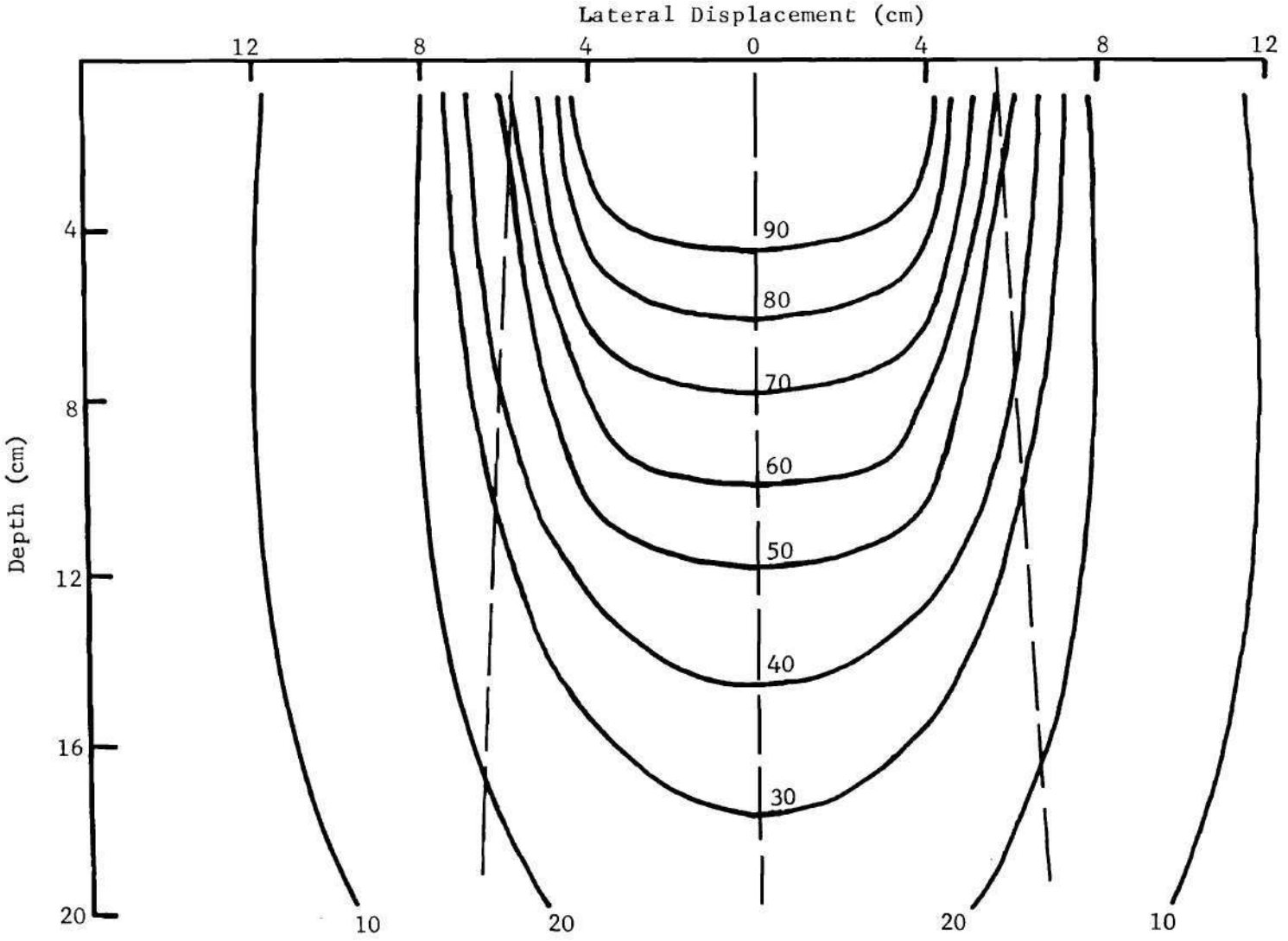

Figure 23. Isodose Contours Derived from Experimental Data in Table 15 for 11.4 × 11.4 cm Field of 14 MeV Neutrons at an SSD of 125 cm

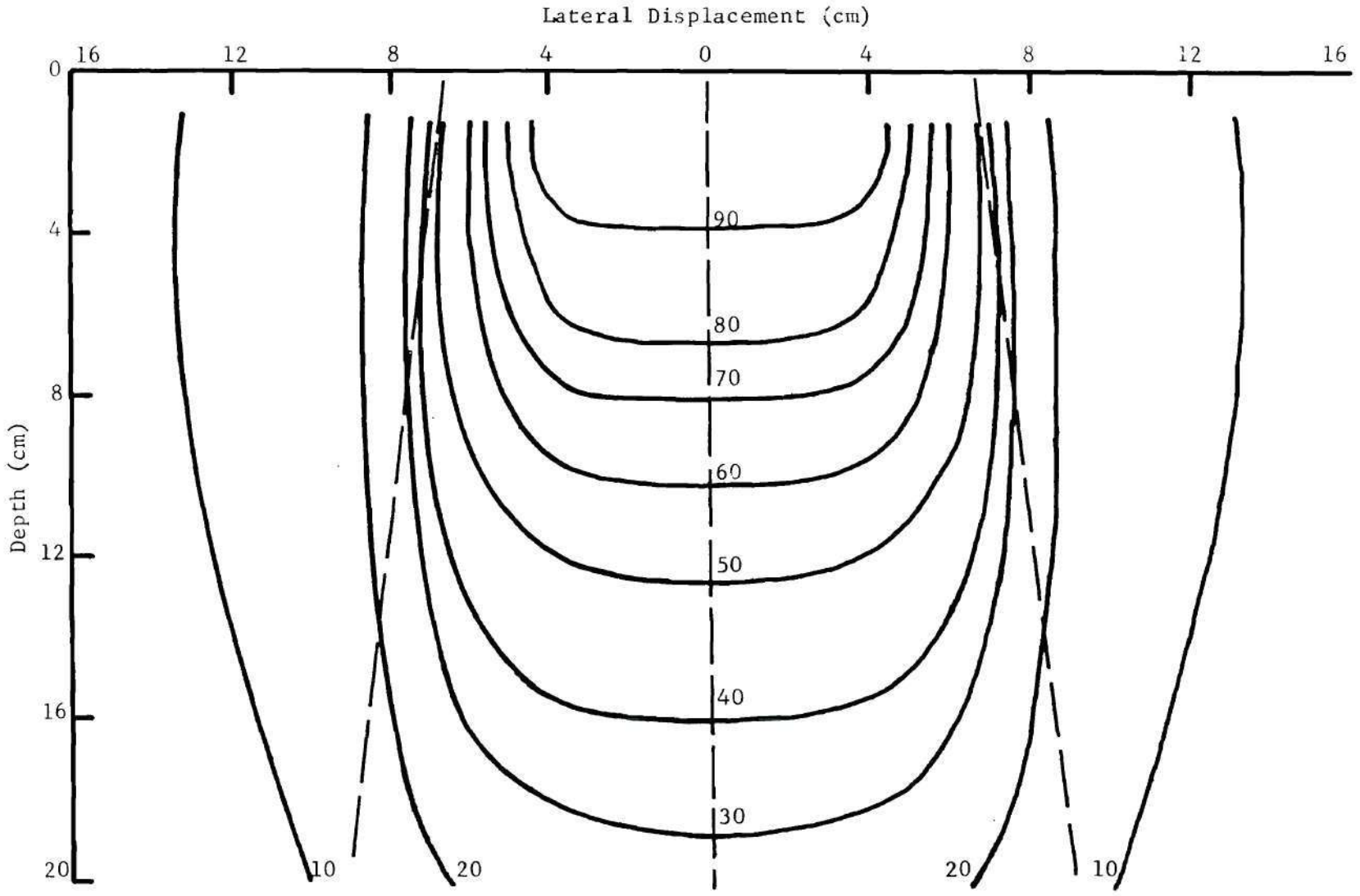

Figure 24. Isodose Contours Derived from Experimental Data in Table 16 for 13 x 13 cm Field of 14 MeV Neutrons at an SSD of 125 cm

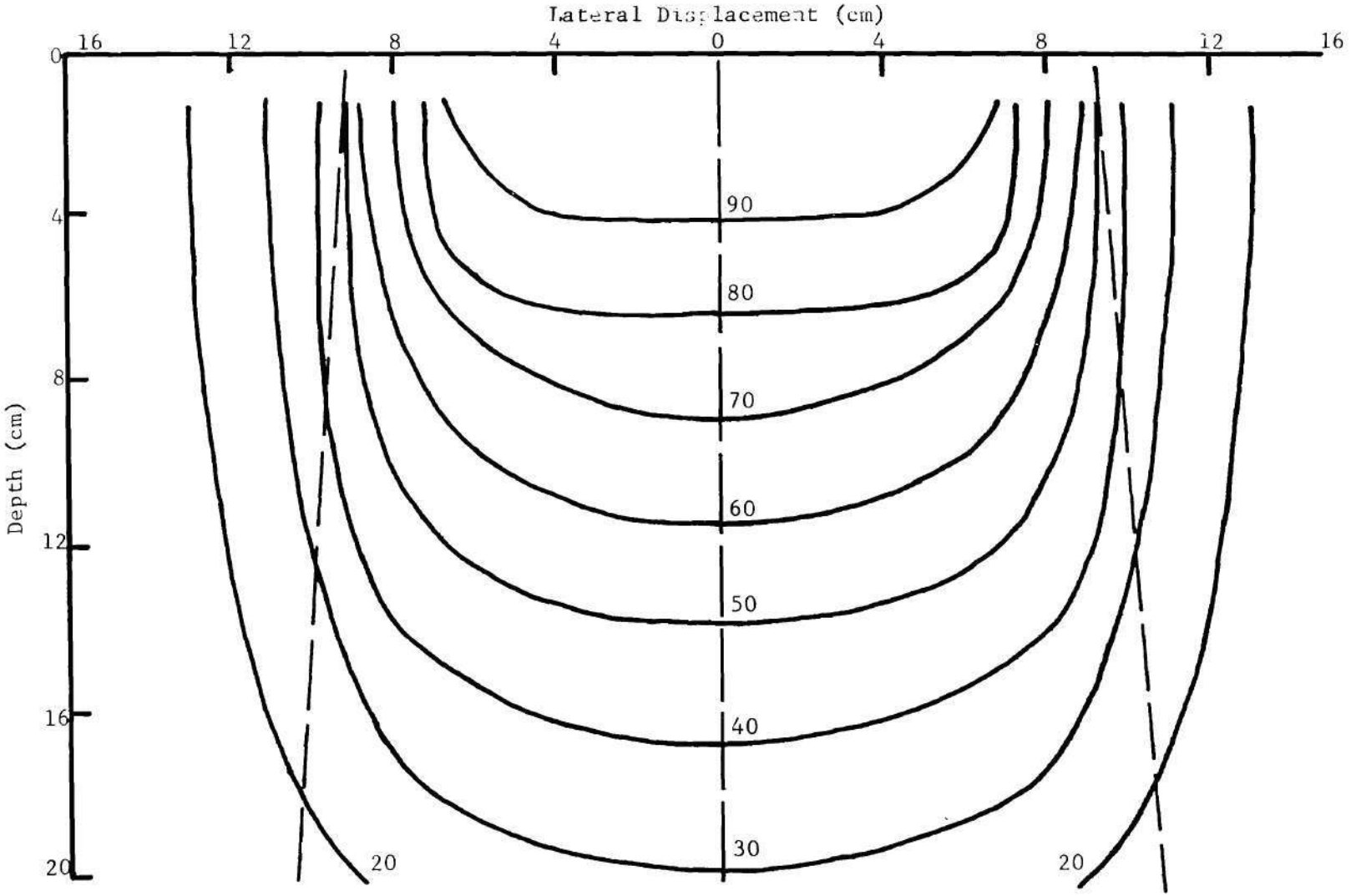

Figure 25. Isodose Contours Derived from Experimental Data in Table 17 for 18.4 x 18.4 cm Field of 14 MeV Neutrons at an SSD of 125 cm

meters outside of the beam is similar to that of therapeutic X ray beams. It would be desirable to reduce this dose component in order to minimize the dose to healthy tissue outside of the neutron beam. This could be accomplished by the use of improved shielding and collimation systems.

The dose distributions of the four fields investigated are similar to those calculated by Wilkie [20] using the Monte Carlo method and assuming perfect beam collimation. Depth dose percentages of 1.0 to 5.0 percent were obtained by Wilkie for points approximately five centimeters outside of the neutron beams. The depth dose percentages obtained at the same points in this investigation are of the order of 10 to 20 percent as a result of the lower degree of beam sharpness and the presence of radiation due to room scatter and penetration of neutrons through the shield. The general features of the isodose curves reported by Goodman and Koch [12] are also similar to the features of the dose distributions obtained in this study.

Treatment Planning Equation

For purposes of fast neutron treatment planning, using digital computers, it is desirable to obtain simple, accurate, and continuous relationships between the percent absorbed dose at a given depth and the conditions of irradiation. The central axis data obtained for the four fields investigated in this study were successfully fitted to equation 14 which was developed by Sterling and co-workers [38] for ^{60}Co radiation. For 14 MeV neutrons the central axis depth dose ($P^{t}_{o,y}$) takes the form

$$P^{t}_{o,y} = \text{antilog}[-0.0425\ y + (0.0198\ y - 0.0395)\ \log(A/E) + 2.106]\ , \quad (37)$$

where

y = depth (cm)

A = area field (cm^2)

E = perimeter of field (cm).

Agreement between experimental and calculated values was found to be within 2.0 percent for the majority of the points along the central axis. In several cases the difference between the calculated and experimental value was as much as 7.5 percent.

A relationship similar to equation 37 was found for the central axis depth dose data reported by Greene and Thomas [34] for 14 MeV neutrons and also for values given by Bewley and Parnell [27] for cyclotron-produced neutrons with a mean energy of 7.65 MeV.

Based on this study and the central axis data reported by the groups mentioned above, the range of application of equation 37 for fast neutrons is for field sizes from 5 × 5 cm to 20 × 20 cm and for depths greater than two centimeters but less than 22 cm. It is therefore possible to express the central axis depth dose due to fast neutrons for all field sizes and depths of clinical interest in the form of a simple equation containing only four fitting constants.

Traverse dose functions (F) were also established for the beams utilized in this work using methods developed by Sterling and co-workers [38] for ^{60}Co radiation. It was found that each traverse distribution in Appendix B was sigmoid in nature and could be fitted to equation 15 but differed from the gamma radiation case in that two sigmoid curves were

required for each traverse distribution. Values of the fitting constants (σ,μ) found for each traverse dose distribution are given in Appendix C. Agreement between observed and calculated dose values using these constants in equation 15 was 5.5 percent or less. Some general trends in changes of the fitting constants can be seen from Appendix C. For example, the values for σ and μ for points in the beam area tend to increase with depth in the phantom and outside of the beam the fitting constant μ increases with depth. No general trend was seen for changes in σ with depth for points outside the geometrical area of the beam.

Combining equations 37 and 15, one obtains a general expression for the percent dose in a plane through the center of a cubical block of tissue irradiated with 14 MeV neutrons from a source located 125 cm from the surface of the block.

$$P^{t}_{x,y} = \{\text{antilog}[-0.0425\ y + (0.0198\ y - 0.0395)\ \log(A/E) + 2.106]\} \quad (38)$$

$$\left\{1 - \frac{1}{\sqrt{2\pi}\ \sigma} \int_{-\infty}^{\ell/L} \exp \frac{((\ell/L) - \mu)^2}{2\sigma^2}\ d(\ell/L)\right\}$$

The range of application of equation 38 is for points such that $2 \leqq y \leqq 20$ cm and $0 \leqq \ell/L \leqq 2$.

Corrections for Bone and Lung

The distortion of soft tissue dose distributions due to the presence of bone and lung was determined in order to obtain realistic treatment planning information. The traverse dose distributions shown in

Figure 26 and Figure 27 were all normalized to the dose obtained at a depth of two centimeters along the central axis without bone present. Values of the percent dose in bone were approximated by use of the following technique. As suggested in ICRU Report 13 [64], the percent dose value measured at a depth of two centimeters in tissue with bone present was reduced by a factor of 1.26 to obtain the percent dose in bone at a depth of approximately three centimeters from the front surface of the phantom. Values of the dose received by tissue as compared to bone reported by Ritts [93] were used to obtain the ratio 1.26. It was assumed that the percent dose in bone follows a simple inverse-square exponential relationship. A linear attenuation coefficient of 0.108 cm^{-1} has been suggested by Wilkie [20] for bone. This value was used in obtaining the dotted curve shown in Figure 27 for points within bone. This portion of the curve is only an approximation of the percent dose in bone and at points less than 0.5 cm from the bone-tissue interface is at best a very rough approximation of the actual dose distribution.

An increase of 7.0 percent in the dose level with bone as compared to the dose without bone was noted for the traverse run at two centimeters depth and also at the surface of the phantom. Both of these distributions were in front of the cylinder of bone-equivalent plastic. This difference in dose level was slightly greater than the statistical uncertainty expected for these measurements and occurred for all of the points near the bone cylinder. The higher density and different elemental composition of bone as compared to tissue may result in "backscattering" of neutrons causing the dose to tissue in front of bone to be increased. Within

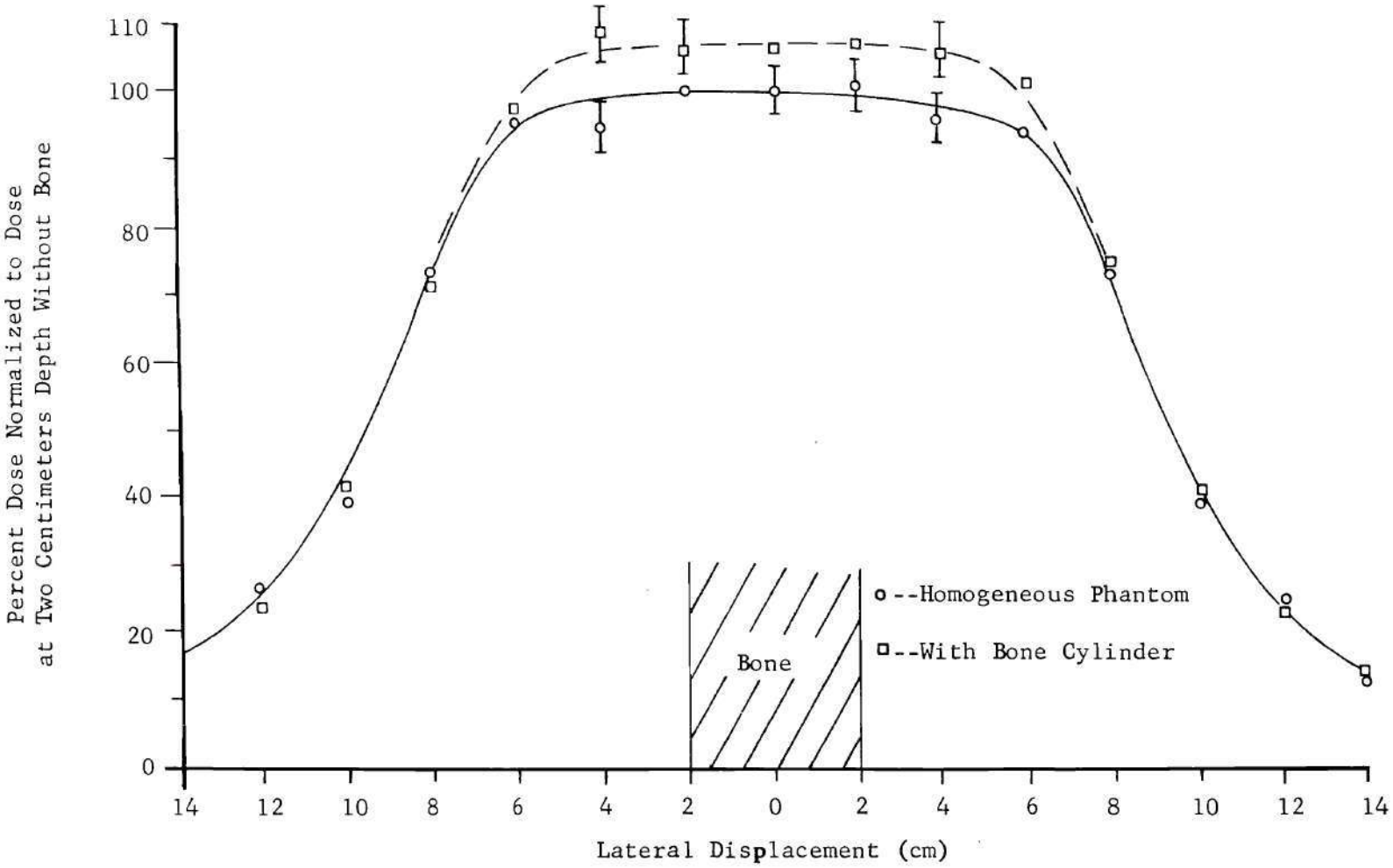

Figure 26. Traverse Dose Distributions for 18.4 × 18.4 cm Field at a Depth of Two Centimeters

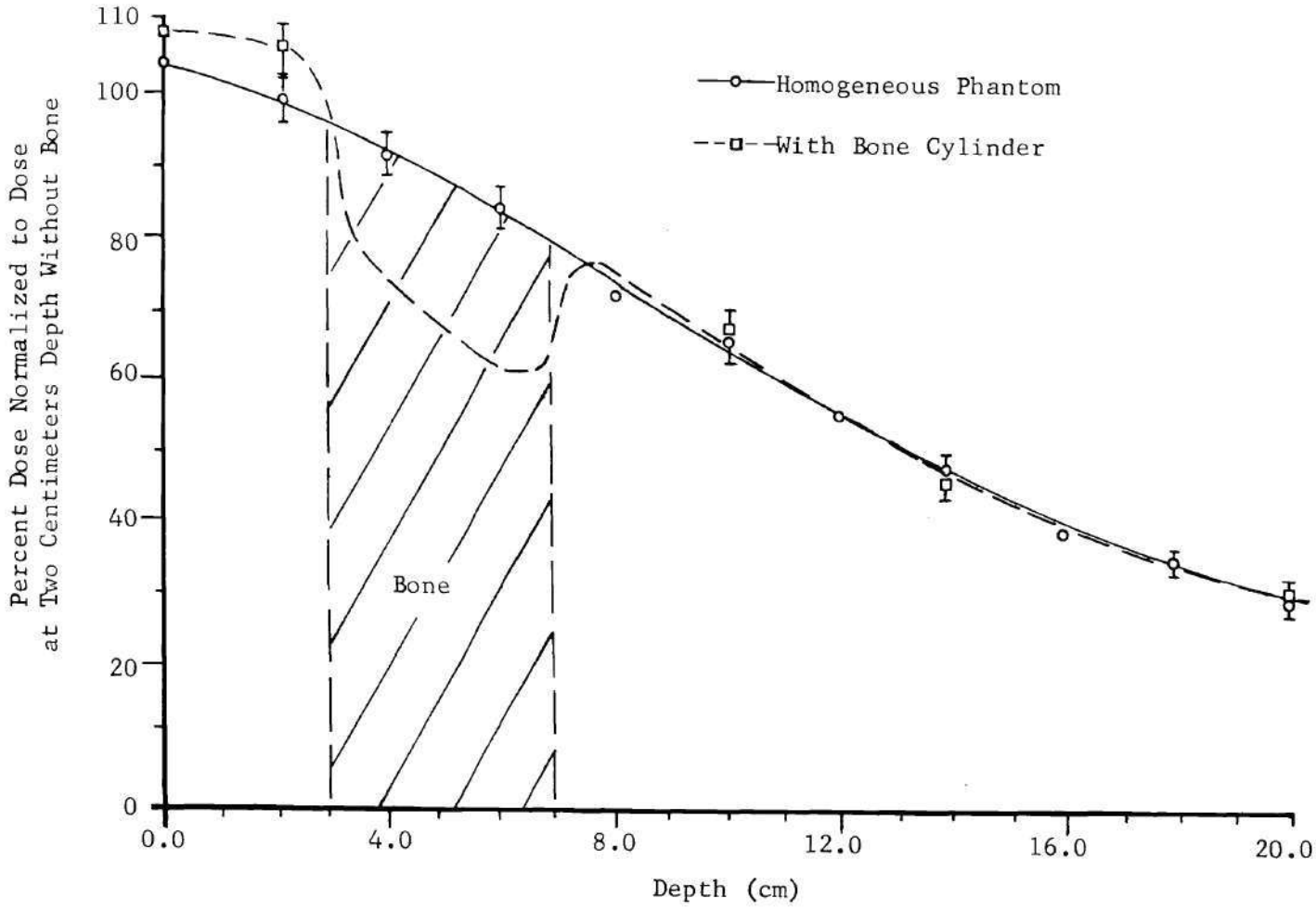

Figure Central Axis Dose Distribution With and Without Bone

experimental error (standard deviation of 4.5 percent) the dose distributions for points behind the bone cylinder (depths of 10, 14, and 20 cm) were the same as the distributions found for the homogeneous phantom. This observation was supported by the experimental work of Poston [79] in which the conclusion was drawn that the upper limit of the dose given to tissue behind a bone-tissue interface is the dose in tissue in the absence of bone. Lawson [94] has made the same suggestion based on theoretical calculations.

The gamma ray dose levels near the bone cylinder were similar to those measured in the cubical phantom without bone plastic. Further study of the dose distribution near bone should be undertaken since the possibility of increased dose due to backscattering of radiation has been demonstrated.

Table 11 gives depth dose values for the central axis of the elliptical and cubical phantom irradiated by an 18.4 × 18.4 cm beam. All percentages indicated in Table 11 were based on the total dose and were normalized to 100 percent at a depth of two centimeters for each field.

In general, the dose levels were slightly less for the elliptical phantom with and without lungs as compared to the dose measurement in the cubical phantom. The gamma dose component for each phantom was the same within experimental uncertainty (± 8.5 percent)

Depth dose data were also obtained with the 18.4 × 18.4 cm beam centered on one of the lungs. Dose measurements were obtained with and without lung in the phantom. Figure 28 shows results of this series of measurements based on neutron dose. Each curve was normalized to 100

Table 11. Depth Dose Distributions in Cubical and Elliptical Phantom for 18.4 x 18.4 cm Field at an SSD of 125 cm

Depth (cm) y	Percent Depth Dose $P^t_{o,y}$ Cubical Phantom (%)	$P^t_{o,y}$ Elliptical Phantom (%)	$P^t_{o,y}$ Elliptical Phantom with Lung (%)
2	100	100	100
4	91.2	95.0	96.0
6	84.5	79.0	78.2
8	72.4	71.5	73.0
10	66.7	63.0	57.3
12	56.0	56.5	54.3
14	48.0	44.2	43.7
16	39.2	35.0	33.4
18	35.2	33.3	37.0
20	29.4	22.8	23.0

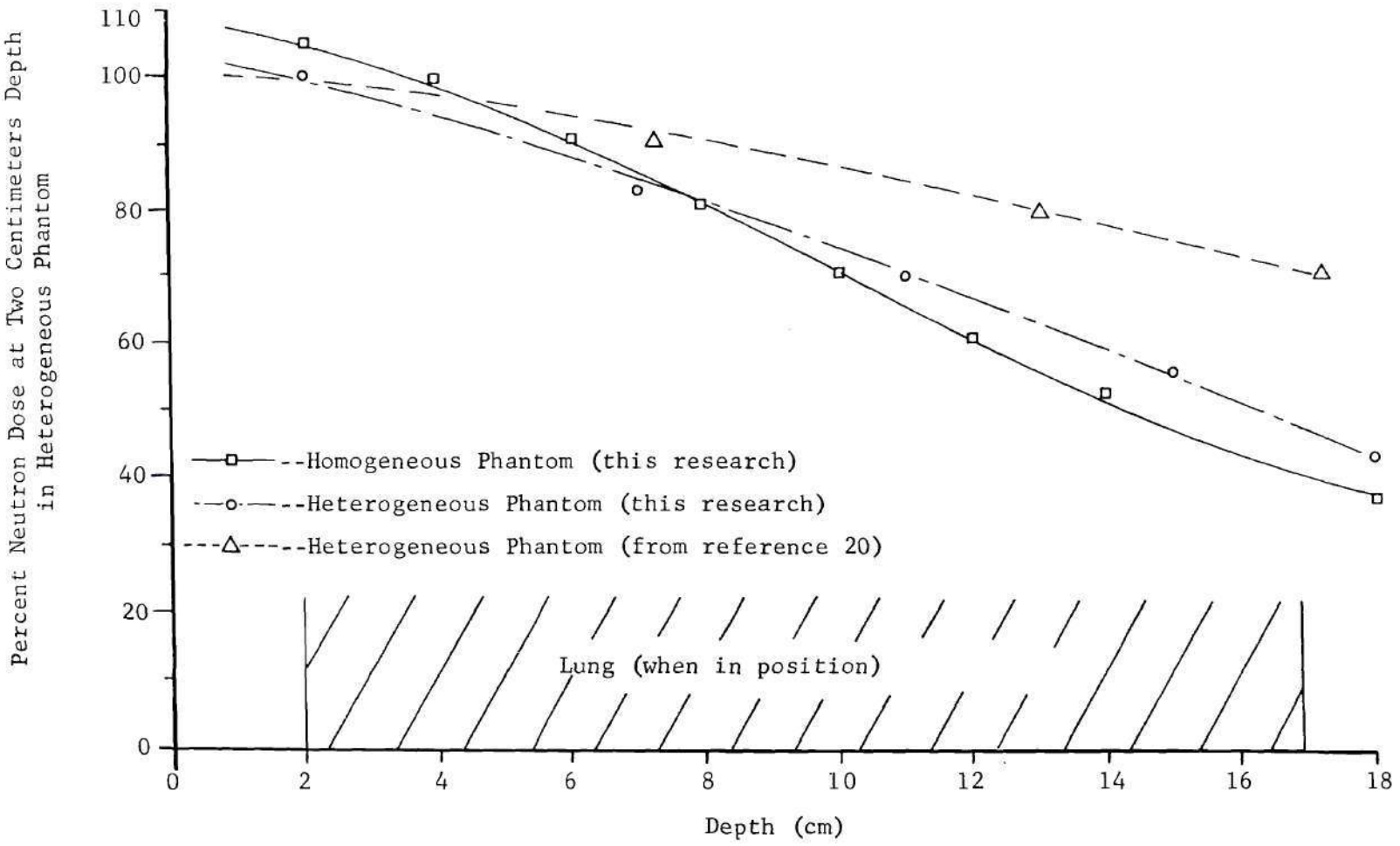

Figure 28. Neutron Depth Dose in Homogeneous and Heterogeneous Phantoms

percent at two centimeters depth with lungs present. Wilkie's Monte Carlo calculation [20] for broad beam irradiation of a 20 x 30 cm elliptical cylinder 60 cm high is also shown in Figure 28. Wilkie's curve falls above the curves for the 18.4 x 18.4 cm beam. These higher percent depth dose values could be due in part to the following factors. In the broad beam case the whole phantom was irradiated; therefore, more scattered neutrons and gamma photons would be present for points along the central axis of the beam than for the case of narrow beams such as the ones used in this investigation.

The reduction of beam intensity due to inverse square effect would also result in lower depth dose values for the 18.4 x 18.4 cm beams as compared to the broad beam case. A decrease of depth dose by a factor of 14.4 and 25.8 percent at 10 and 20 cm depth would result from inverse square attenuation. Application of inverse square corrections to Wilkie's data results in percent dose values that are in reasonable agreement with the values obtained in this study.

Based on these measurements there seems to be a higher dose in and behind lung tissue due to the lesser attenuation of the neutron beam by lung tissue. An increase of 12 percent was seen at 12 cm depth and 17 percent at 18 cm when dose values with and without lungs were compared. This lower attenuation for lung is due to the reduced density of lung tissue as compared to that of soft tissue.

CHAPTER VII

CONCLUSIONS AND RECOMMENDATIONS

Conclusions

An experimental investigation of the dose distribution produced in tissue by beams of 14 MeV neutrons with a source-to-skin distance of 125 cm has been presented. The results of this study clearly show that beams of 14 MeV neutrons exhibit adequate penetration, beam flatness, and beam sharpness for radiotherapy. In tissue located outside the geometrical confines of the beam, dose levels of magnitude similar to that of X ray beams used in radiotherapy are encountered. This situation would be acceptable for fast neutron therapy but it would be desirable to further reduce the radiation dose experienced by healthy tissue outside of the beam. Approximately 50 percent of the radiation dose near the surface of the patient is due to room scattering of neutrons. Therefore, complete shielding of the target would give considerable improvement of the dose distribution near the patient's skin. One of the most striking features of the neutron beam is the low gamma and thermal neutron dose components in air and within the geometrical area of the beam in tissue.

The dose distributions obtained in this study are quite similar to the limited number of experimental distributions reported by other workers [34,12] for beams of 14 MeV neutrons. Reasonable agreement is also obtained between dose distributions calculated by the Monte Carlo method [20,77,90] and the distributions determined in this investigation.

It is concluded that the dose distribution in soft tissue can be expressed as the product of two simple functions. It appears feasible to utilize equations of this type in computer assisted therapy planning.

It is also concluded that small corrections of the soft-tissue dose distribution are required to account for the presence of bone. On the other hand, large positive corrections must be utilized in adjusting the soft-tissue dose distribution to account for the decreased attenuation occurring in the lungs. The dose received by soft tissue in front of bone appears to be increased by a factor of 7.0 percent compared with the dose at the same location without bone. This increased dose can be attributed to backscattering of radiation by bone. These observations are of importance since they can be used to convert the dose distributions obtained in soft tissue to those that would be obtained in a patient irradiated with a collimated beam of 14 MeV neutrons.

Several conclusions can be drawn concerning the performance of the iron-paraffin collimator and shield used in this study. First, a satisfactory shield size, weight, and dose attenuation near the edge of the beam can be obtained. Secondly, a major disadvantage of the shielding system is the relatively high dose level observed for points outside of the beam. Dose levels of approximately three percent of the dose at the center of the beam are obtained as a result of radiation transmitted through the shield. A whole body dose of this magnitude is unacceptable for fast neutron therapy. Thus, it will be necessary to use shielding systems more efficient than the one employed in this investigation for neutron radiotherapy.

Recommendations

Based on this study the following recommendations for future research in this area are made. For treatment planning for 14 MeV neutron therapy, additional depth dose data are needed for many field sizes in the range of areas from 25 cm^2 to 400 cm^2. A detailed study of the dose distribution in tissue in front of bone should be undertaken in order to confirm the backscatter effect observed in this work.

It is recommended that improved collimator and shield designs be developed. Both experimental and Monte Carlo methods should be used in order to establish optimum shield and collimator configurations.

It is also recommended that improved fast neutron calibration of TLD-700 be obtained in order to reduce the uncertainty in mixed-field gamma dose measurements. Accurate calibration could be obtained by use of tissue-equivalent proportional counters such as those developed by Rossi [95]. This instrument has excellent gamma discrimination in terms of absorbed dose and could be used to establish the neutron dose.

To establish the average neutron response of TLD-700, neutron spectral information is required. Monte Carlo programs should be developed for the purpose of calculation of the neutron energy spectrum in tissue for points within and outside of the neutron beam. Experimentally determined beam profiles should be used rather than assuming perfect collimation as has been done in the past.

APPENDICES

APPENDIX A

ERROR ANALYSIS

Definitions

The following definitions of terms associated with errors appearing in the research were adopted from reference 96 for use in this work.

The term "experimental error" will be used to denote the uncertainty associated with an experimental value due to random fluctuations produced by factors such as personal judgment in reading an instrument scale. Error values used to denote the difference between a measured value and the "true" value of some quantity will be referred to as "systematic errors." Measurements with small experimental errors will be considered to have high precision. On the other hand, values with small systematic errors will be considered to have high accuracy. In the discussion that follows, the standard deviation, σ, was used as an index to indicate the magnitude of the experimental error associated with a measurement. The terms standard deviation and experimental error were considered to be equivalent. The standard deviation, σ, was defined as

$$\sigma = \sqrt{\frac{\sum_{1}^{n=k} (x_n - \bar{x})^2}{k - 1}}, \tag{39}$$

where

$\bar{x}$ = arithmetic average of k measurements of the quantity x

x_n = value of n^{th} measurement.

Error in Percent Dose Values

In order to establish the voltage change produced by exposing a Type A chamber to a given dose, the series of voltage measurements shown in Table 12 must be made. The standard deviation values shown in Table 12 are based on repeated voltage readings of the Type A chamber using the Keithley 610B electrometer.

Table 12. Errors in Voltage Measurements Required for Dose Determination

Step	Voltage (volt)	Standard Deviation in Voltage (volt)
Charge-read	V_1	± 0.01
Charge-expose-read	V_2	± 0.01
Recharge-read	V_3	± 0.01

The voltage change (ΔV) caused by the irradiation is obtained from equation 40. The term $(V_1 + V_3)/2$ is the average voltage of the fully charged chamber.

$$\Delta V = ((V_1 + V_3)/2) - V_2 \tag{40}$$

The standard deviation in (ΔV) is given by the square root of the sum of the squares of the standard deviation in voltage V_2 and $(V_1 + V_3)/2$ as shown below.

$$\sigma_{\Delta V} = \sqrt{\sigma_{V_2}^2 + \sigma_{\bar{V}}^2} \qquad (41)$$

$$= \pm 0.014 \text{ volt} ,$$

where

$\sigma_{\Delta V}$ = standard deviation in ΔV

σ_{V_2} = standard deviation in V_2

$\sigma_{\bar{V}}$ = standard deviation in average voltage $\bar{V} = (V_1 + V_3)/2$.

Equation 25 is now used to determine the total dose normalized to a monitor reading of 1×10^5 counts. The dose at some point x,y and the dose at the reference point (0,2 or o,y) are then used in equation 34 or equation 36 to calculate P_y^t or F. Expressing the percent dose in terms of the measured quantities gives equation 42.

$$P^t = \frac{C_a}{C_b}\left(\frac{[(V_1 + V_3)/2 - V_2]_a}{[(V_1 + V_3)/2 - V_2]_b}\right)\left(\frac{(1 \times 10^5/LC)_a}{(1 \times 10^5/LC)_b}\right) , \qquad (42)$$

where

P^t = percent depth dose (central axis depth dose or traverse dose percentage)

a = the chamber used to determine the dose at point x,y

b = the chamber used to measure the dose at the reference point (0,2 cm for the central axis depth dose and o,y for the traverse dose percentage)

LC = long counter reading for given exposure

$C_{a,b}$ = calibration factor for chamber a or b (R/volt).

Temperature and pressure corrections are not included in equation

42 since there were insignificant changes in these parameters during the time required for the two irradiations.

The standard deviation in the percent dose is controlled by the standard deviation of each factor shown in equation 42. The calibration factors (C) have been determined with a percent standard deviation of ± 3.0 percent for a fixed gamma ray dose. The percent standard deviation in the second term, the voltage change caused by the exposure, is given by equation 43.

$$\begin{pmatrix}\text{Percent Standard}\\ \text{Deviation in } \Delta V\end{pmatrix} = \frac{\pm \sigma_{\Delta V}}{\Delta V} \times 100 \qquad (43)$$

where

$\sigma_{\Delta V}$ = standard deviation in voltage drop ΔV (0.014 volt)

ΔV = voltage drop caused by the exposure (volt).

A total dose of about 0.75 rad was used for all measurements within the neutron beam. Therefore, ΔV will be of the order of 1.36 volts and will have associated with it a standard deviation of ± 1.0 percent. An estimated standard deviation of ± 0.5 percent was obtained for the long counter as explained in Chapter IV. All of these factors are combined as shown in equation 44 to obtain the standard deviation in the percent dose.

$$\begin{pmatrix}\text{Percent Standard}\\ \text{Deviation in } P^t\end{pmatrix} = \sqrt{2\left[\begin{pmatrix}\text{Percent}\\ \text{Std. Dev.}\\ \text{in C}\end{pmatrix}^2 + \begin{pmatrix}\text{Percent}\\ \text{Std. Dev.}\\ \text{in } \Delta V\end{pmatrix}^2 + \begin{pmatrix}\text{Percent}\\ \text{Std. Dev.}\\ \text{in LC}\end{pmatrix}^2\right]} \qquad (44)$$

Introducing the percent standard deviations mentioned above into equation 44 leads to a standard deviation of ± 4.5 percent in the percent dose.

It should be noted that systematic errors in the calibration of the ionization chambers will not contribute to the error in relative dose values such as P^t.

Error in Neutron and Gamma Dose

Gamma dose determination by means of the paired chamber system is based on a simultaneous solution of equations 18 and 19. Solving this set of equations for the gamma dose, one obtains equation 45.

$$\gamma = \frac{k\,T - 0.97\,G}{1.03} \tag{45}$$

As can be seen from this equation, the gamma dose component depends directly on the difference between two numbers (k)(T) and 0.97 G. For radiation fields with low gamma contamination, the two numbers are of about the same size. Therefore, several significant figures may be lost in solving for the gamma dose. High percent error may result in the gamma dose due to this reduction of significant figures.

On the other hand, this loss of significant figures is less severe for the determination of the neutron dose. Solving the system of equations for the neutron dose gives the equation shown below.

$$N = \frac{T - G}{0.97 - k}$$

The value of T is considerably larger than G for the case of low gamma contamination and k is of the order of four times smaller than the rad to R conversion factor (0.97). Therefore, the neutron dose has small

percent error compared to the percent error in the gamma dose.

Experimental error arises primarily from variations in the current obtained from the paired ionization chambers. Values of the percent experimental error due to current variations are shown in Table 13. The major source of error for both the gamma and the neutron dose is the large noise to signal ratio of the graphite chamber.

Table 13. Experimental Error in Neutron and Gamma Dose Due to Current Variations

Source	Experimental Error in Gamma Dose (%)	Experimental Error in Neutron Dose (%)
$^{3}_{1}H(d,n)^{4}_{2}He$	± 3	± 1
^{252}Cf	± 24	± 3
$^{2}_{1}H(d,n)^{3}_{2}He$	± 30	± 2
PuBe	± 34	± 3

The variation in the percent error of the gamma dose shown in Table 13 is due primarily to the dose rate obtained from each neutron source used.

Due to uncertainty in the neutron response of the graphite chamber, absolute calibration of each chamber for gamma rays and the ratio of W values for electrons and protons large systematic errors may result in the gamma dose component.

Consideration of the uncertainty due to these sources of systematic error could result in gamma doses that are a factor of two larger than the values given in this study. As a result of this possibility of large systematic error in gamma dose measurements, the relative gamma dose component $P^{\gamma}_{x,y}$ may have an error of the same magnitude.

APPENDIX B

TRAVERSE DOSE FUNCTIONS AND GAMMA DOSE COMPONENTS

Values of the traverse dose function (F) are given in Tables 14, 15, 16, and 17 for each neutron beam investigated in this work. Values of the percent gamma dose component $P^{\gamma}_{x,y}$ are also shown in Tables 14, 15, 16, and 17 and are identified by being enclosed by parentheses.

Table 14. Traverse Functions and Gamma Dose Components for 7.5 × 7.5 cm Field, 14 MeV Neutrons, and SSD of 125 cm

Depth (cm) y	x Displacement from Central Axis (cm)												
	10	8	6	4	3	2	0	2	3	4	6	8	10
2	0.15 (27)	0.14	0.20 (14)	0.43	(10)	0.96	1.00 (8)	0.981	(8)	0.44	0.20 (12)	0.13	0.15 (30)
4	0.15	0.14	0.21	0.48		0.98	1.00	1.02		0.47	0.20	0.14	0.15
6	0.16 (28)	0.14	0.22 (11)	0.521	(6)	1.01	1.00 (8)	0.980	(7)	0.50	0.22 (10)	0.15	0.15 (30)
8	0.16	0.21	0.26	0.516		0.963	1.00	0.936		0.525	0.27	0.21	0.15
10	0.19 (31)	0.26	0.30 (11)	0.546	(10)	0.954	1.00 (9)	0.945	(9)	0.565	0.31 (9)	0.26	0.20 (28)
12	0.21	0.25	0.32	0.578		0.982	1.00	0.952		0.570	0.32	0.26	0.22
14	0.20 (34)	0.28	0.34 (13)	0.552	(9)	0.934	1.00 (10)	0.921	(10)	0.548	0.33 (11)	0.28	0.21 (37)
16	0.20	0.27	0.34	0.558		0.982	1.00	0.946		0.560	0.33	0.26	0.19
18	0.24 (40)	0.31	0.35 (17)	0.574	(9)	1.02	1.00 (12)	0.920	(12)	0.593	0.34 (14)	0.32	0.24 (45)
20	0.23	0.30	0.39	0.607		0.956	1.00	0.931		0.615	0.38	0.30	0.24

NOTE: ( ) = percent gamma dose component $P^{\gamma}_{x,y}$.

Table 15. Traverse Functions and Gamma Dose Components for 11.4 x 11.4 cm Field, 14 MeV Neutrons, and SSD of 125 cm

Depth (cm) y	x Displacement from Central Axis (cm)													
	12	10	8	6	4	2	0	2	3	4	6	8	10	12
2	0.11	0.14	0.20	0.582	0.930	1.01	1.00 (9)	1.02	(8)	0.920	0.571 (9)	0.20	0.15 (28)	0.11
4	0.12	0.14	0.21	0.574	0.862	0.970	1.00	0.980		0.871	0.570	0.20	0.15	0.11
6	0.14	0.18	0.25	0.570	0.864	0.982	1.00 (7)	0.991	(8)	0.885	0.570 (8)	0.25	0.19 (31)	0.14
8	0.15	0.22	0.28	0.584	0.885	0.967	1.00	1.03		0.880	0.575	0.29	0.22	0.15
10	0.16	0.24	0.35	0.590	0.903	1.01	1.00 (9)	1.00	(10)	0.899	0.595 (10)	0.34	0.25 (34)	0.16
12	0.23	0.29	0.34	0.607	0.898	0.988	1.00	0.992		0.900	0.595	0.35	0.29	0.24
14	0.26	0.34	0.45	0.652	0.840	1.02	1.00 (10)	0.982	(12)	0.837	0.660 (11)	0.44	0.34 (40)	0.27
16	0.29	0.36	0.44	0.660	0.842	0.984	1.00	0.973		0.841	0.660	0.45	0.36	0.28
18	0.31	0.39	0.48	0.694	0.823	0.942	1.00 (11)	0.982	(10)	0.810	0.685 (10)	0.48	0.38 (49)	0.31
20	0.31	0.39	0.523	0.742	0.854	1.03	1.00	0.965		0.842	0.730	0.50	0.40	0.32

NOTE: ( ) = percent gamma dose component $P^{\gamma}_{x,y}$.

Table 16. Traverse Functions and Gamma Dose Components for 13 × 13 cm Field, 14 MeV Neutrons, and SSD of 125 cm

Depth (cm) y	x Displacement from Central Axis (cm)																
	14	12	10	8	6	4	3	2	0	2	3	4	6	8	10	12	14
2	0.10	0.10 (30)	0.15	0.21 (30)	0.571	0.982	(8)	0.964	1.00 (8)	1.01	(9)	0.956	0.566	0.21 (27)	0.16	0.11 (28)	0.09
4	0.09	0.13	0.20	0.26	0.603	0.943		0.967	1.00	0.983		0.930	0.617	0.26	0.19	0.13	0.10
6	0.13	0.13 (33)	0.19	0.25 (29)	0.710	0.982	(11)	1.02	1.00 (9)	0.946	(9)	0.965	0.705	0.26 (30)	0.19	0.13 (31)	0.12
8	0.14	0.15	0.22	0.30	0.741	0.942		1.03	1.00	0.982		0.937	0.735	0.31	0.22	0.16	0.13
10	0.14	0.16 (35)	0.23	0.33 (30)	0.758	0.943	(12)	0.987	1.00 (10)	1.02	(11)	0.961	0.760	0.34 (33)	0.23	0.16 (34)	0.13
12	0.16	0.24	0.30	0.43	0.792	1.00		0.992	1.00	0.953		0.972	0.791	0.42	0.30	0.24	0.17
14	0.20	0.26 (41)	0.31	0.45 (37)	0.832	0.974	(12)	0.942	1.00 (12)	0.962	(13)	0.983	0.840	0.45 (38)	0.31	0.25 (40)	0.19
16	0.21	0.27	0.32	0.51	0.830	0.992		1.02	1.00	0.977		0.980	0.822	0.50	0.33	0.27	0.21
18	0.23	0.28 (43)	0.34	0.46 (39)	0.883	0.947	(15)	0.956	1.00 (14)	0.970	(14)	0.954	0.861	0.46 (40)	0.35	0.28 (46)	0.22
20	0.25	0.34	0.40	0.536	0.862	0.962		1.03	1.00	1.02		0.947	0.850	0.55	0.40	0.33	0.25

NOTE: ( ) = percent gamma dose component $P^{\gamma}_{x,y}$.

Table 17. Traverse Functions and Gamma Dose Components for 18.4 × 18.4 cm Field, 14 MeV Neutrons, and SSD of 125 cm

Depth (cm) y	x Displacement from Central Axis (cm)															
	14	12	10	8	6	4	2	0	2	3	4	6	8	10	12	14
2	0.16	0.26	0.39	0.731	0.971	0.954	1.00	1.00 (12)	1.02	(14)	0.967	0.940 (11)	0.725	0.38	0.26 (32)	0.16
4	0.15	0.27	0.43	0.745	0.983	0.947	0.972	1.00	0.981		0.953	0.962	0.736	0.43	0.26	0.17
6	0.21	0.30	0.44	0.756	0.941	0.983	1.02	1.00 (14)	0.986	(13)	0.978	0.930 (12)	0.752	0.44	0.31 (34)	0.20
8	0.18	0.28	0.506	0.773	0.912	0.982	0.965	1.00	0.969		0.971	0.904	0.762	0.503	0.31	0.21
10	0.24	0.34	0.512	0.790	0.924	0.943	0.987	1.00 (13)	0.983	(16)	0.967	0.917 (14)	0.786	0.565	0.36 (35)	0.25
12	0.31	0.39	0.571	0.834	0.953	0.976	1.00	1.00	1.01		0.985	0.942	0.846	0.568	0.40	0.29
14	0.33	0.44	0.630	0.778	0.911	0.946	0.982	1.00 (14)	0.997	(13)	0.973	0.901 (16)	0.764	0.620	0.43 (38)	0.32
16	0.34	0.44	0.657	0.803	0.945	0.974	0.934	1.00	1.02		0.942	0.920	0.788	0.642	0.43	0.33
18	0.36	0.47	0.674	0.823	0.934	0.983	0.991	1.00 (16)	1.04	(15)	0.967	0.900 (16)	0.811	0.682	0.46 (43)	0.35
20	0.35	0.47	0.693	0.841	0.957	1.01	0.984	1.00	1.03		0.934	0.912	0.820	0.681	0.45	0.35

NOTE: ( ) = percent gamma dose component $P^{\gamma}_{x,y}$.

APPENDIX C

FITTING CONSTANTS FOR TRAVERSE EQUATION

Values of a and c for use in equation 38 are given in Table 18 for each field size investigated in this study.

Table 18. Fitting Constants for Traverse Equation (14 MeV Neutrons, SSD = 125 cm)

Depth (cm) y	Field Size	7.5 × 7.5 cm				11.4 × 11.4 cm				13 × 13 cm				18.4 × 18.4 cm			
	ℓ/L Range	0-1		0-2		0-1		0-2		0-1		0-2		0-1		0-2	
	Constant	μ	σ	μ	σ	μ	σ	μ	σ	μ	σ	μ	σ	μ	σ	μ	σ
2		1.02	0.23	0	1.85	1.09	0.30	0	1.66	0.96	0.32	0.08	1.42	1.00	0.23	0.86	0.66
4		1.02	0.25	0	1.90	1.08	0.33	0	1.66	0.98	0.32	0.32	1.32	1.00	0.24	0.86	0.64
6		1.02	0.30	0	1.94	1.07	0.36	0.189	1.72	1.00	0.2	0.34	1.29	1.00	0.26	0.92	0.63
8		1.03	0.30	0	2.40	1.06	0.37	0.579	1.34	1.02	0.26	0.34	1.46	1.02	0.25	0.91	0.63
10		1.05	0.37	0	2.96	1.07	0.38	0.839	1.12	1.03	0.25	0.34	1.46	1.04	0.31	1.00	0.63
12		1.03	0.38	0	3.00	1.06	0.32	0.520	1.96	1.07	0.27	0.68	1.38	1.06	0.30	1.04	0.64
14		1.00	0.37	0	3.38	1.15	0.52	1.00	1.52	1.08	0.27	0.70	1.40	1.09	0.39	1.07	0.62
16		1.01	0.37	0.520	2.10	1.20	0.55	1.05	1.40	1.09	0.28	0.76	1.42	1.10	0.40	1.07	0.64
18		1.03	0.41	0.715	2.24	1.30	0.65	1.20	1.27	1.10	0.28	0.82	1.40	1.12	0.43	1.09	0.65
20		1.04	0.40	0.720	2.20	1.35	0.65	1.20	1.30	1.11	0.29	0.92	1.36	1.12	0.44	1.08	0.66

BIBLIOGRAPHY

1. R. S. Anderson and H. Turkowitz, "The Experimental Modification of the Sensitivity of Yeast to Roentgen Rays," American Journal of Roentgenology 46, 537-542 (1941).

2. L. H. Gray, A. D. Conger, M. Ebert, S. Hornsey, and O. C. A. Scott, "The Concentration of Oxygen Dissolved in Tissue at the Time of Irradiation as a Factor in Radiotherapy," British Journal of Radiology 26, 638-648 (1953).

3. G. W. Barendsen, "The Influence of Oxygen on Damage to the Proliferative Capacity of Cultured Human Cells Produced by Radiation of Different LET," Cellular Radiobiology, Williams and Wilkins Publishers, Baltimore, 1956, pp. 331-335.

4. M. Catterall, R. H. Thomlinson, and C. C. Rogers, "Neutron Radiation Therapy," Neutron Sources and Applications, Proceedings of the American Nuclear Society National Topical Meeting, April 1971, Augusta, Ga., U.S.A.E.C. Report CONF-710402 Vol. II (1971).

5. R. E. Zirkle, D. F. Marchbank, and K. D. Kunck, "Exponential and Sigmoid Survival Curves Resulting from Alpha and X-Irradiation of Aspergillus Spores," Journal of Cellular and Comparative Physiology 39, Suppl. 1, 75 (1952).

6. J. J. Broerse, "Effects of Energy Dissipation by Monoenergetic Neutrons in Mammalian Cells and Tissues," Ph.D. Thesis, University of Amsterdam, 1966.

7. J. R. Andrews and H. Hollister, "The Potentialities for Fast Neutron Beam Cancer Radiotherapy," Proceedings of the XIth International Congress of Radiology Rome, September 1965 Excerpta Medica International Congress Series 105, 914-920 (1965).

8. J. R. Andrews and R. J. Berry, "Fast Neutron Irradiation and the Relationship of Radiation Dose and Mammalian Tumor Cell Reproductive Capacity," Radiation Research 16, 76-81 (1962).

9. J. T. Brennan, "Fast Neutrons for Radiation Therapy," Radiologic Clinics of North America 7, 365-374 (1969).

10. R. C. Lawson, D. M. Clare, and D. E. Watt, "(D,D) and (D,T) Neutron Depth Dose Measurements in a Tissue-Equivalent Phantom," Physics in Medicine and Biology 12, 201-215 (1967).

BIBLIOGRAPHY (Continued)

11. A. C. Lucas and W. M. Quam, "Fast-Neutron Source Studies for Radiation Therapy, Part I: Dosimetry at Hammersmith Cyclotron," E G & G Technical Report S-477-R (1969).

12. L. J. Goodman and U. Koch, "Dosimetry Studies for a Fast Neutron Therapy Beam," U.S.A.E.C. Report NYO-2740-6, 1969, pp. 32-95.

13. J. T. Brennan, A. Raventos, and M. L. Mendelsohn, "14.1 MeV Neutrons in Radiotherapy," Status Report on Planning Grant CA-10059-01, 1967. (U.S. Public Health Service Grant).

14. National Bureau of Standards Handbook 84, "Radiation Quantities and Units," Washington (1964).

15. J. F. Fowler, "Neutrons in Radiotherapy," Biological Effects of Neutron and Proton Irradiations, Vol. II. IAEA, Vienna, 1964, pp. 185-214.

16. E. M. Lent, "Collimation of Fast Neutrons," Lawrence Radiation Laboratory Report UCRL-50857 (1970).

17. M. L. Randolph, "Genetic Damage as a Function LET," Annals New York Academy of Science 114, 85-95 (1964).

18. R. F. Boggs, "Health Physics Aspects of the Operation of Cockroft-Walton Type Neutron Generators," U.S. Department of Health, Education, and Welfare, March 1966.

19. A. C. Lucas and W. M. Quam, "Fast-Neutron Source Studies for Radiation Therapy, Part 2: Dosimetry at the ICT (d,t) Source, LRL-Livermore," E G & G Technical Report S-477-R (1969).

20. W. Wilkie, "Theoretical Image-Forming Quality of Fast-Neutron Radiography," Ph.D. Thesis, Georgia Institute of Technology (1970).

21. R. T. Rogers, "A Phantom Material to Represent Lung," British Journal of Radiology 43, 441-444 (1970).

22. National Bureau of Standards Handbook 85, "Physical Aspects of Irradiation," Washington (1964).

23. H. H. Rossi and G. Failla, "Tissue Equivalent Ionization Chambers," Nucleonics 14, 32-37 (1956).

24. F. R. Shonka, J. E. Rose, and G. Failla, "Conducting Plastic Equivalent to Tissue, Air and Polystyrene," Second United Nations International Conference on the Peaceful Uses of Atomic Energy, Conference paper P/753, (1958).

BIBLIOGRAPHY (Continued)

25. L. J. Goodman, "A Modified Tissue Equivalent Liquid," U.S.A.E.C. Report NYO-2740-6, 1969, pp. 207-208.

26. C. L. Wingate, W. Gross, and G. Failla, "Experimental Determination of Absorbed Dose from X-Rays Near the Interface of Soft Tissue and Other Materials," Radiology 79, 984-999 (1962).

27. D. K. Bewley and C. J. Pannel, "The Fast Neutron Beam from the M.R.C. Cyclotron," British Journal of Radiology 42, 281-288 (1969).

28. T. Jones, D. K. Bewley, and D. D. Vonberg, "Radiation Protection Around the Medical Cyclotron at Hammersmith Hospital," Radiology 98, 665-671 (1971).

29. J. D. Seagrave, E. R. Graves, S. J. Hipwood, and C. J. McDole, "$D(d,n)He^3$ and $T(d,n)He^4$ Neutron Source Handbook," U.S.A.E.C. Report LAMS-2162 (1958).

30. T. G. Provenzano, E. J. Story, F. F. Haywood, and H. T. Miller, "Feasibility Study: Intense 14-MeV Neutron Source for Operation Henre," U.S.A.E.C. Report CEX-65.01 (1965).

31. H. M. Butler and F. F. Haywood, "Radiation Safety Practices: Operation Henre," U.S.A.E.C. Report CEX-65.05 (1970).

32. J. R. Andrews and H. Hollister, "Fast Neutron Beam Radiotherapy," American Journal of Roentgenology 99, 954-961 (1967).

33. J. E. Bounden, P. D. Lomer, and J. D. H. L. Wood, "A Neutron Tube with Constant Output (10^{10} n/sec) for Activation Analysis and Reactor Applications," Nuclear Instruments and Methods 33, 283-288 (1965).

34. D. Greene and R. L. Thomas, "An Experimental Unit for Fast Neutron Radiotherapy," British Journal of Radiology 41, 455-463 (1968).

35. G. W. Hamilton, J. L. Hilton, and J. S. Luce, "Multimomentum 650-mA Ion Source," Plasma Physics 10, 687-697 (1968).

36. C. A. Kelsey, M. L. M. Boone, J. M. Hevezi, A. L. Wiley, Jr., and G. C. Spalek, "Gas Target Source for Neutron Radiation Therapy," Radiology 98, 686-688 (1971).

37. E. W. Webster and K. C. Tsien, "Atlas of Radiation Dose Distributions," International Atomic Energy Agency, Vienna, 1965.

BIBLIOGRAPHY (Continued)

38. T. D. Sterling, H. Perry, and L. Katz, "Derivation of a Mathematical Expression for the Percent Depth Dose Surface of Cobalt 60 Beams and Visualization of Multiple Field Dose Distributions," British Journal of Radiology 37, 544-550 (1964).

39. S. K. Gupta and J. R. Cunningham, "Measurements of Tissue-Air Ratios and Scatter Functions for Large Field Sizes, for Cobalt 60 Gamma Radiation," British Journal of Radiology 39, 7-11 (1966).

40. H. E. Johns and J. R. Cunningham, The Physics of Radiology, Charles C. Thomas Publisher, Springfield, 1969, pp. 313-319 and 358.

41. J. S. Clifton and T. L. Gallagher, "Comparison of Computer Generated Depth Doses," Paper presented at the Second International Conference on Medical Physics, Boston, August 1969.

42. P. G. Orchard, "Decrement Lines: a new presentation of data in cobalt 60 beam dosimetry," British Journal of Radiology 37, 756-763 (1964).

43. J. R. Clarkson, "A Note on Depth Doses in Fields of Irregular Shape," British Journal of Radiology 14, 265-268 (1941).

44. W. J. Meredith and G. J. Neary, "The Production of Isodose Curves and the Calculation of Energy Absorbed from Standard Depth Dose Data," British Journal of Radiology 17, 75-82 (1944).

45. J. J. Weinkam and R. A. Kolde, "Radiation Treatment Planning System Manual," NCI Grant CA-10208, 1970.

46. J. R. Gloven, "An Analysis of Radiation Depth Dose Data," Ph.D. Thesis, The University of Rochester, 1968.

47. G. S. Hurst, "An Absolute Tissue Dosemeter for Fast Neutrons," British Journal of Radiology 27, 353-357 (1954).

48. H. H. Rossi, G. S. Hurst, W. A. Mills, and H. E. Hungerford, Jr., "Intercomparison of Fast-Neutron Dosimeters," Nucleonics 13, 46-47 (1955).

49. U. Fano, "Note on the Bragg-Gray Cavity Principle for Measuring Energy Dissipation," Radiation Research 1, 237-240 (1954).

50. M. L. Randolph, "Energy Deposition in Tissue and Similar Materials by 14.1-MeV Neutrons," Radiation Research 7, 47-57 (1957).

BIBLIOGRAPHY (Continued)

51. J. Rhodes, W. Franzen, and W. E. Stephens, "Ionization Measurement of $B^{10}(n,\alpha)Li^{7}$," Physical Review 87, 141-145 (1952).

52. G. J. Neary, R. J. Munson, and R. H. Mole, "Chronic Radiation Hazards," Pergamon Press, New York (1957).

53. L. H. Gray, "The Ionization Method of Measuring Neutron Energy," Proceedings of the Cambridge Philosophical Society 40, 73-102 (1944).

54. National Bureau of Standards Handbook 75, "Measurement of Absorbed Dose of Neutrons and of Mixtures of Neutrons and Gamma Rays," Washington (1961).

55. J. A. Sayeg and P. S. Harris, "Experimental Determination of Fast and Thermal Neutron Tissue Dose," U.S.A.E.C. Report LA-2174 (1958).

56. G. S. Hurst, "Ionization Methods of Mixed Radiation Dosimetry," Principles of Radiation Protection, K. Z. Morgan and J. E. Turner, eds., John Wiley & Sons, Inc., New York (1967).

57. E. B. Wagner and G. S. Hurst, "A Geiger-Müeller γ-Ray Dosimeter with Low Neutron Sensitivity," Health Physics 5, 20-26 (1961).

58. C. Distenfeld, W. Bishop, and D. Colvett, "Thermoluminescent Neutron-Dosimetry System," Proceedings of an International Conference on Luminescence Dosimetry, June 21-27, 1965, Stanford, F. H. Attix, ed., U.S.A.E.C. Report CONF-650637 1967, p. 457.

59. N. Goldstein, W. G. Miller, and P. F. Rago, "Additivity of Neutron and γ-Ray Exposures for TLD Dosimeters," Health Physics 18, 157-158 (1970).

60. C. L. Wingate, E. Tochilin, and Norma Goldstein, "Response of Lithium Fluoride to Neutrons and Charged Particles," Luminescence Dosimetry, Proceedings of the International Conference on Luminescence Dosimetry, Stanford, June 1965, U.S.A.E.C. Symposium Series No. 8, CONF-650637.

61. E. Tochilin, N. Goldstein, and W. G. Miller, "Beryllium Oxide as a Thermoluminescent Dosimeter," Health Physics 16, 1-8 (1969).

62. D. R. Davy and B. G. O'Brien, "An Adapted Model for the LET Dependance of LiF Thermoluminescence," Health Physics 17, 471-482 (1969).

BIBLIOGRAPHY (Continued)

63. R. Gwin and R. B. Murray, "Scintillation Process in CsI(Tl). II. Emission Spectra and the Possible Role of Self-Trapped Holes," Physical Review 131, 508-512 (1963).

64. International Commission on Radiation Units and Measurements Report 13, "Neutron Fluence, Neutron Spectra and Kerma," Washington (1969).

65. J. R. Cameron, D. Zimmerman, G. Kenney, R. Buch, R. Bland, and R. Grant, "Thermoluminescent Radiation Dosimetry Utilizing LiF," Health Physics 10, 25-29 (1964).

66. V. D. Svikis, "Dense Lithium Fluoride for Gamma-Ray-Free Neutron Shielding," Nuclear Instruments and Methods 25, 93-105 (1963).

67. R. E. Simpson, J. A. Sayeg, and A. C. Lucas, "Depth Dose Distribution in a Beagle Phantom within a Mixed Field of Neutrons and Gamma-Rays," Radiation Protection, W. S. Snyder, ed., Pergamon Press, Oxford, 1968.

68. D. K. Bewley, "Physical Aspects of the Fast Neutron Beam," British Journal of Radiology 36, 81-88 (1963).

69. P. C. Aebersold, "The Production of a Beam of Fast Neutrons," Physical Review 56, 714-727 (1939).

70. P. C. Aebersold, "The Cyclotron: A Nuclear Transformer," Radiology 39, 513-540 (1942).

71. R. B. Allred, A. H. Armstrong, and L. Rosen, "The Interaction of 14-MeV Neutrons with Protons and Deuterons," Physical Review 91, 90-99 (1953).

72. D. Greene and R. L. Thomas, "The Attenuation of 14 MeV Neutrons in Steel and Polyethylene," British Journal of Radiology 14, 45-54 (1969).

73. A. Langsdorf, Jr., "Neutron Collimation and Shielding for Experimental Purposes," Fast Neutron Physics, Part I, J. B. Marion and J. L. Fowler eds., Interscience Publishers, New York, 1960.

74. J. T. Brennan, Private Communication, Hospital of the University of Pennsylvania (1970).

75. D. Greene, Private Communication, Christie Hospital and Holt Radium Institute (1969).

BIBLIOGRAPHY (Continued)

76. P. H. McGinley, "Fast Neutron Central Axis Depth Dose Equation," Physics in Medicine and Biology 15, 121-126 (1970).

77. T. D. Jones, W. S. Snyder, and J. A. Auxier, "Absorbed Dose, Dose Equivalent, and LET Distribution in Cylindrical Phantoms Irradiated by a Collimated Beam of Monoenergetic Neutrons," To be published in Health Physics.

78. C. C. Burkell, T. A. Watson, H. E. Johns, and R. J. Horsley, "Skin Effects of Cobalt 60 Telecurie Therapy," British Journal of Radiology 27, 171-176 (1954).

79. J. W. Poston, "Neutron Depth Dose Distributions in Heterogeneous Phantoms," Ph.D. Thesis, Georgia Institute of Technology (1971).

80. H. Skoldform, "On the Design, Physical Properties and Practical Application of Small Condenser Ionization Chambers," ACTA Radiological, Supplement 187 (1959).

81. J. W. Poston, Private Communication, Oak Ridge National Laboratory (1970).

82. D. C. Lawrence, "Mixed Radiation Dosimetry of a Plutonium-Beryllium Neutron Source," Health Physics 7, 179-184 (1962).

83. W. C. Reinig, "Advantages and Applications of ^{252}Cf as a Neutron Source," Nuclear Applications 5, 24-25 (1963).

84. D. Nachtigall, "Average and Effective Energies, Fluence-Dose Conversion Factors and Quality Factors of the Neutron Spectra of (α,n) Sources," Health Physics 13, 213-219 (1967).

85. J. B. Smathers, Private Communication, Texas A & M University, 1971.

86. C. J. Parnell, "Fast Neutron Depth Doses and Spectra Obtained by Bombarding Various Targets with 16 MeV Deuterons," Neutron Sources and Applications, Proceedings of the American Nuclear Society National Topical Meeting, April 1971, Augusta, Ga., U.S.A.E.C. Report CONF-710402, Vol. II (1971).

87. J. H. Thorngate, D. R. Johnson, and P. T. Perdue, "Neutron and Gamma-Ray Leakage from the Ichiban Critical Assembly," U.S.A.E.C. Report CEX-64.7 (1965).

88. J. A. Auxier, F. F. Haywood, and L. W. Gilley, "General Correlative Studies - Operation BREN," U.S.A.E.C. Report CEX-62.03 (1963).

BIBLIOGRAPHY (Concluded)

89. H. L. Fisher, Jr. and W. S. Snyder, "Distribution of Dose in the Body from a Source of γ Rays Distributed Uniformly in an Organ," Radiation Protection, W. S. Snyder ed., Pergamon Press, Oxford, 1968.

90. J. A. Auxier, W. S. Snyder, and T. D. Jones, "Neutron Interactions and Penetration in Tissue," Radiation Dosimetry Vol. I, F. H. Attix and W. C. Roesch eds., Academic Press, New York (1968).

91. G. F. Stone and J. H. Thorngate, "Experimentally Determined Proton-Recoil Spectra in Tissue-Equivalent Material from 3 and 15 MeV Neutrons," U.S.A.E.C. Report ORNL-TM-1927 (1967).

92. L. J. Goodman, Private Communication, Columbia University (1970).

93. J. J. Ritts, "The Calculation of Doses in Human Tissue," Masters Thesis, The University of Tennessee (1970).

94. R. C. Lawson, "The Recoil Proton Dose at a Bone-Tissue Interface Irradiated by Fast Neutrons," Physics in Medicine and Biology 12, 551-554 (1967).

95. H. H. Rossi and W. Rosenzweig, "A Device for the Measurement of Dose as a Function of Specific Ionization," Radiology 64, 404-444 (1955).

96. Y. Beers, Introduction to the Theory of Error, Addison-Wesley Publishing Company, Cambridge, Mass., 1953.

VITA

Patton Hopkins McGinley was born in Narrows, Virginia on December 25, 1935. Mr. McGinley attended the Georgia Institute of Technology from 1954 until 1958 when he received the Bachelor of Science Degree in Physics.

From 1958 to 1959 he was employed by the Pulaski High School, Pulaski, Virginia, as a physics instructor. In 1959 Mr. McGinley entered the armed forces as a combat engineer.

During the years 1961 to 1966, Mr. McGinley was employed as an Instructor of Physics by the Virginia Polytechnic Institute. In 1963 he took a leave of absence in order to enter graduate school. He received his M.S. degree in Radiological Health Physics from Rutgers in 1964.

In 1966, he was employed by the Longwood College, Farmville, Virginia, as an Assistant Professor of Physics.

Mr. McGinley married the former Bennie Ruth Williams on March 17, 1962 and has two children, Patton Jr. and Mary Darden.